

INFORMATION TO USERS

This manuscript has been reproduced from the microfilm master. UMI films the text directly from the original or copy submitted. Thus, some thesis and dissertation copies are in typewriter face, while others may be from any type of computer printer.

The quality of this reproduction is dependent upon the quality of the copy submitted. Broken or indistinct print, colored or poor quality illustrations and photographs, print bleedthrough, substandard margins, and improper alignment can adversely affect reproduction..

In the unlikely event that the author did not send UMI a complete manuscript and there are missing pages, these will be noted. Also, if unauthorized copyright material had to be removed, a note will indicate the deletion.

Oversize materials (e.g., maps, drawings, charts) are reproduced by sectioning the original, beginning at the upper left-hand corner and continuing from left to right in equal sections with small overlaps.

Photographs included in the original manuscript have been reproduced xerographically in this copy. Higher quality 6" x 9" black and white photographic prints are available for any photographs or illustrations appearing in this copy for an additional charge. Contact UMI directly to order.

ProQuest Information and Learning
300 North Zeeb Road, Ann Arbor, MI 48106-1346 USA
800-521-0600

UMI[®]

University of Alberta

**Programming Supramolecular Systems Using
Hydrogen Bonding and Metal Chelation**

by

Elisa Murguly



A thesis submitted to the Faculty of Graduate Studies and Research in partial fulfillment
of the requirements for the degree of
Master of Science

Department of Chemistry

Edmonton, Alberta

Spring 2001



**National Library
of Canada**

**Acquisitions and
Bibliographic Services**

**395 Wellington Street
Ottawa ON K1A 0N4
Canada**

**Bibliothèque nationale
du Canada**

**Acquisitions et
services bibliographiques**

**395, rue Wellington
Ottawa ON K1A 0N4
Canada**

Your file Votre référence

Our file Notre référence

The author has granted a non-exclusive licence allowing the National Library of Canada to reproduce, loan, distribute or sell copies of this thesis in microform, paper or electronic formats.

The author retains ownership of the copyright in this thesis. Neither the thesis nor substantial extracts from it may be printed or otherwise reproduced without the author's permission.

L'auteur a accordé une licence non exclusive permettant à la Bibliothèque nationale du Canada de reproduire, prêter, distribuer ou vendre des copies de cette thèse sous la forme de microfiche/film, de reproduction sur papier ou sur format électronique.

L'auteur conserve la propriété du droit d'auteur qui protège cette thèse. Ni la thèse ni des extraits substantiels de celle-ci ne doivent être imprimés ou autrement reproduits sans son autorisation.

0-612-60476-4

Canada

University of Alberta

Library Release Form

Name of Author: Elisa Murguly

Title of Thesis: Programming Supramolecular Systems Using Hydrogen Bonding and Metal Chelation

Degree: Master of Science

Year this Degree Granted: 2001

Permission is hereby granted to the University of Alberta Library to reproduce single copies of this thesis and to lend or sell such copies for private, scholarly or scientific research purposes only.

The author reserves all other publication and other rights in association with the copyright in the thesis, and excepts as herein before provided, neither the thesis nor any substantial portion thereof may be printed or otherwise reproduced in any material form whatever without the author's prior written permission

Elisa Murguly
6067 Trent Drive
Prince George, B.C.
V2N 2G4

January 2001

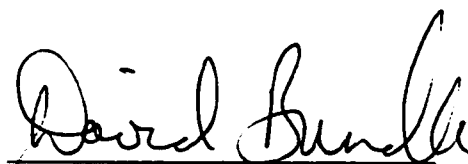
University of Alberta

Faculty of Graduate Studies and Research

The undersigned certify that they have read, and recommend to the Faculty of Graduate Studies and Research for acceptance, a thesis entitled Programming Supramolecular Systems Using Hydrogen Bonding and Metal Chelation submitted by Elisa Murguly in partial fulfillment of the requirements for the degree of Master of Science.



Assistant Professor Neil R. Branda



Professor David R. Bundle



Professor Edward Knaus

01/25/14

To family and friends:

your love and support is overwhelming. Thank you!

Programming Supramolecular Systems Using Hydrogen Bonding and Metal Chelation

by

Elisa Murguly

Abstract

Supramolecular building blocks were designed and synthesized for use in self-assembly syntheses. The utility of hydrogen and/or dative bonds to direct the self-assembly process for the fabrication of supramolecular complexes capable of specific tasks was investigated.

Photochromic chiral dithienylethenes formed optically pure helicates in a spontaneous “chiral-directed” self-assembly process. The rigid positioning of the photochrome within the helicate resulted in the preferential formation of one of the stereoisomers during the *ring-closing* photochromic reaction. The resulting two states of the photochrome (*ring-open* and *ring-closed*) exhibited contrasting ORD curves. This formed the basis for a non-invasive write-read-erase system.

A series of racemic helicenes were prepared. Their ability to selectively and spontaneously self-assemble into predictable architectures was investigated. The discriminating self-assembly process for [7]-helicene was enantiospecific in solution and diastereoselective in the crystal.

Novel synthons, containing both hydrogen and dative bond recognition sites, were synthesized for the construction of discrete self-assembled arrays with potential applications in inclusion chemistry.

The keto-enol equilibrium of terpyridine derivatives was evaluated in the gas, solution and solid-state using IR spectroscopy, variable temperature ^1H and ^{13}C NMR spectroscopy and X-ray crystallography. The results showed the enol to be predominant in the gas phase, while the more polar keto form is predominant in solution. In the solid-state a mixed dimer (1:1) is present.

Table of Contents

1	Concepts and Methods in Supramolecular Chemistry	1
1.1	Supramolecular Glue	2
1.2	Characterization of Supramolecular Architectures	4
1.2.1	Structure Elucidation of Aggregate	4
1.2.2	Kinetic Information	6
1.2.3	Thermodynamic Information	8
1.3	Summary and Overview	8
1.4	References	9
2	Dative Bonding, Photochromes and Erasable Memory Media	12
2.1	Molecular Recognition and the Dative Bond	12
2.1.1	Properties of Dative Bonds	13
2.1.2	Selected Examples of Metal-Directed Assemblies	14
2.2	Molecular Programming and Dithienylethenes	16
2.2.1	Choice of Photochrome	16
2.2.2	Detection of Dithienylethene Photochromes	18
2.2.3	Use of Optical Rotation for Non-Destructive Detection	19
2.2.4	Chirality of Dithienylethene Photochromes	20
2.2.5	Dative Bonds and Optically Pure Helicates	22
2.2.6	Dative Bonds and Dithienylethenes	24
2.3	Dithienylethenes – Results and Discussion	25
2.3.1	Synthesis	25

2.3.2	Electrospray Mass Spectroscopic Analysis	27
2.3.3	X-Ray Crystallographic Analysis	28
2.3.4	UV-Vis Spectroscopic Analysis	30
2.3.5	Solution-State Studies Using ^1H NMR Analysis	32
2.3.6	Circular Dichroism and Optical Rotatory Dispersion Analysis	36
2.4	Conclusions	37
2.5	Experimental	38
2.5.1	General Information	38
2.5.2	Synthesis	39
2.6	References	45
3	Hydrogen Bonding, Helicenes and Chiral Discrimination	49
3.1	Molecular Recognition and The Hydrogen Bond	50
3.1.1	Primary Hydrogen Bonds	50
3.1.2	Secondary Hydrogen Bonds	50
3.1.3	Isomers of Hydrogen Bond Arrays	53
3.1.4	Selected Examples of Hydrogen Bond Directed Assemblies	54
3.2	Molecular Programming and Helicenes	54
3.2.1	Choice of the Scaffold	54
3.2.2	Viability of the Scaffold	57
3.2.3	Synthesis of the Helicene	58
3.2.4	Design of Specific Helicene Scaffold	60
3.3	[7]-Helicene: Results and Discussion	61

3.3.1	Synthesis	62
3.3.2	Solution-State Studies Using ^1H NMR Analysis	64
3.3.3	X-Ray Crystallographic Analysis	66
3.4	[5]- and [9]-Helicene: Results and Discussion	70
3.4.1	Synthesis	70
3.4.2	Solution-State Studies Using ^1H NMR Analysis	72
3.4.3	X-Ray Crystallographic Analysis	74
3.5	Alternate Helicenes	76
3.6	Diaza-helicene as Helical Catalysts	78
3.6.1	Synthesis	79
3.7	Conclusions	80
3.8	Experimental	81
3.9	References	103
4	Dative Bonding, Hydrogen Bonding and Molecular Squares	106
4.1	Dative Bonds and Molecular Squares	106
4.1.1	Dative and Hydrogen Bonds and Molecular Squares	109
4.1.2	Design of a Bifunctional Synthon	111
4.2	Results and Discussion	113
4.2.1	Synthesis of Ligands 4 and 8	113
4.2.2	Self-Assembly Involving Ligand 8	115
	4.2.2.1 Solution-State Studies Using ^1H NMR Analysis	115
	4.2.2.2 Mass Spectrometry Analysis	117

4.2.3	Synthesis of Ligand 13	118
4.2.4	Self-Assembly Involving Ligand 13	119
4.2.4.1	Solution-State Studies for 13 Only	120
4.2.4.2	Solution-State Studies for [Pt(dppp)OTf ₂ + 13]	122
4.3	Conclusions	125
4.4	Experimental	126
4.4.1	Synthesis	126
4.5	References	129
Appendix I – Tautomerism of 4-Hydroxypyridine		131
I.1	Introduction	131
I.2	Results and Discussion	133
I.2.1	X-Ray Crystallographic Analysis	133
I.2.2	Solid-State Analysis using ¹³ C NMR Spectroscopy	138
I.2.3	Infrared Spectroscopic Analysis	139
I.2.4	Solution-State Studies Using ¹ H NMR Analysis	141
I.3	Conclusion	147
I.4	Experimental	148
I.5	References	151
Appendix II – X-Ray Crystallography		155

List of Tables

Chapter 1

Table 1	Examples of Supramolecular “Glue”	3
---------	-----------------------------------	---

Chapter 2

Table 1	Examples of Photochromic Molecules	18
Table 2	Diastereoselectivities of Photochromic Processes	34

Chapter 3

Table 1	Comparison of Activation Barriers to Racemization	56
---------	---	----

Chapter 4

Table 1	Molecular Library of Cyclic Molecular Arrays	108
---------	--	-----

Appendix I

Table 1	Selected Interatomic Distances from X-Ray Crystal Structure	136
Table 2	^{13}C CPMAS DPD NMR Data for Terpyridine	138
Table 3	^1H NMR Data for Terpyridine in CDCl_3	142

Appendix II

Table 1	Selected Interatomic Distances from X-Ray Crystal Structure	155
---------	---	-----

List of Figures

Chapter 1

Figure 1.	NMR Titration Graphs	7
-----------	----------------------	---

Chapter 2

Figure 1a	Geometries of Selected Metals	13
Figure 1b	Schematic of Metal Directed Assemblies	14
Figure 2	X-Ray Crystal Structure of Copper (I) Complex	28
Figure 3	X-Ray Crystal Structure of Psuedooctahedral Environment	29
Figure 4a	UV-Vis Spectra of Copper Complex	31
Figure 4b	UV-Vis Spectra Comparing Complexes	32
Figure 5	^1H NMR Spectra of Diastereoselectivity	33
Figure 6a	CD Spectra of <i>Open/Closed</i> Forms without Copper	35
Figure 6b	CD Spectra of <i>Open/Closed</i> Forms with Copper	35
Figure 7	ORD Specta of <i>Open/Closed</i> Forms with Copper	36
Figure 8	Modulation of Optical Rotation	37

Chapter 3

Figure 1	Jorgensen's Secondary Electrostatic Model	52
Figure 2	Effects of Preorganization on Association Constants	53
Figure 3	Self-assembly of Racemic and Optically Pure 8	55
Figure 4	Examples of Functional Helicenes	58
Figure 5	Schematic Representation of Hydrogen-bonded Assemblies	62

Figure 6	Dilution Titration of [7]-Helicene in Pyridine	66
Figure 7	X-Ray Crystal Structure of Protected [7]-Helicene	67
Figure 8	X-Ray Crystal Structure of [7]-Helicene	69
Figure 9	Packing Diagram of [7]-Helicene	70
Figure 10	X-Ray Crystal Structure and Packing Diagram of [5]-Helicene	75
Figure 11	Planar Nucleophilic Catalyst	78
Figure 12	Diaza helicene as Nucleophilic Catalyst	78

Chapter 4

Figure 1	Self-Assembly of Molecular Square	107
Figure 2	Base Quartet formed between Self-Complementary Base Pairs	110
Figure 3	Dilution Titration of 8 and [Pt(dppp)OTf ₂ + 8]	116
Figure 4	ES-MS of [Pt(dppp)OTf ₂ + 8] in CH ₂ Cl ₂	118
Figure 5	Two Modes of 13 Binding to a Sodium Ion	122
Figure 6	Variable Temperature ³¹ P NMR Spectra	123

Appendix I

Figure 1	X-Ray Crystal Structure of Mixed Dimer	135
Figure 2	Packing Diagram of Mixed Dimer	137
Figure 3	FT-IR Spectra of Terpyridine in Gas, Solution and Solid State	140
Figure 4	N.O.e. Assignment of Terpyridine	142
Figure 5	N.O.e. Assignment of Terpyridine Derivative	144
Figure 6	NMR Cooling Experiment of Terpyridine	146

List of Schemes

Chapter 2

Scheme 1	Self-assembly of Molecular Boxes	15
Scheme 2	Synthesis of Dithienylethene Photochrome	26
Scheme 3	Synthesis of Copper (I) Complex	27
Scheme 4	Mechanism of <i>Ring-closing</i> Reaction	30

Chapter 3

Scheme 1	Synthesis of [7]-Helicene	63
Scheme 2	Synthesis of [5]-Helicene	71
Scheme 3	Synthesis of [9]-Helicene	73
Scheme 4	Synthesis of Alternative [5]-Helicene	77
Scheme 5	Synthesis of Diazahelicene	80

Chapter 4

Scheme 1	Molecular Capsule as a Catalyst	109
Scheme 2	Assemblies of Linear Ligand 4 and Square-Planar Metal Pt ²⁺	112
Scheme 3	Synthesis of Ligand 4	113
Scheme 4	Synthesis of Ligand 8	114
Scheme 5	Synthesis of Ligand 13	120

Appendix I

Scheme 1	Keto-enol equilibrium	132
----------	-----------------------	-----

List of Abbreviations

Ac	acetyl
Bn	benzyl
Bu	<i>n</i> -butyl
CD	circular dichroism
(COCl) ₂	oxalyl chloride
cod	cyclooctadiene
CP MAS	cross polarization magic angle spin
de	diastereomeric excess
DMF	dimethylformamide
DMSO	dimethylsulfoxide
DPD	dipolar dephasing
DPPA	diphenylphosphorylazide
dppp	1,3-bis(diphenylphosphino)propane
ee	enantiomeric excess
en	ethylenediamine
Et	ethyl
Hex	<i>n</i> -hexyl
<i>i</i> -Pr	isopropyl
IR	infrared
Me	methyl
mp	melting point
MS	mass spectrometry

<i>n</i>	refractive index
NBS	N-bromosuccinimide
NMR	nuclear magnetic resonance
ORD	optical rotatory dispersion
Ph	phenyl
PPh ₃	triphenylphosphine
py	pyridine
rt	room temperature
SOCl ₂	thionyl chloride
<i>t</i> -Bu	<i>tert</i> -butyl
TEA	triethylamine
Tf	trifluoromethanesulfonyl
TFA	trifluoroacetic acid
THF	tetrahydrofuran
TIPS	triisopropylsilyl
TMS	trimethylsilyl

Chapter 1 –Concepts and Methods in Supramolecular Chemistry

Recently, the area of supramolecular chemistry has become one of the most actively pursued fields of science.¹ Both the concept and the term were introduced as “chemistry beyond the molecule”,^{1a} which can be understood to mean the chemistry of assemblies of high complexity that result from the spontaneous assembly of two or more building blocks. These sophisticated architectures have potential applications in general areas such as medicine, information and communication technology and chemical reactivity and separation.²

Fabricating large molecular arrays with well-defined architectures is challenging. In this regard, the concept of self-assembly synthesis is appealing.³ The self-assembly approach, based on the spontaneous assembly of smaller subunits to generate higher ordered aggregates, offers an efficient alternative to the classic organic approach, as it requires fewer synthetic steps and hence is not plagued by the lower yields often seen in multistep reactions. The kinetically labile interactions that are used as the supramolecular “glue” allows for self-correcting or self-healing resulting in the most stable defect-free aggregates being formed. The feasibility of this approach hinges on the rational design of simple building blocks that on mixing are capable of selective and spontaneous assembly. Synthon design demands the consideration of two key issues: what functionality will act as effective “glue”, and how will the recognition features be incorporated and placed into the components to facilitate a discriminating self-assembly process? In the literature these two points are frequently referred to as the *molecular recognition elements* and *molecular programming*, respectively. *Molecular programming* is a key theme in this thesis and the

examples discussed in later chapters will highlight the various design principles involved in constructing effective supramolecular building blocks.

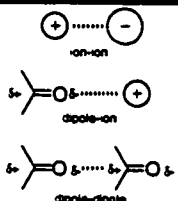
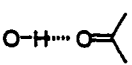
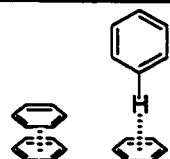
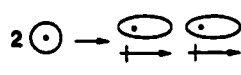
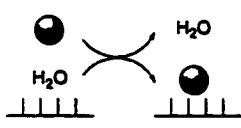

The remainder of this introduction will serve to present the basic principles involved in supramolecular chemistry, from the types of supramolecular “glue” that may be used, through the characterization of the architectures that are formed, to an introduction of the practical applications of supramolecular complexes.

1.1 Supramolecular Glue

The different types of “glue” that are used to hold supramolecular architectures together have been typically defined as “non-covalent” and include: ionic interactions (ion-ion, ion-dipole and dipole-dipole), hydrogen bonds, π - π stacking, dispersion forces, coordination or dative bonds and the hydrophobic effect.⁴ A summary of each type of interaction is given in Table 1.

The term “non-covalent” has brought up many debates about the definition of a chemical bond centred around the legitimacy of making a distinction between a covalent and a non-covalent bond. A covalent bond is strictly defined as one in which a pair of electrons is shared by two nuclei.⁴ With the exception of dispersion forces and the hydrophobic effect, all of the interactions listed in Table 1 also depend on electron-pair sharing to hold the components together. The difference between the interactions listed in Table 1 and typical covalent bonds lies in the extent to which a pair of electrons is shared between two nuclei. Therefore, in order to avoid any ambiguities, all the interactions will be referred to as “intermolecular forces” and not as non-covalent interactions.

Table 1. Examples of Supramolecular Glue

Interaction	Bond Strength ^a (kcal mol ⁻¹)	Description	Example
electrostatics	>45 (ion-ion) 10-40 (ion-dipole) 1-10 (dipole-dipole)	coulombic interactions between opposite charges	 <p>ion-ion dipole-ion dipole-dipole</p>
hydrogen bonds	4-25 (strong) 1-4 (moderate) <1 (weak)	donor-acceptor interactions specifically involving hydrogen as the proton donor and a base as the proton acceptor	 <p>O-H...C=O</p>
π-π interactions	2-5 (face to face) 5-10 (edge to face)	attractive forces between electron rich interior of an aromatic ring with the electron poor exterior of an aromatic ring	
dispersion forces	<2	also called London forces – momentary induced dipole-dipole interactions	 <p>2 \odot → $\oplus \ominus$ $\oplus \ominus$</p>
hydrophobic effects	1-10	the attraction of water molecules for one another resulting in agglomeration of other species	 <p>H₂O H₂O</p>
dative bonds	varied 5-90	coordination of a metal by a ligand donating two or more electrons	 <p>M</p>

^a Association constants are measured in chloroform-*d*.

The methodologies required to construct the building blocks for the creation of supramolecular complexes demand a solid basis in synthetic chemistry. The

supramolecular synthons can incorporate one or more of the interactions listed in Table 1. The combination of two or more, either similar or different, interactions increases selectivity and adaptability of the building blocks and also increases the stability of the complexes resulting from the self-assembly process.

1.2 Characterization of Supramolecular Architectures

Complete characterization of supramolecular aggregates can be a challenge as these structures are generally of greater complexity and lability than molecular species. In particular, the following questions must be addressed:

- 2 What is the final architecture of the aggregate?
- 3 How rapidly is it formed?
- 4 How strong are the interactions holding the complexes together?

1.2.1 Structure Elucidation of Aggregates⁵

With respect to gaining architectural information, X-ray crystallography and NMR spectroscopy are the most diagnostic techniques. An X-ray crystal structure clearly shows atom positioning. However, this analysis is only valid for the crystalline solid-state. Factors such as crystal packing, which are absent in the solution or gas phase, may alter the structure of the complex. In order to investigate and understand the structure in the solution phase a variety of techniques can be employed, most notably NMR spectroscopy.

Simple one-dimensional NMR spectroscopy measures the degree to which the nuclei in question are shielded by their electronic environment in terms of chemical shift.⁶ Movements of these resonance signals can provide evidence of intermolecular interactions, as spectra changes indicate a change in chemical environment. Proton NMR is most widely used not only because of practical reasons such as sensitivity but also because these nuclei are positioned on the periphery of the molecule and therefore are more exposed and better able to sense small changes in the environment. In a typical titration experiment, a NMR spectrum of the host is recorded and then the guest is added in small aliquots. If binding occurs, the guest will alter the electronic environment of the host and hence alter the chemical shifts of host's nuclei.

The development of other techniques, such as Nuclear Overhauser Effect Spectroscopy (NOESY), has made NMR spectroscopy an even more powerful tool for structure elucidation.⁷ NOESY experiments provide significant information about through-space interactions that are in the 4Å range. Cross-correlation peaks indicate that the two protons in question are physically close to one another. In many instances this technique can provide the exact coordination geometry between supramolecular synthons. NMR methods can provide great insight into the mode of binding between building blocks but does not provide direct information about the stoichiometry of the building blocks used to construct the supramolecular complex.

Mass spectrometry (MS) is gaining wide spread acceptance as a method for studying the stoichiometry of both solution and gas-phase supramolecular reactions.⁸ The step-wise approach in the numerous MS techniques commonly involves the transfer of the chemical species to the gas phase, ionization of the molecules and subsequent

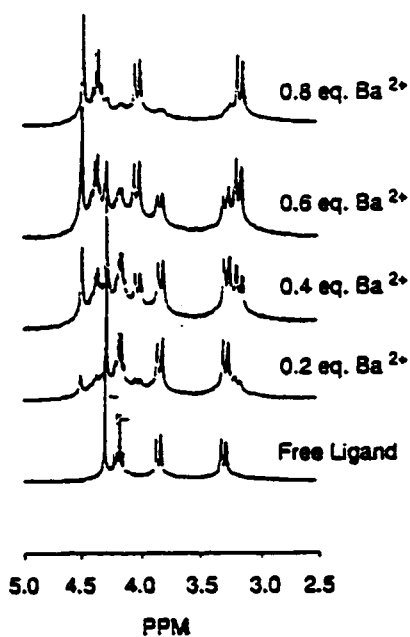
separation of the gaseous ions based on mass-to-charge (m/z) ratios. New developments in MS have focused on “softening” the ionization technique for detection of complexes held together by weaker interactions. Electrospray ionization (ES) has shown to be one of the most promising techniques for the study of supramolecular complexes. However, this method does not always provide an accurate representation of the solution equilibrium, as this technique is dependent on complete desolvation of charged complexes. If the complex is a neutral species in solution, inducing it with a charge can drastically alter the complex’s stability. Likewise, desolvation enhances the importance of electrostatic interactions but decreases the stability of other interactions such as the hydrophobic effect. This can result in detection of non-specific associations, which are associations that are weak or non-detectable in solution but are strengthened in the gas phase, or insufficient detection of interactions which are clearly taking place in the solution state.

Many other techniques can be employed to help elucidate the overall structure such as absorption and emission spectroscopy, computer-aided molecular modeling and chirotopical methods (circular dichroism, for example) but will not be discussed in this chapter. Alone, each of the analytical techniques provides only part of the picture. Together they can provide great insight into the aggregates’ overall structure in solution as well as in the solid-state.

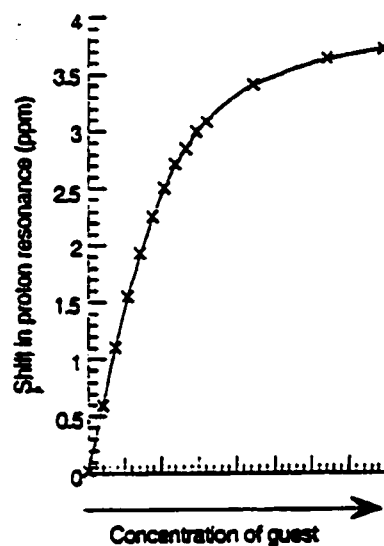
1.2.2 Kinetic Information

The polymolecular structures formed during the self-assembly process are held together “reversibly” by intermolecular forces, which results in a dynamic system between bound and unbound forms of the synthons. These two forms have different

NMR responses that can provide insight into the binding kinetics.⁹ If the binding is *slow* compared to the NMR time scale (slower than 10^{-2} – 10^{-3} s), the NMR resonances for both forms appear as individual signals with the resonance corresponding to free synthon gradually diminishing as complexation increases (Figure 1a). If, however, binding is *fast*, then the NMR resonances for the two forms are observed as an average peak. In the typical titration experiment mentioned previously, the addition of a guest causes the time-averaged peak to shift continuously until the host is saturated with guest. Plotting the change in chemical shift as a function of concentration results in a titration curve (Figure 1b).



(a)

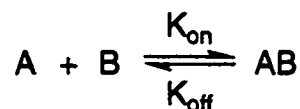


(b)

Figure 1. (a) A series of NMR spectra in which metal binding is *slow*. Therefore resonances for both the ionophore and metal-ligand complex are clearly visible. (b) A titration curve in which the binding of a substrate is *fast*. The addition of the substrate causes the time average peak to shift until the host is saturated with a guest. Reprinted from Oxford Chemistry Primers, Supramolecular Chemistry, 1999,45. Copyright (1999) P. D. Beer, P. A. Gale, D. K. Smith.

1.2.3 Thermodynamic Information

Titration experiments provide insight into not only the kinetics but also the thermodynamics of association and dissociation.⁹ Examination of the simple 1:1 complex formation equilibrium:



gives a binding or association constant of:

$$K_a = \frac{[AB]}{[A][B]}$$

When binding is *slow* one can easily calculate the binding constant K_a by measuring the relative intensities of the individual NMR signals of the bound and unbound forms. The integration of the peaks gives the relative concentrations of all three species, **A**, **B** and **AB**. When the binding is *fast*, the structural features of the titration curve (Figure 1b) such as slope and shape provide the information about the association constant. Iterative fitting procedures by non-linear least squares programs that fit theoretical models of the complexation process to the experimental data are used to determine the association constant.

1.3 Summary and Overview

The exact knowledge of the binding modes of the intermolecular interactions such as strength and directionality, coupled with the ability to properly characterize these interactions have allowed for effective design of fascinating supramolecular architectures

such as helices, macrocycles, racks, ladders, grid and tubes. Even more impressive, is that these architectures can now perform specific applications in areas such as:

- medicine – drug delivery systems,¹⁰ sensors,¹¹ ion channels¹²
- information and communication technology¹³ – erasable memory media
- chemical reactivity and separation – zeolites,¹⁴ new separation media for use in chromatography,¹⁵ catalysts¹⁶

The remaining chapters in this thesis will focus on specific examples to illustrate not only the basic principles behind building block design but also to introduce practical applications of supramolecular complexes. Chapters Two and Three explore the utility of using coordination (dative) bonds and hydrogen bonds, respectively, as the “glue” to construct supramolecular aggregates capable of accomplishing specific tasks. Chapter Four describes the combination of hydrogen bonds and metal coordination to direct the self-assembly process.

1.4 References

1. For an overview of *Supramolecular Chemistry*, see: (a) J. -M. Lehn, *Supramolecular Chemistry: Concepts and Perspectives*, VCH, Weinheim, 1995; (b) F. Vögtle, *Supramolecular Chemistry*, John Wiley and Sons, New York, 1991; (c) P. D. Beer, P. A. Gale, D. K. Smith, *Supramolecular Chemistry*, Oxford University Press Inc., New York, 1999; (d) *Molecular Self-Assembly – Organic versus Inorganic Approaches*, Ed. M. Fujita, Springer-Verlag Berlin Heidelberg, New York, 2000.

2. For a comprehensive survey of supramolecular technology, see: *Comprehensive Supramolecular Chemistry*, Vol. 10, Ed. J. L. Atwood, J. E. D. Davies, D. D. MacNicol; F. Vögtle, Elsevier, Oxford, 1996.
3. J. -M. Lehn, *Angew. Chem. Int. Ed. Engl.* **1990**, *29*, 1304.
4. J. March, *Advanced Organic Chemistry*, John Wiley and Sons, New York, 1992.
5. For a comprehensive overview on supramolecular methodology, see: H. -J. Schneider, A. Yatsimirsky, *Principles and Methods in Supramolecular Chemistry*, John Wiley and Sons, New York, 2000 and references cited therein.
6. G. A. Jeffrey, *An Introduction to Hydrogen Bonding*, Oxford University Press Inc., New York, 1997.
7. H. Mo, T. C. Pochapsky, *Prog. Nucl. Magn. Reson. Spectrosc.* **1997**, *30*, 1.
8. (a) K. Wang, G. W. Gokel, *Pure Appl. Chem.* **1996**, *68*, 1267; (b) R. D. Smith, J. E. Bruce, L. Wu, Q. P. Lei, *Chem. Soc. Rev.* **1997**, *26*, 191; (c) M. Przybylski, M. O. Glocker, *Angew. Chem. Int. Ed. Engl.* **1996**, *35*, 807.
9. K. A. Connors, *Binding Constants, The Measurement of Molecular Complex Stability*, John Wiley and Sons, New York, 1987.
10. J. M. Rivera, T. Martin, J. Rebek, *Science* **1998**, *279*, 1021.
11. (a) A. P. DeSilva, *Chem. Rev.* **1997**, *97*, 1515; (b) P. D. Beers, *Acc. Chem. Res.* **1998**, *31*, 71.
12. (a) J. D. Lamb, J. J. Christensen, S. R. Izatt, K. Bedke, M. S. Astin, R. M. Izatt, *J. Am. Chem. Soc.* **1980**, *102*, 3399; (b) H. C. Visser, D. N. Reinhoudt, F. de Jong, *Chem. Soc. Rev.* **1994**, *75*; (c) F. M. Menger, D. S. Davis, R. A. Persichetti, J. J. Lee, *J. Am. Chem. Soc.* **1993**, *115*, 2451.

13. (a) D. Philp, J. F. Stoddart, *Angew. Chem. Int. Ed. Engl.* **1996**, *35*, 1155; (b) Y. -Z. Hu, D. V. Luyen, O. Schwarz, S. Bossman, H. Dürr, V. Huch, M. Veith, *J. Am. Chem. Soc.* **1998**, *120*, 5822.
14. (a) G. R. Desiraju, *Angew. Chem. Int. Ed. Engl.* **1995**, *34*, 2311; (b) A. Müller, H. Reuter, S. Dillinger, *Angew. Chem. Int. Ed. Engl.* **1995**, *34*, 2328.
15. (a) W. H. Pirkle, T. C. Pochapsky, *Chem. Rev.* **1989**, *89*, 347; (b) T. Webb, C. S. Wilcox, *Chem. Soc. Rev.* **1993**, 383.
16. (a) L. E. Orgel, *Acc. Chem. Res.* **1995**, *28*, 109; (b) M. M. Conn, E. A. Wintner, J. Rebek, *J. Am. Chem. Soc.* **1994**, *116*, 8823; (c) L. G. Mackay, R. S. Wylie, J. K. M. Sanders, *J. Am. Chem. Soc.* **1994**, *116*, 3141.

Chapter 2 – Dative Bonding, Photochromes and Erasable Memory Media

Advances in computer technology and the demand for small, quick, large capacity data storage systems has fostered an explosion of research in the area of nanosize molecular devices capable of controlling and storing information.¹ Recent proposals of these new organic devices have them behaving as "on-off" switches (1 and 0 in binary systems).^{1,2} This requires the presence of two different forms of a chemical species, having different detectable properties, such as absorption spectra, that can be reversibly interconverted by means of an external stimulus. These devices can operate at the molecular level, but they can also be built into supramolecular architectures, which should yield functional assemblies displaying novel physical properties.^{1b}

In order for these devices to function at the supramolecular level a number of factors must be considered including: (1) the supramolecular glue that will be chosen to act as constructive recognition elements and direct the self assembly synthesis, (2) the molecular scaffold that is to be used as the switching device and (3) the incorporation of the molecular recognition elements into the resulting complex such that they will not only promote but also enhance the function of the molecular device.

This chapter will explore the utility of incorporating dative bonds into molecular devices for applications in non-destructive erasable memory media. The strength and directionality of dative bonds are first discussed and then the utility of this "glue" is highlighted in the examples illustrated in this chapter.

2.1 Molecular Recognition and the Dative Bond

2.1.1 Properties of Dative Bonds

The use of transition metal ions to direct molecular assemblies has three major advantages.³ First, metal-ligand dative bonds have varying degrees of binding energies. Therefore the kinetic stability of the complex can be weak or strong depending on the choice of the metal. In general the metal-ligand bond strength *decreases* with increasing atomic number for main group elements but *increases* within a transition metal triad.^{4a} Second, transition metals most often have coordination spheres with well-defined geometric environments. This gives metal ions the ability to control the precise geometry of ligands during the self-assembly process.^{4b,c} Examples of metal ions which possess different geometries are given in Figure 1a.

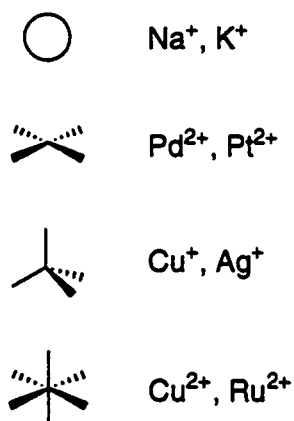


Figure 1a

Third, the number and relative placement of available coordination sites on the metal ion can be easily altered by placement of non-labile ligands (protecting groups), which can give rise to drastically different assemblies using a single metal ion (Figure 1b).

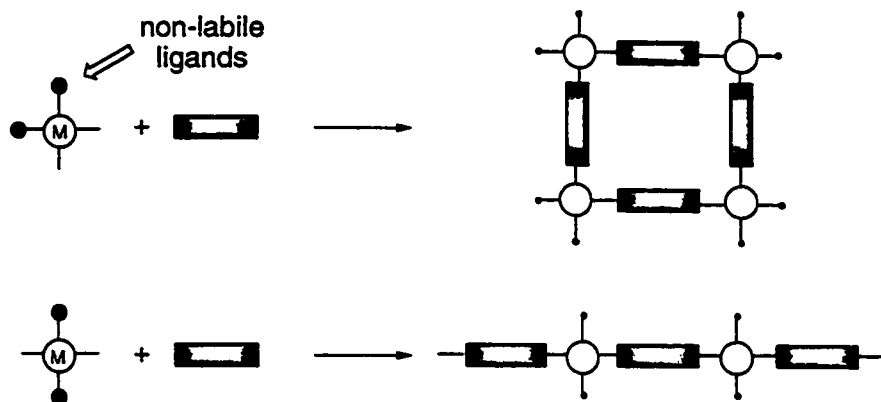


Figure 1b. Schematic presentation of planar ligands with two linking sites and their coordination assemblies with a protected square planar metal

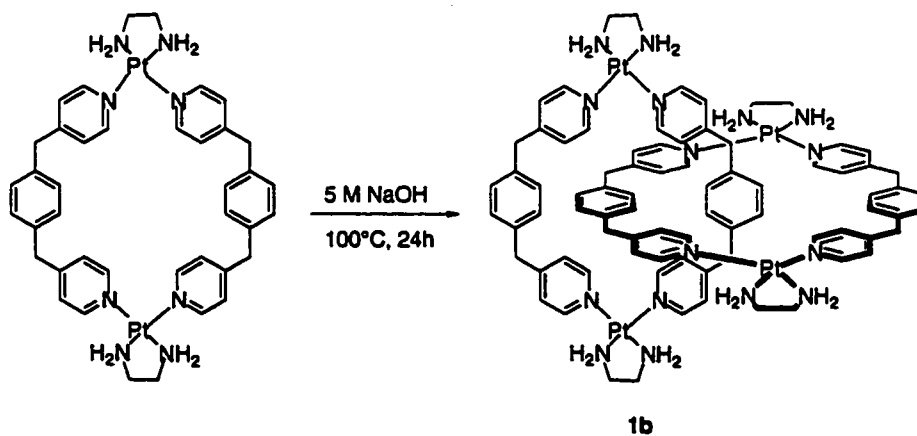
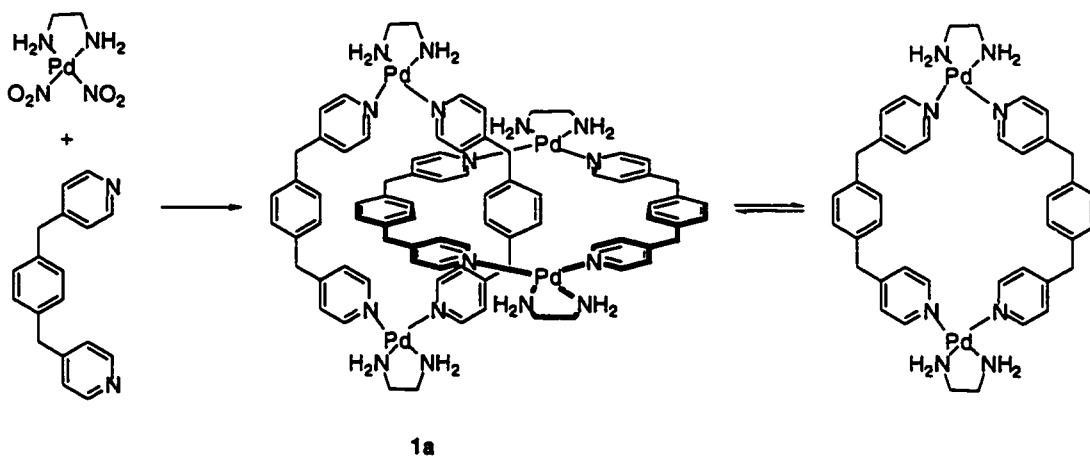
2.1.2 Selected Examples of Metal-Directed Assemblies

Self-assembly synthesis has been applied to the area of coordination chemistry to produce a variety of elegant structures including catenates,⁵ helicates,⁶ squares,⁷ racks,⁸ and ladders.⁹ In most instances, supramolecular complexes are formed with transition metal-pyridyl σ -bonds. An impressive feature of some metal-directed assemblies is the construction of chiral superstructures from achiral synthons. A few of these structures are shown in Scheme 1.

Chiral catenate **1a** consist of two interlocked macrocycles which are stabilized by π - π stacking (Scheme 1).¹⁰ The nitrogen-palladium bonds are labile and so an equilibrium exists between the macrocycle and the catenate. At low concentrations the macrocycle predominates while at higher concentrations the catenate prevails. The *topological* bond which holds the two macrocycles together can form in two stereochemically different ways creating topological chiral isomers.^{10c} Interestingly, in the analogous system containing Pt(II), where the dative bonds are not as labile, **1b** exists

exclusively as the macrocycle. Only under extreme conditions of high temperatures and polar solvents do the Pt-N bonds become labile enough to break and form the catenate.

Scheme 1



2.2 Molecular Recognition and Dithienylethenes

2.2.1 Choice of Photochrome

The viability of any compound in erasable memory devices hinges on the basic requirement of the reversible transformation of a chemical species between two states that display different physical properties. The two different chemical forms can be the result of a number of different responses such as isomerization, electron transfer or complexation ability, to name a few. The interconversion between these two forms can be achieved through light, heat, pressure, magnetic or pH changes.¹¹ Molecules that undergo reversible changes upon photoisomerization, such as *cis-trans* isomerizations or pericyclic reactions, are particularly promising as light has maximal velocity and can be easily controlled using fibreoptics.¹²

There are many well studied examples of molecules that undergo reversible colour changes upon photoisomerization (photochromes) including strained olefins, thioindigos, azabenzenes, spirobenzopyrans, fulgides and diarylethenes (Table 1). These photo-induced reactions can be grouped into two general processes: *cis-trans* isomerization and photocyclization (*ring opening/ring closing*). However, despite meeting the basic requirement of the reversible presence of two different chemical forms of a molecule there are a number of other requirements that are fundamental for practicable applications of any compound in erasable memory devices.¹³ The most relevant are:

- fatigue resistance – numerous on/off cycles without significant degradation
- thermal stability – no thermal interconversion between the two states

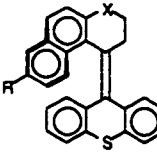
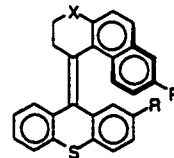
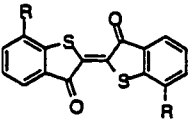
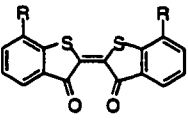
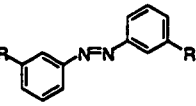
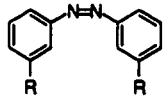
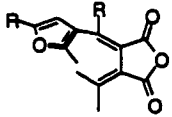
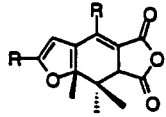
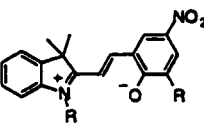
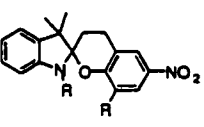
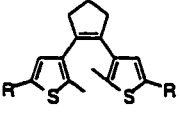
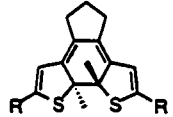
- detectability – ease of identifying both photochromic states
- nondestructive readout – the ability to read the stored information without erasing it

With respect to these critical properties, Table 1 briefly highlights some of the drawbacks for each of the photochromic molecules mentioned above. For instance, the *cis* form of azabenzenes are very susceptible to thermal racemization ($t_{1/2}$ = 4 days at 20°C) and therefore, because of significant and rapid degradation of this conformation, limits their use as data storage devices.¹⁴ Even under ideal conditions, modified azabenzenes exhibit thermal decay after just a few weeks. On the other hand, appropriately chosen dithienylethenes show no thermal interconversion within a very large temperature range ($t_{1/2}$ = greater than 3 months at 80°C).^{13a}

Spiropyrans not only show thermal reversion ($t_{1/2}$ = 10 min at 80°C) but also exhibited limited multi-cycle durability.¹⁵ Photochromic performance of these molecules is lost after 100 colouration/decolouration cycles. This is very poor as compared to dithienylethenes where the *ring-closing/ring-opening* reaction cycle can be repeated more than 10⁴ times without the loss of photochromic performance.

The appeal of photochromic 1,2-dithienylethene derivatives in optical device applications such as information processing and optical switching stems from their striking display of advantageous photochromic properties including thermal irreversibility and fatigue resistance. However, practical applications of dithienylethenes in erasable memory devices also requires that both photochromic states can be detected in the readout event in a facile, economical and non-invasive manner.

Table 1. Photochromic Molecules and Some of Their Properties.

Reaction Type	Example	Form A	Form B	Properties
<i>cis-trans isomerization</i>	strained olefin			<ul style="list-style-type: none"> • must have optically pure starting material • slow response time
	thioindigos			<ul style="list-style-type: none"> • difficult to synthesize
	azabenzenes			<ul style="list-style-type: none"> • not thermally stable
<i>ring opening-ring closing</i>	fulgides			<ul style="list-style-type: none"> • form A isomerizes to non-productive <i>E</i> isomer
	spiropyrans			<ul style="list-style-type: none"> • not thermally stable • epimerization at spiro carbon center
	dithienylethenes			<ul style="list-style-type: none"> • thermally stable, no isomerization, easy to derivatize

2.2.2 Detection of Dithienylethene Photochromes

Typically, the readout event involves the use of UV-Vis spectroscopy to record the spectra changes near the absorption bands corresponding to the two photochromic states. These absorptions, however, are the same ones that induce the *ring-opening* and

ring-closing reactions. A detection method that relies on sampling near these photoactive absorption bands inevitably causes partial switching of the photochrome and erases the stored information. Efforts to circumvent this problem have focused on the development of photochromic systems that, upon photoisomerization, display variations in other optical properties such as refractive index,¹⁶ luminescence¹⁷ or optical rotation.¹⁸ It is the detection of these accompanying changes that will ultimately lead to effective non-destructive information processing systems.

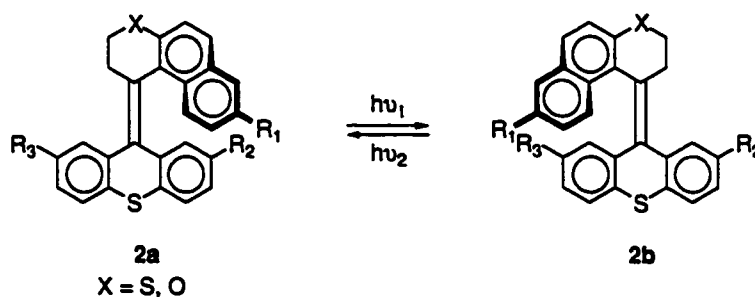
Recording changes in optical rotation is a particularly promising alternative for non-destructive readout because the detection event can often be performed outside the photoactive spectral regions. The utility of this technique is dependent upon the design of photochromes that exhibit significantly contrasting optical rotating strengths between two states of the molecule. The photo-induced photochromic reaction should, therefore maximize the formation of one stereoisomer in order to enhance the readout signal or when plagued with small enantiomeric (ee) or diastereomeric excesses (de), use molecules that produce very large optical rotations. Ideally, one should incorporate both techniques to obtain maximum signal while using minimum amounts of material.

2.2.3 Use of Optical Rotation for Non-Destructive Detection

The strong rotatory power of helical molecules makes them ideally suited for data processing systems that use light outside the absorption bands for non-destructive readout methods because the enhanced read-out signals provided by helical chirality allows for easy detection even at low concentrations.¹⁹

For example, Feringa and co-workers have developed a series of chiroptical molecular switches based on sterically-overcrowded alkenes **2a** and **2b** (Equation 1). Unfavorable steric interactions around the central olefinic bond force the molecule into a helical topology.²⁰ Irradiation of enantiomerically pure **2a** results in the reversal of helicity (*M* to *P* or *P* to *M*).²¹ The two helical forms display distinct chiroptical properties such as opposing ORD and CD signals that can be used for non-destructive detection purposes as applied to *write-read-erase* memory devices. Although further improvements are required with respect to slow response times and low ee, the ease and success of using changes in optical rotation as a nondestructive detection method is an attractive feature of this photochromic system.

Equation 1.

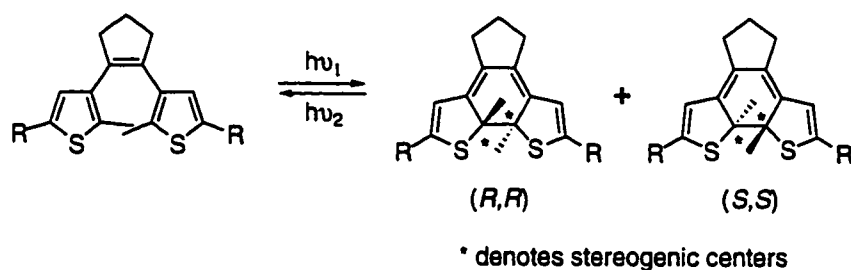


2.2.4 Chirality of Dithienylethene Photochromes

As mentioned above, dithienylethenes are among the most promising photoswitches known today because of their excellent display of advantageous photochromic properties. The photogenerated *ring-closed* isomers of dithienylethene derivatives are necessarily chiral (Equation 2) making them excellent candidates for incorporation into chiroptical devices.^{13, 20} However, the photo-induced *ring-closing*

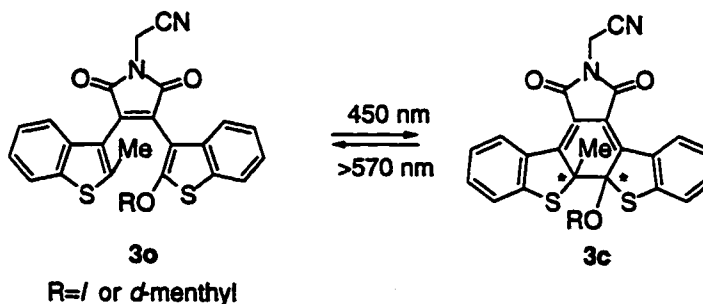
reaction produces both *R,R* and *S,S* stereoisomers of equal amounts, rendering the desirable chiroptic readout method ineffective for the *ring-closed* form.

Equation 2



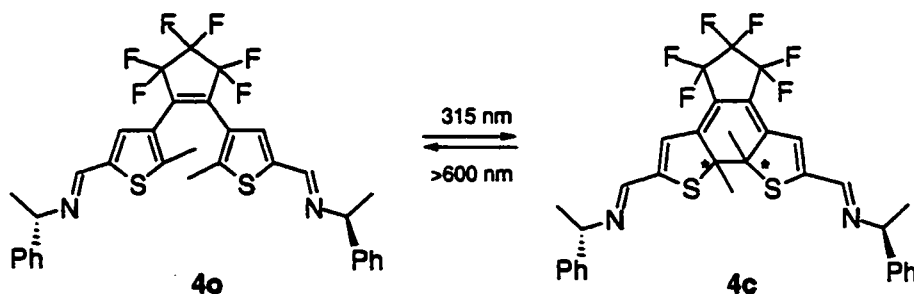
The presence of an optically active chiral auxilliary such as a *l*- or *d*-menthyl group at the 2-position of the benzo[*b*]thiophene ring in diarylmaleimide photochrome **3o** (“o” represents the *open* form) has been shown to induce stereodifferentiation with values of de (diastereomeric excess) up to 86% in the photocyclization reaction to **3c** (Equation 3).^{18c} Restrictive environmental conditions such as nonpolar solvents (toluene) and higher temperatures (40°C) needed to ensure high stereoselectivity coupled with long irradiation times limits the use of the existing system in optoelectronic devices such as optical memory.

Equation 3



Moving the chiral auxillary to the periphery of the photochromes' backbone, **4o** for example, also promotes stereodifferentiation with de up to 36% during the photochromic ring closing reaction to **4c** (Equation 4).²² Interestingly, it was found that even with low diastereoselectivity the ring *open* and *closed* forms show distinctly different CD spectra. To date, though, these changes have not been capitalized on for nondestructive write-read-erase systems. In addition, derivatives of **4o** have been introduced as dopants in an effort to modulate liquid-crystalline phases for display technology, but problems with low stereoselectivity during the *ring-closing* reaction hinders their use in these devices. Improvements with respect to the high molar concentration required to produce the small signal readouts are required for practical applications of these systems, especially in light of the low concentrations of the photochromic materials required in “real” solid-state devices.

Equation 4

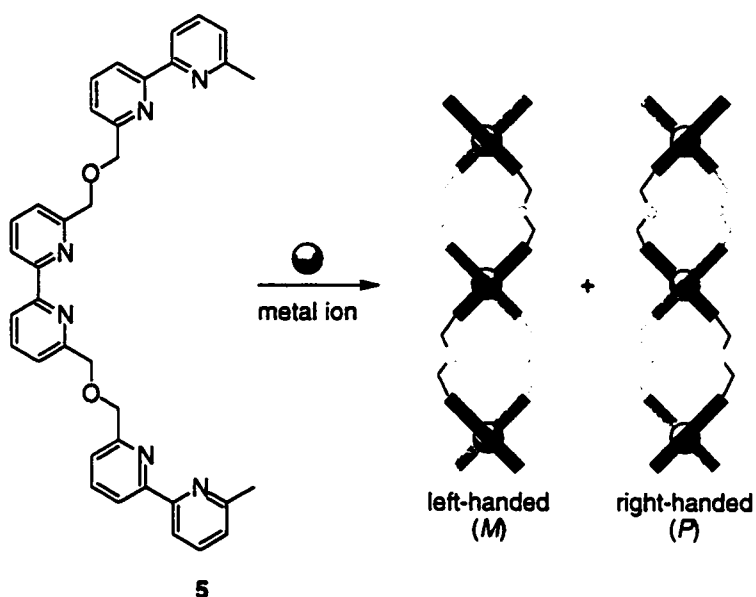


2.2.5 Dative Bonds and Optically Pure Helicates

As discussed in section 2.2.3, the appeal of helical compounds for applications in nondestructive read-out methods stems from their strong optical rotating abilities even at low concentrations. Helicity can be generated by a variety of methods. One of the most

appealing methods is the spontaneous self-assembly of helicates from flexible polyvalent ligands.²³ The formation of helical morphology results when two ligand, such as **5**, twist around a metal-metal axis. This method, however, results in racemic mixtures as the winding process occurs in either direction to generate both left and right handed helicates (Equation 5).

Equation 5

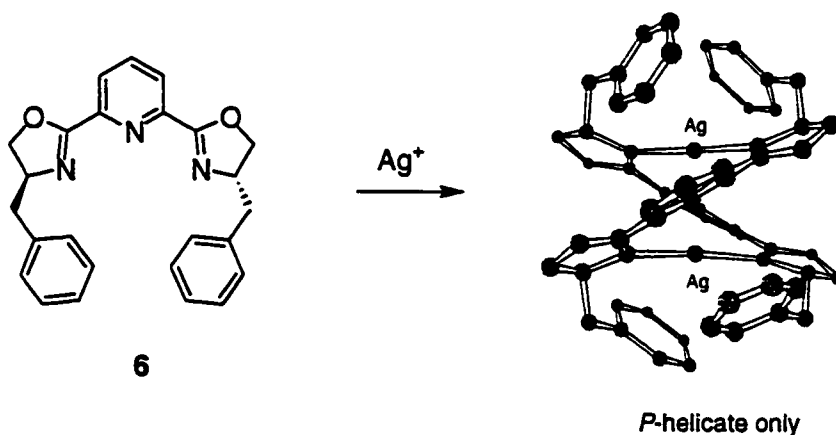


Stereoselective assembly of helicates has been achieved by introducing chiral auxiliaries onto the backbone of a flexible polyvalent ligand, such as the placement of the benzyl groups on the bis(oxazoline) backbone of ligand **6** (Equation 6).²⁴ Initial complexation of two chiral ligands to a single silver ion sets the stage for the direction of winding to coordinate to the second silver ion. Twisting in one direction will result in strong steric interactions between the two benzyl groups, while winding in the other

direction will not. It is this communication between the chiral auxiliaries that initiates and amplifies the handedness of the resulting helicate.

Inspired by this and other similar examples,^{24b-d} in which remote stereogenic centers guide the creation of stereochemically pure metallohelicates, we began to explore the unique properties of self-assembled helicates in stereoselective photochromic transformations. The goal of this project is the achievement of a non-destructive *write-read-erase* system based on chiral photochromic dithienylethene derivatives.

Equation 6



2.2.6 Dative Bonds and Dithienylethenes

Chiral bis(oxazoline) compounds **7o** and **8o** were prepared (Scheme 2) as the polyvalent ligands for this study. It was expected that the transformation of **7o** or **8o** and copper(I) into double-stranded helicates $\text{Cu}_2(\mathbf{7o})_2$ and $\text{Cu}_2(\mathbf{8o})_2$ (Scheme 3) would show stereoselectivity due to a discrimination process that occurs when the chiral oxazoline moieties on the periphery of the individual strands are brought into close proximity. Unfavorable steric interactions between the two chiral auxiliaries within the helix should result in helicates of a single handedness. Formation of optically pure helicates $\text{Cu}_2(\mathbf{7o})_2$

and $\text{Cu}_2(\mathbf{8o})_2$ is expected to pre-orient the pro-stereogenic centers such that on photocyclization of these helicates only one major diastereomer will form. The dramatic changes in optical rotation that are expected to accompany the stereoselective *ring-closing* process can be recorded as the read-out signal in a non-destructive manner.

2.3 Dithienylethenes – Results and Discussion

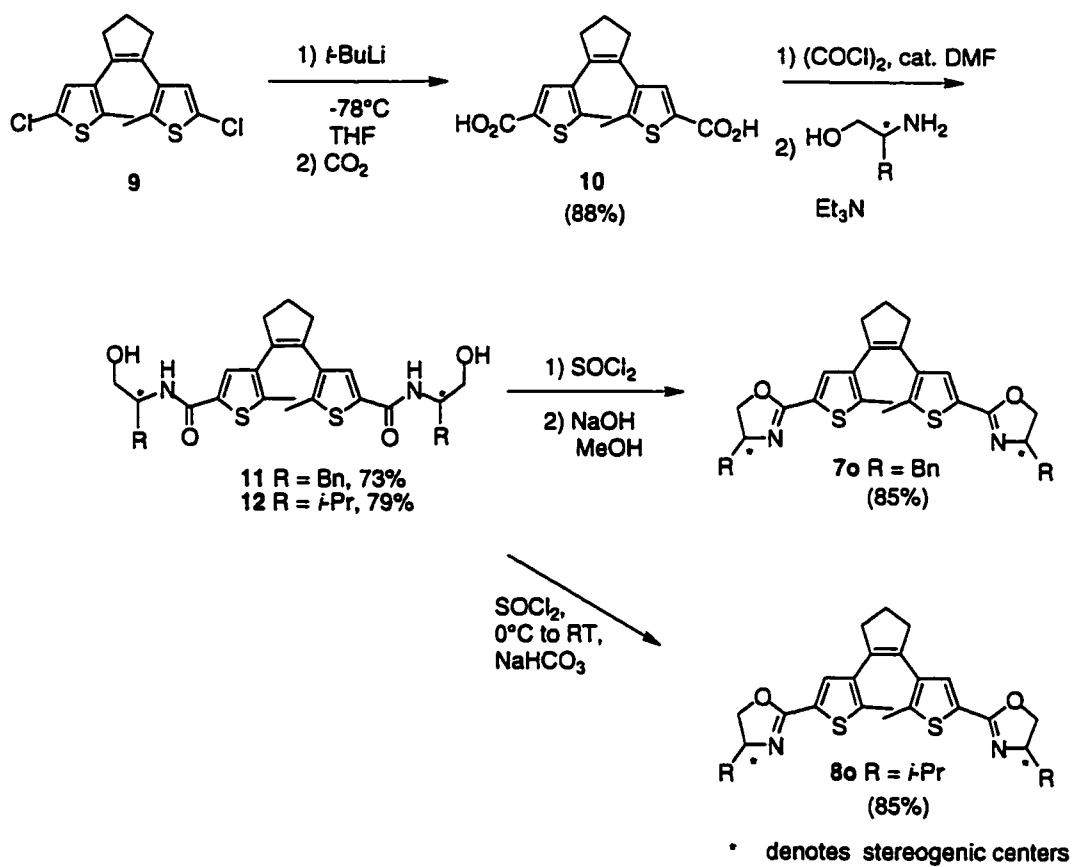
2.3.1 Synthesis

Both (*R,R*) and (*S,S*) enantiomers of photochromic bis(oxazolines) **7o** and **8o** were prepared in four steps from 1,2-bis-(5-chloro-2-methyl-3-thienyl)cyclopentene **9**²⁵ as outlined in Scheme 2. Lithiating **9** with excess *tert*-butyllithium followed by quenching with carbon dioxide afforded diacid **10**. Treatment of **10** with oxalyl chloride and catalytic DMF resulted in the corresponding diacid chloride, which was carried on without purification. Amide alcohols **11** and **12** were prepared by acylating optically pure phenylalanine or isoleucinol with the photochromic diacid chloride. Subsequent dehydrative ring closure yielded optically pure bisoxazolines **7o** and **8o**. All new compounds were characterized by UV-Vis spectroscopy, FT-IR spectroscopy, multinuclear NMR spectroscopy and high-resolution mass spectrometry.

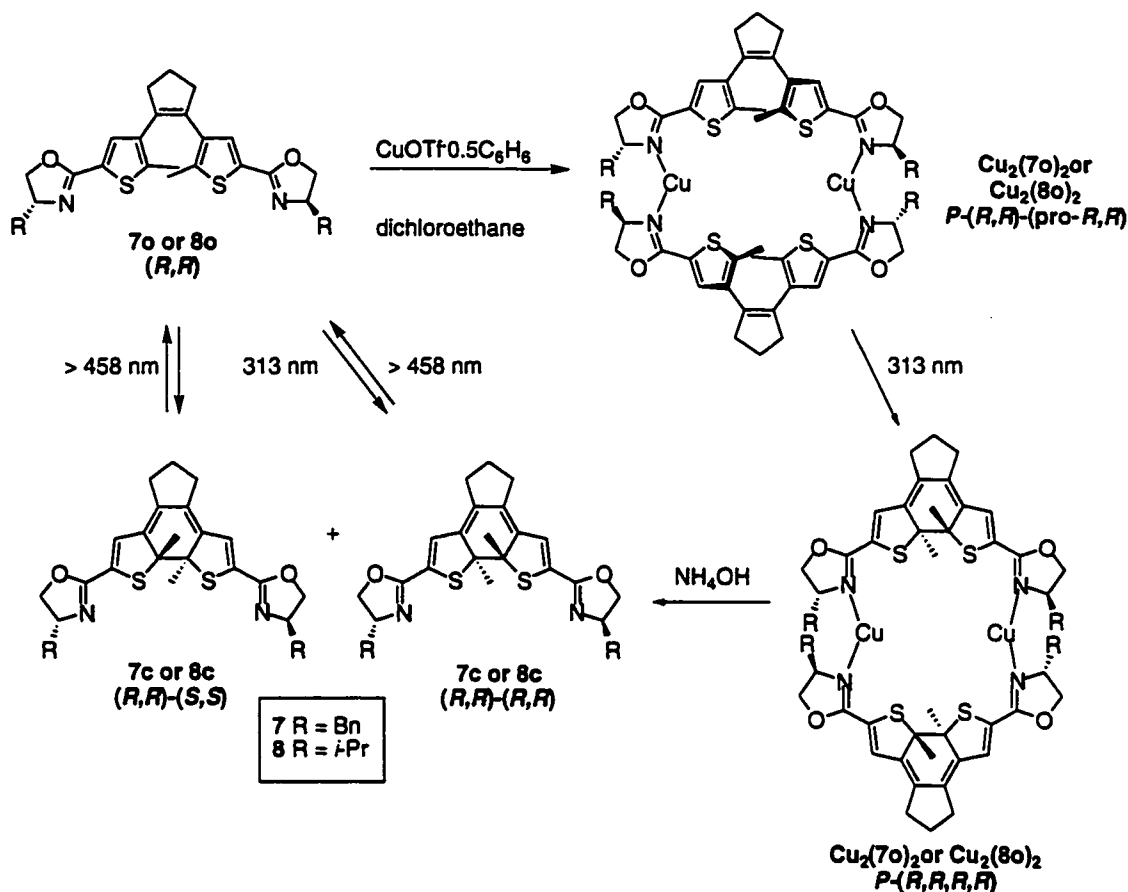
Copper(I) complexes $\text{Cu}_2(\mathbf{7o})_2$ and $\text{Cu}_2(\mathbf{8o})_2$ were prepared by adding, through a canula, an equimolar amount of ligand **7o** or **8o** in degassed dichloroethane to copper(I) trifluoromethanesulfonate ($\text{CuOTf} \cdot 0.5\text{C}_6\text{H}_6$) under argon (Scheme 3). Care was taken when handling the copper(I) reagent to ensure a moisture and oxygen free atmosphere in order to minimize the oxidation of the metal to copper(II). With the exception of single

crystals grown for X-ray analysis, no attempts were made to isolate the copper(I) complexes.

Scheme 2



Scheme 3



2.3.2 Electrospray Mass Spectroscopic Analysis

Electrospray mass spectrometry of dichloromethane solutions of a freshly prepared mixture of ligand **7o** and CuOTf shows peaks at m/z 579.1 and 641.1 corresponding to the free ligand **7o** and a mixture of the coordination compounds $\text{Cu}_2(\text{7o})_2$ and Cu(**7o**), respectively. The isotopic abundance of the peak at m/z 641.1 shows the typical (0.5) peak separation of a doubly charged species confirming the presence of the binuclear complex $\text{Cu}_2(\text{7o})_2$. The isotopic distribution pattern verifies the presence of $\text{Cu}_2(\text{7o})_2$ along with mononuclear Cu(**7o**). The ratio of $\text{Cu}_2(\text{7o})_2$ to Cu(**7o**) increased when the solutions were concentrated. This observation clearly emphasizes the

need to control the concentration of the coordination compound, a condition that will be illustrated in later studies.

2.3.3 X-ray Crystallographic Analysis

Single crystals of both (*R,R*) and (*S,S*) enantiomers of $\text{Cu}_2(\mathbf{70})_2\cdot\text{OTf}_2$ suitable for X-ray crystallographic analysis were obtained by layering hexane upon freshly prepared dichloromethane solutions of the copper(I) complexes. The crystal structure of the (*S,S*) enantiomer (Figure 2) highlights the metals' role in the self-assembly process. The resulting solid-state architecture is the anticipated binuclear double helix. Bis(oxazoline) ligand **70** acts as a bis(monodentate) ligand coordinating two copper (I) metal ions with Cu-N bond lengths of 1.871(8) Å and 1.882(7) Å and N-Cu-N angles of 178.2(5)° and 177.5(5)°.

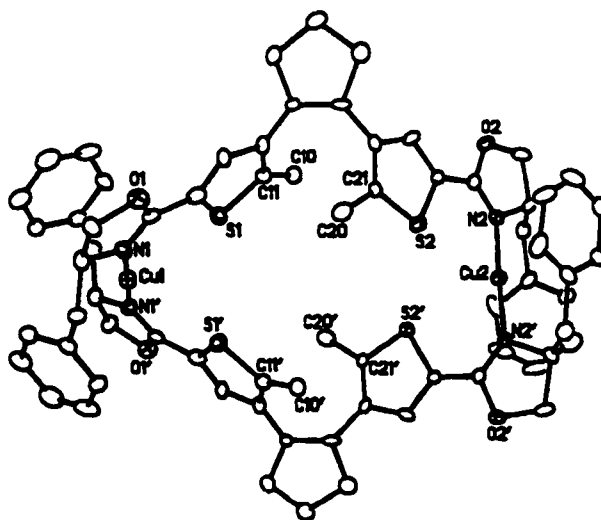


Figure 2. The structure of the copper(I) complex (*S,S*)- $\text{Cu}_2(\mathbf{70})_2$ in the crystal. All non-heteroatomic hydrogens have been removed for clarity. The thermal ellipsoids are drawn at the 20% probability level. The structure of the (*R,R*)-enantiomer is a perfect mirror image.

The angle of rotation of the binuclear double helix is $83.4(5)^\circ$, as measured by the rotation between the vectors defined by the bonds N1-Cu1 and Cu2-N2. The Cu-Cu distance is $10.687(2)$ Å. In addition to the D_2 symmetry of the double helix, there exist pseudotwofold axes passing through the copper ions and through the cyclopentane rings.

On first impression, the metal centers appear to reside in a linear geometry with the nitrogen acting as the sole Lewis base. Closer inspection reveals that the metal is actually in the expected tetrahedral environment (Figure 3) comprised of two Cu-N bonds and two long Cu-S bonds (average bonds lengths of 3.18 Å). In addition two weak cation- π interactions (the average ring-to-metal distance is 3.46 Å) exist creating a psuedo-octahedral environment around the copper metal. While both of these sets of bonds appear long, they are comparable to those found in similar copper induced octahedral environments.²⁶ The presence of these weak interactions in $\text{Cu}_2(70)_2$ may be one of the major factors leading to the stability of this coordination compound.

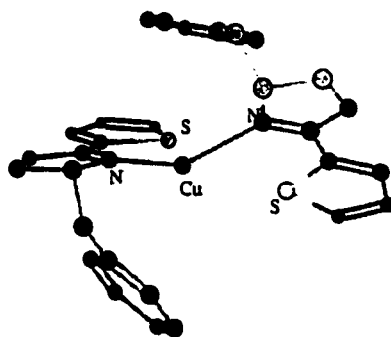
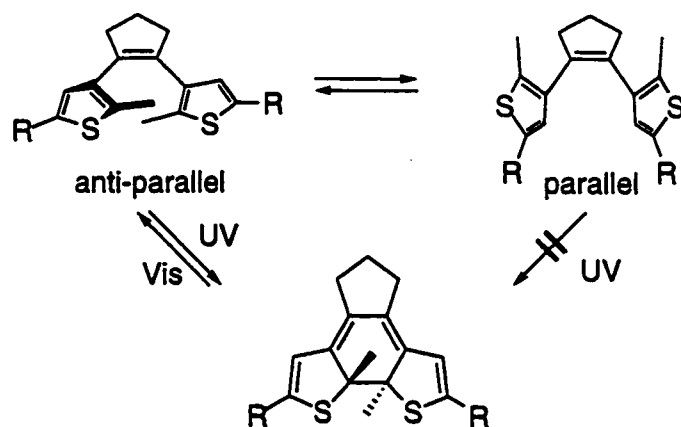


Figure 3. The crystal structure shows the copper ion bound strongly by four ligands and weakly by two π -cation interactions, creating a pseudooctahedral environment around the metal.

The impact of the helical architecture is felt on many levels. It locks the photochrome into its productive antiparallel conformation, as shown in Scheme 4, a

factor that is advantageous because it minimizes the amount of structural reorganization that must take place in order to facilitate the photocyclization process. More importantly, the coordination of the oxazoline ligands to the metal ion brings together the two chiral auxiliaries so that they can influence the helicate's stereochemistry. In all cases, (*S,S*)-**7o** generates solely the *M* helix and (*R,R*)-**7o** generates solely the *P* helix. The helical handedness, in turn, biases the relative orientation of the methyl groups on the thiophene heterocycles (C10, C10', C20 and C20') and sets the carbons involved in forming the new single bond in the photo-induced ring closure (C11, C11', C21 and C21') as pro-(*S,S*) for the *M* helix and pro-(*R,R*) for the *P* helix. To date, crystals of the corresponding complex prepared from the isopropyl analogue **8o** have not been grown.



Scheme 4. The open form of diarylethenes can exist in two conformations: parallel and antiparallel. The conrotatory photocyclization reaction can only proceed from the antiparallel conformation.

2.3.4 UV-Vis Spectroscopic Analysis

The UV-Vis spectra of the *open* (**7o**) and *closed* (**7c**) isomers of the benzyl-substituted photochrome and the corresponding *in situ* generated copper(I) complexes are

shown in Figures 4a and 4b with wavelengths of maximum absorption (λ_{max}) labeled for comparison. The copper containing *ring-closed* isomer $\text{Cu}_2(7\text{c})_2$ was cleanly produced as the sole product, shown by the presence of the isobestic point at 337 nm (Figure 4a), by irradiating dichloroethane solutions of $\text{Cu}_2(7\text{o})_2$ (obtained by mixing an equimolar mixture of **7o** and $\text{CuOTf}\cdot 0.5\text{C}_6\text{H}_6$) with a hand-held 313 nm lamp.²⁷ After 2 minutes of irradiation, the photostationary states (pss) were formed which showed 90% conversion to the *closed* isomers as measured by ^1H NMR. Subsequent irradiation of the *closed* isomer $\text{Cu}_2(7\text{c})_2$ at wavelengths greater than 458 nm restored the spectrum to its original trace by regenerating the *open* isomer $\text{Cu}_2(7\text{o})_2$ quantitatively. As expected, the spectral characteristics of both (*R,R*) and (*S,S*) enantiomers were identical.

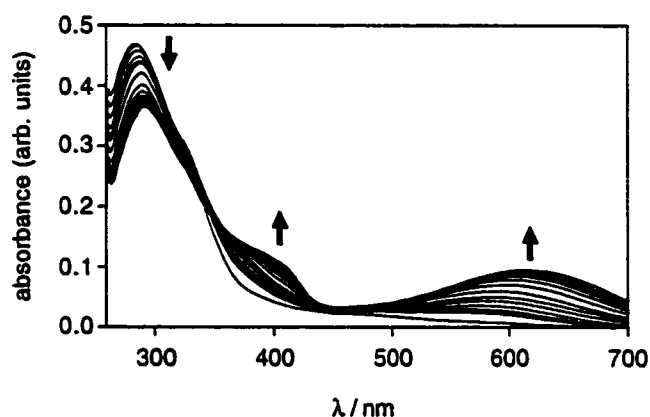


Figure 4a. Change in UV-VIS absorption spectra of $\text{Cu}_2(7)_2$ in dichloroethane by 313 nm light irradiation, starting from $\text{Cu}_2(7\text{o})_2$.

As seen in Figure 4b, coordination to copper(I) has two significant effects on the UV-Vis spectrum: 1) it induces the appearance of an additional absorption peak in the far UV region and 2) it separates the absorption peaks of the *open* and *closed* isomers

(compare $\Delta\lambda = 315$ nm for the coordination compounds and $\Delta\lambda = 270$ nm for the free ligands). This shift, which is in accordance with other metal-ligand complexations reactions,^{23b} increases the non-absorbing region between the two photoactive peaks of the switch.

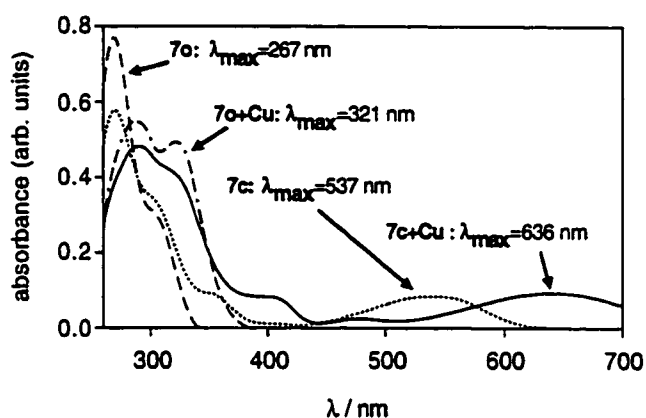


Figure 4b. UV-VIS absorption spectra of (a) $\text{Cu}_2(7\text{o})_2$, (b) $\text{Cu}_2(7\text{c})_2$, (c) 7o and (d) 7c . All spectra were run in dry degassed dichloroethane at 3.5×10^{-5} M.

2.3.5 Solution-State Studies Using ^1H NMR Analysis

Irradiation of the *open* isomer (*S,S*)- 7o at 313 nm also produces characteristic shifts of the signals in the ^1H NMR spectrum. Of particular importance is the resonance assigned to the protons on the thiophene rings which appears as a singlet at 7.23 ppm in 7o and as two singlets of nearly equal intensity at 6.47 and 6.48 ppm for the corresponding ring-closed product 7c . These two singlets (Figure 5, top trace) are clearly a result of the production of two diastereomers in the conrotatory ring closing reaction of the 1,2-diarylethene photochrome (as seen in Equation 2). The relative integrations of the two singlets indicate that both diastereomeric products are being formed to nearly the same extent in the photocyclization reaction.

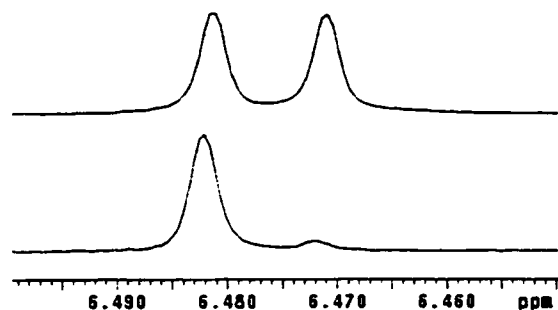


Figure 5. ^1H NMR (500 MHz, CD_2Cl_2) spectra of the thiophene protons in (top) **7c** generated from **7o** without $\text{CuOTf}\cdot 0.5\text{C}_6\text{H}_6$ and (bottom) **7c** generated from **7o** with $\text{CuOTf}\cdot 0.5\text{C}_6\text{H}_6$ after washing with NH_4OH to remove the metal.

Upon metal complexation the number of signals in the ^1H NMR spectrum of **7o** and $\text{CuOTf}\cdot 0.5\text{C}_6\text{H}_6$ in CD_2Cl_2 remain constant but their positions shift significantly, indicating the formation of a symmetrical metal-ligand complex. The singlet, corresponding to the protons on the thiophene ring, found at 7.23 ppm shifts downfield ($\Delta\delta = 0.42$) to 7.65 ppm upon metal complexation. The proximity of the thiophene ring to the deshielding metal center is the likely cause of the downfield shift. More importantly, when the photocyclization reaction of **7o** is repeated in the presence of copper(I) there is preferential formation of one stereoisomeric product with a diastereoselectivity of 86% as shown by the non-equivalency of the signals in the ^1H NMR spectrum (Figure 5, bottom trace). This stereoselection can best be justified by invoking the existence of the helical binuclear complex $\text{Cu}_2(\text{7o})_2$ in solution.

The results of the stereoselective ring-closing reaction are shown in Table 2. The increase in diastereoselectivity as the concentration was increased (entries 1-3) can be attributed to the predominance of the binuclear complex $\text{Cu}_2(\text{7o})_2$ at higher concentrations (see mass spectrometry discussion). The high degree of diastereoselectivity at 10^{-3} M is accompanied, however, by a coinciding increase in the

amount of photochemical degradation (undesired side product formed was measured to be 17%). Reducing the amount of $\text{CuOTf} \cdot 0.5\text{C}_6\text{H}_6$ to less than one molar equivalent decreased the diastereoselectivity, as did decreasing the reaction time (entries 5 and 6). The diastereoselectivity was also lower (51%) when the photocyclization reactions were repeated with the isopropyl ligand **8o** (entries 7 and 8). We attribute this to the formation of a less robust coordination compound. Whether this difference in stability is due to steric and/or electronic factors is currently under investigation.

Table 2. Conversions and diastereoselectivities in the photochromic processes.^[a]

Entry	Photochrome	Concentration [M]	% Conversion ^[b]	% de
1	(S,S)- 7o + Cu(I)	0.001	95	98
2		0.0001	94	86
3		0.00001	85	74
4	(R,R)- 7o + Cu(I)	0.0001	92	89
5	(S,S)- 7o + 0.5Cu(I)	0.001	94	68
6	(S,S)- 7o + Cu(I)	0.001	60	52
7	(S,S)- 8o + Cu(I)	0.0001	70	55
8	(R,R)- 8o + Cu(I)	0.0001	79	49

[a] In a typical reaction, the ligand and $\text{CuOTf} \cdot 0.5\text{C}_6\text{H}_6$ were mixed in deoxygenated dichloroethane and exposed to 313 nm light for 20 minutes. After washing with excess NH_4OH to remove the metal, the % conversions and % de's of the products were measured by ^1H NMR spectroscopy in CD_2Cl_2 . [b] Based on the disappearance of the *open* isomers.

2.3.6 Circular Dichroism and Optical Rotatory Dispersion Spectroscopic Analysis

The circular dichroism (CD) and optical rotatory dispersion (ORD) spectra of the photochromic reaction are shown in Figures 6 and 7, respectively. Once again the dramatic effects of the ligand coordinating to the copper ions are observed. The CD spectrum of the *open* R-isomer of **7o** displays a very weak negative double Cotton

effect²⁸ while the *closed* form exhibits a red shifted spectrum that is of the opposite sign (Figure 6a). As expected, the spectral characteristics of (*R,R*) and (*S,S*) enantiomers were mirror images of one another. Conversely, the copper(I) R-isomer complex $\text{Cu}_2(\mathbf{7o})_2$ exhibits intense multiple Cotton effect curves (Figure 6b) and the absorption bands have red shifted to $\lambda_{\text{max}} = 380$ nm. After irradiation, the copper(I) complex of the *closed* R-isomer of **7c** displays a dramatically different CD spectrum as the major areas of absorption have red shifted from 280 nm to 635 nm (Figure 6b).

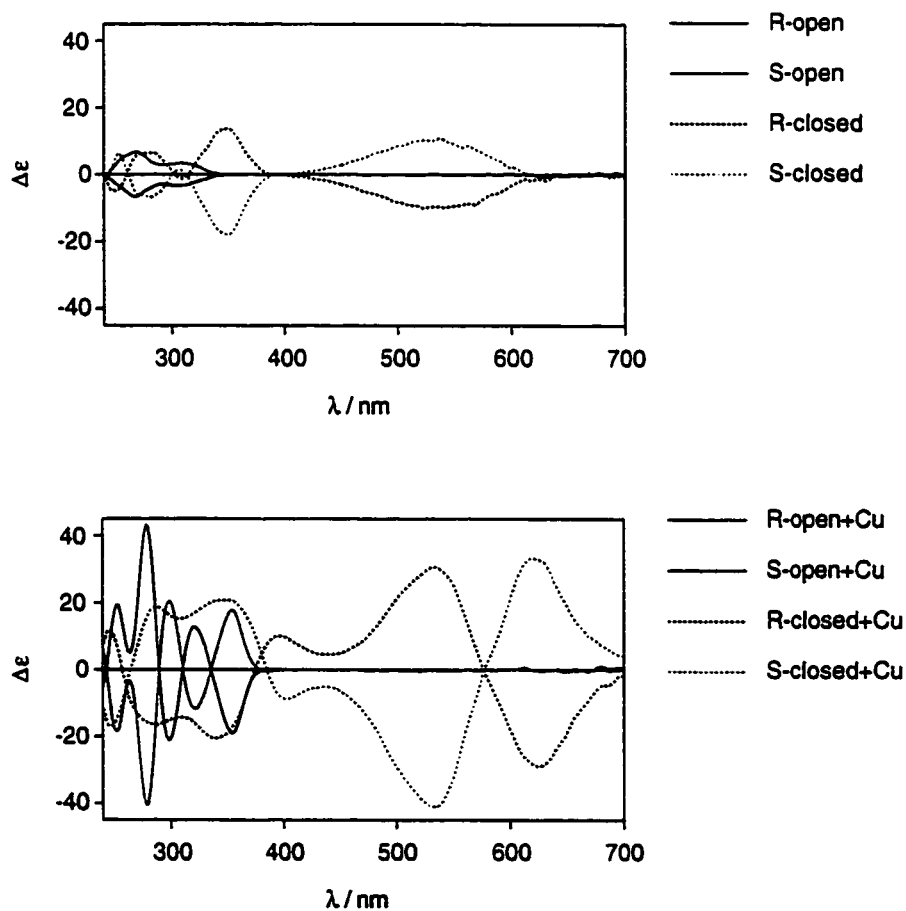


Figure 6. (a) CD spectra of **7o** and **7c** without $\text{CuOTf} \cdot 0.5\text{C}_6\text{H}_6$ and (b) CD spectra of **7o** and **7c** with $\text{CuOTf} \cdot 0.5\text{C}_6\text{H}_6$. All spectra were run in dry degassed dichloroethane at 2.8×10^{-4} M.

The ORD spectra of the photochromic reaction (Figures 7) follow a similar trend. Both the open and closed form of the ligand without copper display small optical rotatory powers, while the copper(I) complex of the *open* form $\text{Cu}_2(\mathbf{7o})_2$ displays strong optical rotatory powers in the 230 to 360 nm region (Figure 7). The *closed* form of this complex shows regions of optical rotation extending from 240 to 700 nm. These changes from the *open* to the *closed* forms are dramatic and provide regions for non-destructive read-out.

Of special interest is the region between 400 and 500 nm as this region is just outside the absorption bands for both the *open* and *closed* forms. At 450 and 475 nm the copper(I) complex of the *open* isomer shows almost no optical rotatory powers, conversely the *closed* form displays a strong negative Cotton effect. These differences can be exploited by toggling between $\text{Cu}_2(\mathbf{7o})_2$ and $\text{Cu}_2(\mathbf{7c})_2$ by alternate irradiation at 313 nm and greater than 458 nm (Figure 8) demonstrating the utility of this system for reversible data processing. This detection method is non-invasive as illustrated by the lack of variation in the UV-Vis spectrum upon extended irradiation at 475 nm.

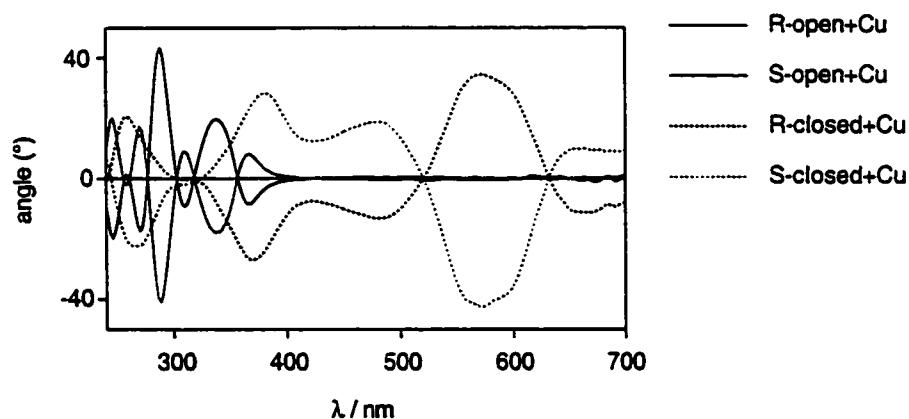


Figure 7. ORD spectra of **7o** and **7c** and $\text{CuOTf} \cdot 0.5\text{C}_6\text{H}_6$. All spectra were run in dry degassed dichloroethane at 2.8×10^{-4} M.

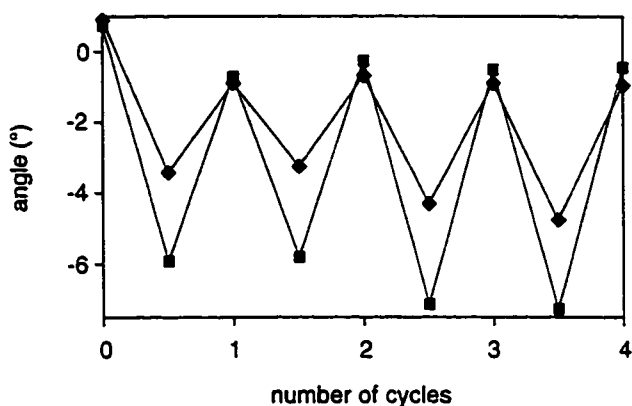


Figure 8. Modulated optical rotation at 450 nm (◆) and 475 nm (■) of a dichloroethane solution of $\text{Cu}_2(7\text{o})_2$ (2.8×10^{-4} M) during alternating irradiation at 313 nm and greater than 458 nm.

2.4 Conclusions

Chiroptic molecular switches $\text{Cu}_2(7\text{o})_2$ and $\text{Cu}_2(8\text{o})_2$, based on the spontaneous self-assembly of ligands **7o** or **8o** with copper(I) into stereochemically pure helicates, provides a viable solution to the problem of non-destructive read-out for photochromic re-writable optical memories. It has the distinct advantage over already existing chiroptic switches in that it shows preferential formation of one stereoisomer, large changes in optical rotary powers in non-photoactive regions, good fatigue resistance over a large number of photochemical cycles and no racemization. Other examples of chiral photochromic molecules such as strained olefins are susceptible to racemization, leading to decreased read-out signals over large number of cycles, that limits their use in information processing.

Further development of photochromic compounds for optical data storage hinges on their being incorporated into polymers or polymer like materials such as liquid crystals (LC). Polymers are excellent supporting materials for practical applications of these new materials because they aid in stability and processibility. Two important

conditions must be met, however. Incorporation of the photochrome into a matrix cannot inhibit the performance of the molecule and the molecule cannot display any fluctuations in its physical properties. To this end, molecular switches based on dithienylethenes are ideal candidates as initial studies show that these molecules maintain photochromic performance upon incorporation into liquid crystals.

2.5 Experimental

2.5.1 General Information

All solvents (Caledonia) were distilled prior to use. Dichloroethane used for UV-Vis spectroscopy and photoisomerization reactions was deoxygenated by bubbling argon through the solvent. Solvents for NMR analysis (Cambridge Isotope Laboratories) were used as received. All reagents and starting materials were purchased from Aldrich or Acros Organics. Trifluoromethanesulfonic acid copper (I) salt benzene complex was purchased from TCI America. 1,2-Bis(5-chloro-2-methylthien-3-yl)cyclopentene was prepared as described in literature.²⁹

¹H NMR characterizations were performed on a Varian Inova-500 instrument, working at 499.92 MHz or on a Varian Inova-300 instrument, working at 299.96 MHz. Chemical shifts (δ) are reported in parts per million relative to tetramethylsilane using the residual solvent peak as a reference standard. First order coupling constants (J) are reported in Hertz. UV-Vis spectra were recorded on a JASCO Ubest-50 UV-Vis spectrophotometer. CD spectra were recorded on a JASCO 7500 CD/ORD spectrophotometer. ORD spectra were obtained, by utilizing the data processing unit,

from CD measurements. High resolution mass spectrometry measurements were performed using Kratos MS-50 with an electron impact source, while low resolution mass spectrometry measurements were performed using an Agilent Technologies 1100 MSD spectrometer with an electrospray source.

Standard lamps used for visualizing TLC plates (Spectroline E-series, 470 $\mu\text{W}/\text{cm}^2$) were used to carry out the *ring-closing* reaction of **7o** to **7c** and **8o** to **8c** with and without copper. The *ring-opening* reactions were carried out using the light of a 150-W tungsten source that was passed through a 458 nm cutoff filter to eliminate higher energy light.

2.5.2 Synthesis

1,2-Bis(5'-carboxyl-2'-methylthien-3'-yl)cyclopentene (10). To a cooled ($-78\text{ }^{\circ}\text{C}$) solution of 2-bis(5'-chloro-2'-methylthien-3'-yl)cyclopentene **9** (1.90g, 5.8 mmol) in anhydrous THF (130 mL) under an argon atmosphere was added dropwise over 10 min *t*-butyl lithium (1.7 M in hexane, 7.48 mL, 12.8 mmol). The reaction was then stirred for a further 30 min. Anhydrous CO_2 was then bubbled through the reaction mixture for 20 min, the solution turned into a thick slurry and THF (20 mL) was added. The reaction was warmed to ambient temperature and stirred for 1 h. The THF was removed under pressure, the residue dissolved in CH_2Cl_2 (250 mL) and washed with 5% NaOH (2 x 250 mL). The combined aqueous layers were acidified by concentrated HCl and the resulting white precipitate was collected by vacuum filtration. Trituration of the precipitate with cold CH_2Cl_2 (2 x 10 mL) subsequently removed any mono-substituted

acid to afford desired diacid **10a** (1.75g, 88%). Single crystals suitable for x-ray diffraction were grown by layering a MeOH solution of **12a** with H₂O. mp >265 °C (dec); ¹H NMR (300 MHz, CD₃OD) δ: 7.47 (s, 2H), 2.82 (t, *J* = 6.5 Hz, 4H), 2.10 (m, 2H), 1.96 (s, 6H); ¹³C NMR (300 MHz, CD₃OD) δ: 165.24, 144.25, 138.12, 136.34, 135.75, 131.55, 39.46, 23.91, 14.81; FT-IR (microscope): 2953, 2841, 2578, 1663, 1550, 1463, 1373, 1308, 1271 cm⁻¹; EI-HSMS *m/z* (%): calcd for C₁₇H₁₆O₄S₂ 348.0490, found 348.0492 (100).

1,2-Bis(5'-carbonyl chloride -2'-methylthien-3'-yl)cyclopentene. To a suspension of **10** (52 mg, 0.15 mmol) in freshly distilled CH₂Cl₂ (10 mL) was added anhydrous DMF (25 μL) and the solution was cooled to 0 °C. A solution of oxalyl chloride (270 mg, 2.1 mmol) in freshly distilled CH₂Cl₂ (10 mL) was added dropwise to the rapidly stirring solution over 30 min. After 1 h, a light green homogenous solution was formed and the reaction was warmed to ambient temperature and stirred for 16 h. The solvent was removed under reduced pressure affording a moss green solid. The crude product was carried onto the next step without further purification. mp 115–120 °C; ¹H NMR (300 MHz, CDCl₃) δ: 7.63 (s, 2H), 2.81 (t, *J* = 6.5 Hz, 4H), 2.10 (m, 2H), 2.01 (s, 6H); EI-HRMS *m/z* (%): calcd for C₁₇H₁₄³⁷Cl³⁵ClO₂S₂ 385.9782, found 385.9768 (43); calc'd for C₁₇H₁₄³⁵ClO₂S₂ 349.0124, found 349.0107 (100).

1,2-Bis(5'-(*N'* *N'*' -bis-((2''*S*)-(3''-methyl-1''-hydroxybutyl)-amide))-2'-methylthien-3'-yl)cyclopentene (12). A solution of (*S*)-2-amino-3-methyl-1-butanol (102 mg, 1.0

mmol) and triethylamine (680 mg, 6.7 mmol) in freshly distilled CH₂Cl₂ (10 mL) was cooled to 0 °C. Non-isolated 1,2-bis(5'-acylchloride-2'-methylthien-3'-yl)cyclopentene (173 mg, 0.451 mmol) dissolved in CH₂Cl₂ (15 mL) was added dropwise over 30 min. The solution was warmed to ambient temperature and stirred for an additional 12 h. The mixture was diluted with CH₂Cl₂ (30 mL) and was washed with H₂O (50 mL). The aqueous phase was extracted CH₂Cl₂ (2 x 15 mL). The combined organic phases were washed with saturated aqueous NaCl and dried over Na₂SO₄. The solvent was removed under reduced pressure and the residue was purified by column chromatography over silica gel (1–5% MeOH/CHCl₃) to afford 183 mg (79%) of a slightly pink solid. mp 110–114 °C; ¹H NMR (300 MHz, CDCl₃) δ: 7.06 (s, 2H), 6.23 (d, *J* = 9.0 Hz, 2H), 3.79 (m, 2H), 3.72 (d, *J* = 3.9 Hz, 4H), 2.95 (bs, 2H), 2.74 (t, *J* = 6.4 Hz, 4H), 2.00 (s, 6H), 1.88 (m, 2H), 0.93 (t, *J* = 6.4 Hz, 12H); ¹³C NMR (300 MHz, CDCl₃) δ: 162.65, 140.43, 136.31, 135.26, 134.27, 129.74, 63.44, 57.32, 37.88, 29.34, 23.11, 19.63, 19.29, 14.72; FT-IR (CHCl₃ cast): 3319, 3059, 2958, 2925, 2871, 1741, 1621, 1557, 1531, 1463 cm⁻¹; ES-MS *m/z*: calcd for C₂₇H₃₈N₂O₄S₂Na 541.2171; found 541.2169; [α]_D²⁰ -66.6° [0.0001 M, CH₂Cl₂]; a sample of the product derived from (*R*)-2-amino-3-methyl-1-butanol was spectroscopically identical and possessed an optical rotation of [α]_D²⁰ +62.6° [0.0001 M, CH₂Cl₂].

1,2-Bis(5'-((4''*S*)-(4''-*iso*-propyl-1'',3''-oxazoline))-2'-methylthien-3'-yl)cyclopentene (8o). To a rapidly stirring CH₂Cl₂ (10 mL) solution of **12** (177 mg, 0.34 mmol) at 0 °C was added SOCl₂ (220 mg, 1.8 mmol) dropwise. The reaction was warmed to ambient

temperature. After 45 min the amide alcohol ($R_f = 0.5$ amide-alcohol, 10% MeOH/ CHCl_3) was completely converted to the oxazoline ($R_f = 0.65$). Cold saturated NaHCO_3 (5 mL) was added to the flask and the solution rapidly stirred for an additional 45 min. The two layers were separated and the organic layer washed with saturated aqueous NaCl solution and dried over Na_2SO_4 . The solvent was removed under reduced pressure and the residue was purified by column chromatography over silica gel (1:4 hexane/EtOAc) to afford 140 mg (85%) of a white solid. mp 59–62 °C; ^1H NMR (300 MHz, CD_2Cl_2) δ : 7.24 (s, 2H), 4.35 (m, 2H), 4.01 (m, 4H), 2.77 (t, $J = 6.5$ Hz, 4H), 2.04 (m, 2H), 1.92 (s, 6H), 1.75 (m, 2H), 0.98 (d, $J = 6.9$ Hz, 6H), 0.88 (d, $J = 6.9$ Hz, 6H); ^{13}C NMR (300 MHz, CDCl_3) δ : 159.02, 139.81, 136.40, 134.69, 131.14, 126.25, 72.76, 70.41, 38.72, 32.88, 22.93, 19.11, 18.12, 14.63; FT-IR (CH_2Cl_2 cast): 2956, 2924, 2871, 1648, 1547, 1467, 1384, 1351 cm^{-1} ; ES-MS m/z : calcd for $\text{C}_{27}\text{H}_{35}\text{O}_2\text{N}_2\text{S}_2\text{Na}$ 483.2140, found 483.2147; $[\alpha]_{589} -50.8^\circ$ [0.0001 M, CH_2Cl_2]; a sample of the product derived from (*R*)-2-amino-3-methyl-1-butanol was spectroscopically identical and possessed an optical rotation of $[\alpha]_{589} +50.6^\circ$ [0.0001 M, CH_2Cl_2].

1,2-Bis(5'-(*N*'*N*'-bis-((2''*S*)-(3''-phenyl-1''-hydroxypropyl)-amide))-2'-methylthien-3'-yl)cyclopentene (11). A solution of (*S*)-2-amino-3-phenyl-1-propanol (105 mg, 0.70 mmol) and triethylamine (200 mg, 2.0 mmol) in freshly distilled CH_2Cl_2 (25 mL) was cooled to 0 °C. Non-isolated 1,2-bis(5'-acylchloride-2'-methylthien-3'-yl)cyclopentene (127 mg, 0.33 mmol) dissolved in CH_2Cl_2 (15 mL) was added dropwise over 30 min. The

solution was warmed to ambient temperature and stirred for an additional 12 h. The mixture was diluted with CH₂Cl₂ (30 mL) and was washed with H₂O (50 mL). The aqueous phase was extracted CH₂Cl₂ (2 x 15 mL). The combined organic phases were washed with saturated aqueous NaCl and dried over Na₂SO₄. The solvent was removed under reduced pressure and the residue was purified by column chromatography over silica gel (1:1 hexane/EtOAc) to afford 150 mg (73%) of a white solid. mp 108.5–109.5 °C; ¹H NMR (300 MHz, CD₂Cl₂) δ: 7.27 (m, 10H), 6.98 (s, 2H), 6.06 (d, *J* = 7.8 Hz, 2H), 4.21 (m, 2H), 3.64 (m, 4H), 2.90 (d, *J* = 7.2 Hz, 4H), 2.76 (m, 4H), 2.06 (q, *J* = 7.2 Hz, 2H), 2.00 (s, 6H); ¹³C NMR (300 MHz, CDCl₃) δ: 162.44, 140.66, 138.71, 137.62, 136.31, 135.20, 134.09, 129.83, 129.34, 128.75, 126.88, 63.70, 53.11, 37.92, 37.23, 23.12, 14.89; FT-IR (CHCl₃ cast): 3316, 3061, 3026, 3923, 1620, 1556, 1529, 1496, 1454, 1293, 1038 cm⁻¹; ES-MS *m/z*: calcd for C₃₅H₃₈N₂O₄S₂Na 637.2171, found 637.2179 [M + Na]; [α]₅₈₉ -90.0° [0.0001 M, CH₂Cl₂]; a sample of the product derived from (*R*)-2-amino-3-phenyl-1-propanol was spectroscopically identical and possessed an optical rotation of [α]₅₈₉ +92.0° [0.0001 M, CH₂Cl₂].

1,2-Bis(5'-(*NN'*-bis-((2''*S*)-(3''-phenyl-1''-hydroxypropyl)-amide))-2'-methylthien-3'-yl)cyclopentene. To a cooled (0 °C) rapidly stirring solution of **11** (120 mg, 0.195 mmol) in CH₂Cl₂ (15 mL) was added SOCl₂ (100 mg, 0.85 mmol) dropwise. The solution was stirred at 0 °C for 10 min and then allowed to warm to ambient temperature. After 90 min of stirring at ambient temperature the diol (*R_f* = 0.42, 4:1 hexane/EtOAc, SiO₂) was

completely converted to the dichloride ($R_f = 0.92$) at which point the solvent was removed under pressure and the pink solid residue placed under high vacuum for 3 h. The crude product was used in the next step without further purification. mp 138.5–140.5 °C; ^1H NMR (300 MHz, CDCl_3) δ : 7.26 (m, 10H), 7.16 (s, 2H), 5.96 (d, $J = 8.1$ Hz, 2H), 4.57 (m, 2H), 3.67 (dd, $J = 4.2, 11.4$ Hz, 2H), 3.54 (dd, $J = 3.0, 11.1$ Hz, 2H), 3.02 (dd, $J = 3.0, 8.7$ Hz, 2H), 2.93 (dd, $J = 8.7, 13.5$ Hz, 2H), 2.78 (t, $J = 8.1$ Hz, 4H), 2.06 (q, $J = 8.1$ Hz, 2H), 1.95 (s, 6H); ES-MS m/z : calcd for $\text{C}_{35}\text{H}_{36}\text{Cl}_2\text{N}_2\text{O}_2\text{S}_2\text{Na}$ 673.1493, found 673.1504 [M + Na].

1,2-Bis(5'-((4''*S*)-(4''-benzyl-1'',3''-oxazoline))-2'-methylthien-3'-yl)cyclopentene (7o). The above non-isolated 1,2-bis(5'-(*N N'*-bis-((2*S*)-(3''-phenyl-1''-chloropropyl)-amide))-2'-methylthien-3'-yl)cyclopentene in MeOH (20 mL) was added NaOH (2 mL, 1.25 M) solution and the reaction was brought to reflux for 2.5 h. The solvent was removed under reduced pressure and the residue taken up in CH_2Cl_2 (15 mL), washed with H_2O (2 x 10 mL) and dried over Na_2SO_4 . The solvent was removed under reduced pressure and the residue was purified by column chromatography over silica gel (3:1 hexane/EtOAc) to afford 96 mg (85%) of a white solid. mp 92.5–94 °C; ^1H NMR (300 MHz, CD_2Cl_2) δ : 7.27 (m, 12H), 4.50 (m, 2H), 4.32 (dd, $J = 8.2, 8.2$ Hz, 2H), 4.06 (dd, $J = 8.2, 8.2$ Hz, 2H), 3.08 (dd, $J = 6.0, 13.8$ Hz, 2H), 2.78 (t, $J = 8.1$ Hz, 4H), 2.75 (dd, $J = 8.1, 13.8$ Hz, 2H), 2.05 (q, $J = 8.1$ Hz, 2H), 1.94 (s, 6 H); ^{13}C NMR (300 MHz, CDCl_3) δ : 159.55, 140.23, 138.71, 136.82, 135.10, 131.50, 129.76, 128.83, 126.75, 126.75, 72.64, 68.43, 42.02, 38.96, 23.35, 14.76; FT-IR (CHCl_3 cast): 2918, 2843, 1644, 1494, 1477,

1453, 1439, 1354, 1019 cm^{-1} ; ES-MS m/z : calcd for $\text{C}_{35}\text{H}_{39}\text{N}_2\text{O}_2\text{S}_2$ 579.2134, found 579.2179 $[\text{M} + \text{H}]$; $[\alpha]_{589} +15.1^\circ$ [0.0001 M, CH_2Cl_2]; a sample of the product derived from (*R*)-2-amino-3-phenyl-1-propanol was spectroscopically identical and possessed an optical rotation of $[\alpha]_{589} -14.2^\circ$ [0.0001 M, CH_2Cl_2].

2. 6 References

1. (a) J. C. Crano, R. J. Gugliemetti, *Organic Photochromic and Thermochromic Compounds Vol. 2*, Plenum Publishers, New York, 1999; (b) J. -M. Lehn, *Supramolecular Chemistry: Concepts and Perspectives*, VCH, Weinheim, 1995.
2. I. Willner, S. Rubin, *Angew. Chem. Int. Ed. Engl.* **1996**, *35*, 367.
3. P. D. Beer, P. A. Gale, D. K. Smith, *Supramolecular Chemistry*, Oxford University Press Inc., New York, 1999.
4. (a) M. Bochmann, *Organometallics 1: Complexes with Transition Metal-Carbon σ -Bonds*, Oxford University Press Inc., New York, 1994; (b) M. Fugita, J. Yazaki, K. Ogura, *J. Am. Chem. Soc.* **1990**, *112*, 5645; (c) M. Fugita, K. Ogura, *Bull. Chem. Soc. Jpn.* **1996**, *69*, 1471.
5. R. Kramer, J. -M. Lehn, *J. Chem. Soc. Chem. Commun.* **1993**, 990.
6. (a) U. Koert, M. M. Harding, J. -M. Lehn, *Nature* **1994**, *346*, 339; (b) E. C. Constable, *Tetrahedron* **1992**, *48*, 10013.
7. S. Leininger, B. Olenyuk, P. J. Stang, *Chem. Rev.* **2000**, *100*, 853 and references therein.

8. G. S. Hanan, C. R. Arana, J. -M. Lehn, G. Baum, D. Fenske, *Chem. Eur. J.* **1996**, *2*, 1292.
9. P. N. W. Baxter, G. S. Hanan, J. -M. Lehn, *Chem. Commun.* **1996**, 2019.
10. (a) M. Fujita, F. Ibukura, H. Hagihara, K. Ogura, *Nature* **1994**, *367*, 720; (b) M. Fujita, K. Ogura, *Acc. Chem. Res.* **1999**, *32*, 53; (c) E. Wasserman, *J. Am. Chem. Soc.* **1960**, *82*, 4433.
11. (a) B. L. Feringa, W. F. Jager, B. de Lange, *Tetrahedron* **1993**, *49*, 8267; (b) M. Gómez-López, J. F. Stoddart, *Bull. Chim. Soc. Belg.* **1997**, *106*, 491.
12. S. Kawata, Y. Kawata, *Chem. Rev.* **2000**, *100*, 1777.
13. a) M. Irie, *Chem. Rev.* **2000**, *100*, 1685; b) M. Irie, In *Organic Photochromic and Thermochromic Compounds: Edited by Crano, J. C., Gugliemetti, R. J.*; Plenum Press: New York, NY, 1999; Vol. 1, Chapter 5.
14. F. Vögtle, *Supramolecular Chemistry*, John Wiley and Sons, New York, 1991.
15. G. Berkovic, V. Krongauz, V. Weiss, *Chem. Rev.* **2000**, *100*, 1741.
16. (a) E. Kim, K. H. Choi, S. B. Rhee, *Macromolecules* **1998**, *31*, 5726; (b) T. Kawai, T. Koshido, K. Yoshino, *Appl. Phys. Lett.* **1995**, *67*, 795; (c) N. Tanio, M. Irie, *J. Appl. Phys.* **1994**, *33*, 1550.
17. (a) L. Gobbi, P. Seiler, F. Diederich, *Angew. Chem. Int. Ed.* **1999**, *111*, 740; *Angew. Chem. Int. Ed.* **1999**, *38*, 674; (b) A. Fernandez-Acebes, J. -M. Lehn, *Chem. Eur. J.* **1999**, *5*, 3285; (c) M. Takeshita, M. Irie, *Chem. Lett.* **1998**, 1123; (d) Y. Yokoyama, S. Uchida, Y. Yokoyama, T. Sagisaka, Y. Uchida, T. Inada, *Enantiomer* **1998**, *3*, 123; (e) G. M. Tsivgoulis, J. -M. Lehn, *Chem. Eur. J.* **1996**, *2*, 1399; (f) M. Seibold, H. Port, H. C. Wolf, *Mol. Cryst. Liq. Cryst.* **1996**, *283*, 75; (g) N. P. M. Huck and B. L.

- Feringa, *J. Chem. Soc., Chem. Commun.* **1995**, 1095; (h) T. Saika, T. Iyoda, K. Honda and T. Shimidzu, *J. Chem. Soc., Chem. Commun.* **1992**, 591.
18. (a) T. Yamaguchi, T. Inagawa, H. Nakazumi, S. Irie, M. Irie, *Chem. Mater.* **2000**, *12*, 869; (b) C. Denekamp, B. L. Feringa, *Adv. Mater.* **1998**, *10*, 1080; (c) T. Yamaguchi, K. Uchida, M. Irie, *J. Am. Chem. Soc.* **1997**, *119*, 6066; (d) L. Eggers, V. Buss, *Angew. Chem. Int. Ed.* **1997**, *109*, 885; *Angew. Chem. Int. Ed.* **1997**, *36*, 881; (e) N. P. M. Huck, J. F. Wolter, G. De Lange, B. L. Feringa, *Science* **1996**, *273*, 1686; (f) G. Agati, A. F. McDonagh, *J. Am. Chem. Soc.* **1995**, *117*, 4425.
19. (a) *Optical Rotatory Dispersion and Circular Dichroism in Organic Chemistry*, G. Snatzke, Ed.; Heyden and Son Limited, Great Britian, 1967; (b) P. Crabbé, *ORD and CD in Chemistry and Biochemistry*, Academic Press Inc., New York, 1972.
20. B. L. Feringa, R. A. van Delden, N. Kourmura, E. M. Geertsema, *Chem. Rev.* **2000**, *100*, 1789 and references therein.
21. For a description of *M* and *P* nomenclature, see: E. L. Eliel, S. H. Wilen, *Stereochemistry of Organic Compounds*, Wiley, New York, 1994; Chapter 14, pp 1121.
22. A. Fernandez-Acebes, *Chirality* **2000**, *12*, 149. For examples of diastereoselectivity in the crystalline state, see: (a) T. Kodani, K. Matsuda, T. Yamada, S. Kobatake, M. Irie, *J. Am. Chem. Soc.* *In press*; (b) T. Kodani, K. Matsuda, T. Yamada, M. Irie, *Chem. Lett.* **1999**, 1003.
23. For recent reviews on helicates, see: (a) A. von Zelewsky, O. Mamula *J. Chem. Soc. Dalton Trans.* **2000**, *3*, 219; (b) C. Piguet, G. Bernardinelli, G. Hopfgartner, *Chem.*

- Rev.* **1997**, *97*, 2005. For selected examples, see: G. Bernardinelli, C. Piguet, A. F. Williams, *Angew. Chem. Int. Ed. Engl.* **1992**, *31*, 1622.
24. C. Provent, E. Rivara-Minten, S. Hewage, G. Brunner, A. F. Williams, *Chem. Eur. J.* **1999**, *5*, 3487.
25. L. N. Lucas, J. van Esch, R. M. Kellogg, B. L. Feringa, *Chem. Commun.* **1998**, 2313.
26. (a) A. W. Addison, E. Sinn, *Inorg. Chem.* **1983**, *22*, 1225; (b) G. C. van Stein, G. van Koten, A. L. Spek, A. J. M. Duisenberg, E. A. Klop, *Inorg. Chem. Acta*, **1983**, *78*, L61.
27. Standard lamps used for visualizing TLC plates (Spectroline E-series, 470 $\mu\text{W}/\text{cm}^2$) were used to carry out the ring-closing reaction of **7o** to **7c** and **8o** to **8c** with and without copper. The ring-opening reactions were carried out using the light of a 150-W tungsten source that was passed through a 458 nm cutoff filter to eliminate higher energy light.
28. If a compound presents one or several optically active absorption bands, its ORD and CD curves will show peaks or troughs in the spectral region in which the chromophore absorbs. These curves are anomalous and called Cotton effect curves. The sign of the Cotton effect (positive or negative) is determined by whether a peak or trough, respectively, is met first when going from longer wavelengths to shorter wavelengths.
29. L. N. Lucas, J. van Esch, R. M. Kellogg, B. L. Feringa, *Chem. Commun.* **1998**, 2313.

Chapter 3 – Hydrogen Bonding, Helicenes and Chiral Discrimination.

The design and synthesis of molecules that distinguish between stereoisomers can provide models to rationalize substrate-receptor selectivity, create chiral environments for asymmetric synthesis and separation, and supply building blocks for constructing supramolecular complexes having novel chemical and topological properties.¹ This last goal requires a great degree of stereocontrol and can be achieved by taking advantage of the appealing concept of auto-resolution where, through the interaction of molecular recognition elements, molecules sort themselves into stereochemically pure assemblies based on their handedness.

Programming molecules to spontaneously and selectively assemble into stereochemically predictable architectures requires the consideration of three critical factors. First, the most appropriate functionality must be chosen to act as constructive recognition elements (hydrogen bonds, van der Waal's interactions or dative metal bonds, for example) and to guide the self-assembly reaction along the desirable pathway. Second, undesirable assemblies must be eliminated through the rational choice of a scaffold onto which the molecular recognition sites are fused. Third, the choice of scaffold must also consider the molecular requirements needed to induce spontaneous resolution.

This chapter will explore the utility of using hydrogen bonds and helical scaffolds to foster the selective self-recognition of uncharged species into topologically predictable supramolecular aggregates in both the solution and the solid state. The strength and

directionality of hydrogen bonds are first discussed and then the utility of this “glue” is highlighted by using representative examples.

3.1 Molecular Recognition and The Hydrogen Bond

3.1.1 Primary Hydrogen Bonds

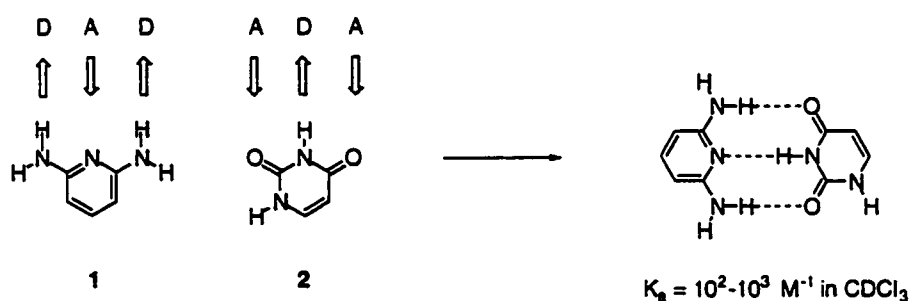
The design and synthesis of supramolecular building blocks requires the selection of intermolecular interactions that are strong and possess well-defined directionality. In this regard, the hydrogen bond is not ideal. The binding energy, which is determined by the attraction between an electropositive hydrogen atom (donor) and an electronegative heteroatom (acceptor), is low ($1\text{--}1.5\text{ kcal mol}^{-1}$ in aprotic solvents such as chloroform).² Furthermore, the directionality is not well defined. Many reported examples display significant bending (interatomic angle can vary from the ideal angle of 180° to 150°) with little loss in binding energy.³ The strengths of hydrogen bonds is also extremely solvent dependent. For example, dramatic decreases in binding constants result with the addition of 1% methanol to chloroform.⁴ Therefore, the design of hydrogen-bonding ligands must rely on multiple hydrogen bond donor (D) and acceptor (A) sites to ensure that the overall interactions are strong enough and that the geometry is better defined.

3.1.2 Secondary Hydrogen Bonds

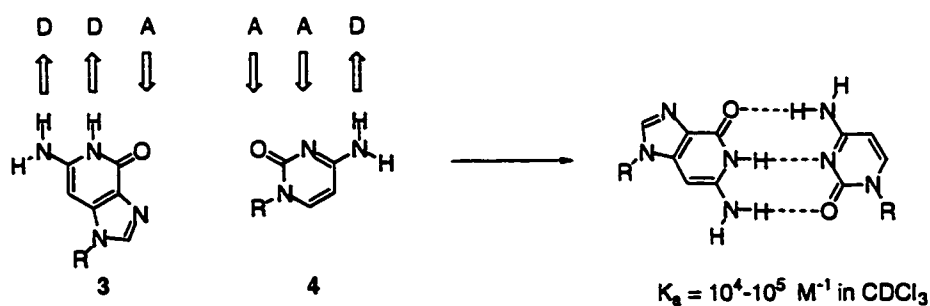
Using arrays of hydrogen bonds, however, is not as straightforward as it may seem. The arrangement of hydrogen bond donor and acceptor groups with respect to one another has a dramatic effect on the extent of association.⁵ This concept is effectively

illustrated by comparing the association between diaminopyridine **1** and uracil **2** (Equation 1) to the association between guanine **3** and cytosine **4** (Equation 2). Each of the four compounds contains three potential hydrogen-bonding sites, but the arrangement of these sites differs. Diaminopyridine **1** possesses a donor-acceptor-donor (DAD) hydrogen-bonding array and uracil **2** contains a complementary ADA arrangement. Guanine **3** and cytosine **4** have DDA and AAD motifs, respectively. Surprisingly, the DAD•ADA arrangement (Equation 2) has an association constant (K_a) that is two orders of magnitude smaller than the DDA•AAD arrangement.

Equation 1



Equation 2



Jorgensen proposed that it is the *diagonal interactions* in the array that account for the differences in association constants and labeled them as *secondary electrostatic*

interactions.⁶ Figure 1 provides a schematic representation of the three possible triple hydrogen bonded arrangements. In the first hydrogen-bonding array (ADA•DAD), all of the diagonal interactions are between like charges. These are considered to be negative interactions and weaken the binding. In the last hydrogen-bonding array (AAA•DDD) all of the diagonal interactions are between opposite charges. This results in constructive secondary interactions, which strengthen the binding. Calculations indicate that *secondary electrostatic interactions* are worth about 0.5 kcal mol⁻¹ per bond in non-protic solvents. Looking back to Equations 1 and 2, the DAD•ADA array contains only *destructive* secondary interactions. On the other hand, the DDA•AAD arrangement has two repulsive and two attractive secondary interactions. This results in no net secondary interactions and consequently the DDA•AAD motif has a stronger binding constant than the DAD•ADA pattern.

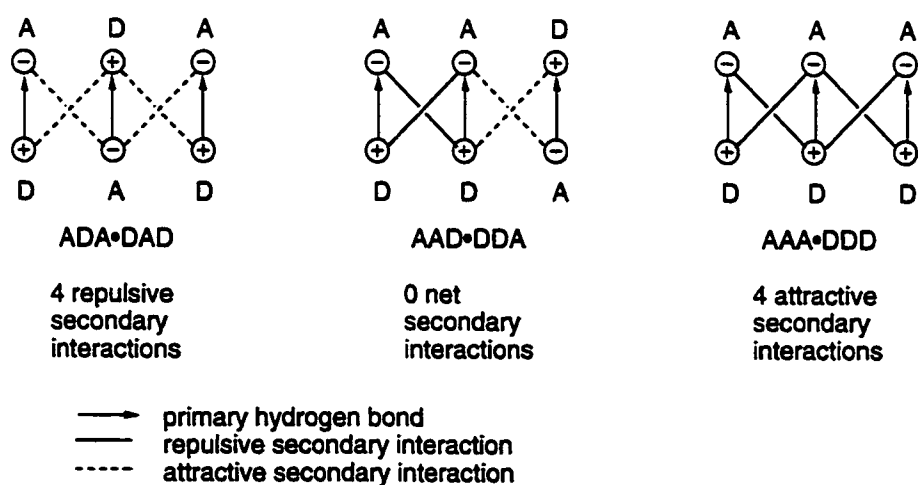


Figure 1. Jorgensen's secondary electrostatic model.

3.1.3 Isomers of Hydrogen Bond Arrays

Studies have also illustrated that systems that are poorly organized and require bonds to be “fixed” or “frozen” for complexation to occur have lower association constants.⁷ For example, crown ethers bind metal ions more strongly than their acyclic analogs because the host is already organized for binding. There are several examples that effectively illustrate the hydrogen bond analogy to this concept, one of which is shown in Figure 2. The strength of complexation between **5**•**7** is significantly weaker than that of **6**•**7**, even though both systems contain identical hydrogen bond motifs (ADDA•DAAD). The higher stability of **6**•**7** can be attributed to the intramolecular hydrogen bond in the complex. This interaction preorganizes the four hydrogen bond donor and acceptor groups and increases the complexes' stability by an extra 1-2 kcal mol⁻¹.

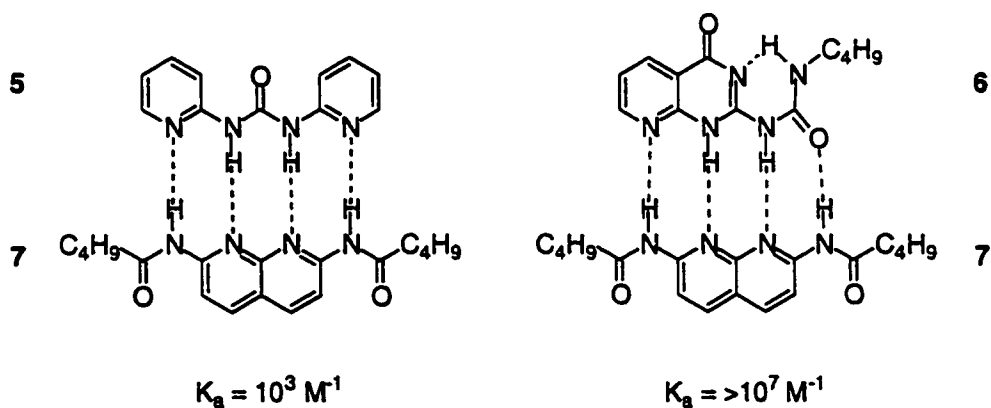


Figure 2. Preorganization and its dramatic effects on association constants. Association constants are measured in CDCl₃.

Synthons that possess two or more tautomeric forms can also affect the resulting complexes' strength and specificity. Incorrect tautomeric forms can result in wrong structures being assembled. There is a cost in energy to switch the tautomeric equilibrium toward the desired form. This concept is discussed in greater depth in Appendix 1. (pp 131)

3.1.4 Selected Examples of Hydrogen-Bond-Directed Assemblies

Many examples have employed hydrogen bond motifs to control the construction of supramolecular assemblies such as 2-dimensional ribbons⁸ and rosettes⁸, and 3-dimensional zeolites¹⁰ and capsules.¹¹ These molecular assemblies can be composed of identical or non-identical molecules. They can also, depending on hydrogen bond array placement, be linear (network) or cyclic (discrete).

An interesting example of how the stereochemical aspects of hydrogen bond arrays may be used to successfully control the topological features of self-assembled superstructures is shown in Figure 3. X-ray crystallographic analysis of crystals grown from solutions of either racemic or optically pure **8** reveals that two very different structures are formed.¹² Racemic solution of **8** produce crystals composed of linear arrays of doubly hydrogen bonded components of alternating chirality. Conversely, homochiral solutions of **8** produce crystals comprised of cyclic tetramers.

3.2 Molecular Programming and Helicenes

3.2.1 Choice of the Scaffold

Successful control of topological features arising from the self-assembly process relies on the design of the scaffold. While the directionality of hydrogen-bonding recognition surfaces serves to align the organic fragments along predetermined vectors, it

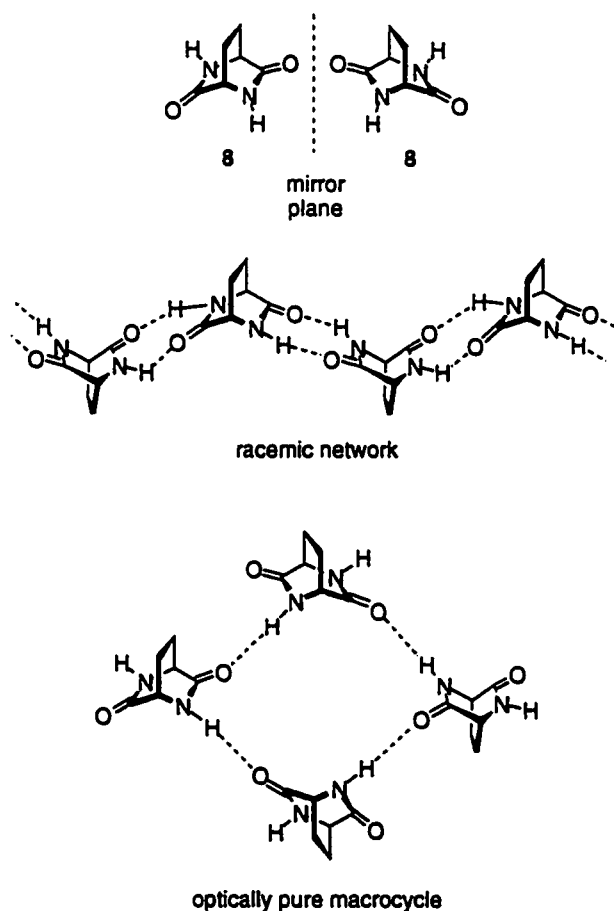


Figure 3. Self-assembly of hydrogen-bonded supramolecular complexes with racemic **8** and optically pure **8**.

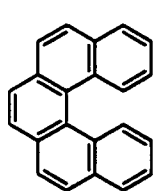
is the scaffold that controls the spatial orientation of these recognition sites and directs self-assembly processes in both the solution and solid-state.

The twisted backbones in *ortho*-fused aromatic rings (helicenes) result in stereo-discrimination because they possess a high degree of structural integrity which minimizes

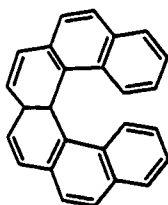
conformational scrambling that would otherwise result in the possible recognition of more than one substrate stereoisomer. The high optical stability (often greater than 35 kcal mol⁻¹) of hexahelicene and larger [n]-helicenes is testament to this stability (Table 1).¹³

Table 1. Comparison of Activation Barriers for Racemization

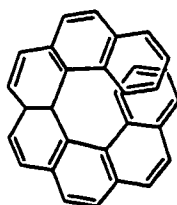
helicene	$\Delta\Delta G$	$\Delta\Delta H$
	[kcal mol ⁻¹]	[kcal mol ⁻¹]
I	24.1	22.9
II	36.2	35.0
III	41.7	40.5
IV	42.4	41.0
V	43.5	41.7



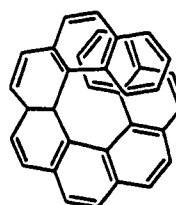
[5]-helicene
I



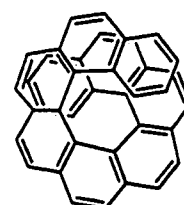
[6]-helicene
II



[7]-helicene
III



[8]-helicene
IV



[9]-helicene
V

The formation of optically pure solid-state aggregates (conglomerates) is rare (less than 10%) and their prevalence is largely dependent upon the class of organic compounds involved. For example, molecules that possess C_2 or C_3 symmetry such as helicenes and binaphthyl and bicyclononane derivatives, respectively, display a greater tendency to crystallize as conglomerates.¹⁴

The above considerations make the combination of hydrogen bonding and helicenes ideally suited for supramolecular projects where stereocontrol is paramount.^{15,16}

3.2.2 Viability of the Scaffold

Many research groups have utilized the advantageous properties of helicenes, including the high optical stability and pronounced asymmetric character, in chiral recognition^{15c,17} and asymmetric catalysis¹⁸ experiments, several examples of which are shown in Figure 4. Diederich and co-workers have synthesized a series of helical receptors for carboxylate recognition.^{15c} Receptor **9** is chiral due to its helical shape, which places the two (DA) hydrogen bond sites in an asymmetric environment. Acids **10a** and **10b**, which differ only by the *Z/E* configuration at their double bond, bind to optically pure **9** in aprotic solvents with differing strengths. The association of **9** with **10a** is two orders of magnitude stronger than that with **10b**. It has been shown that the magnitude of this selectivity is dependent upon the total number of hydrogen bonding interactions between host and guest. The geometry of acid **10a** satisfies four hydrogen bond requirements of its host, while the geometry of **10b** allows it to only satisfy two.

Optically active crown ethers, such as **11**, have also been used for chiral recognition of primary ammonium salts.¹⁷ Here, the distorted backbone of the helicene alters the relative orientation of the crown ethers' hydrogen bonding groups. The induced asymmetric character of the crown ether can now effectively discriminate between chiral amines. The results indicate that a stereoselective process between enantiomeric salts is taking place (ee = 75%).

Furthermore, Katz has shown that helical dihydroxyl ligand **12** catalyzes the addition of diethylzinc to aldehydes to afford chiral alcohols with ee as high as 81%.^{18c} The selectivity and yields are higher than those obtained with traditional chiral catalysts containing binaphthyl backbones.

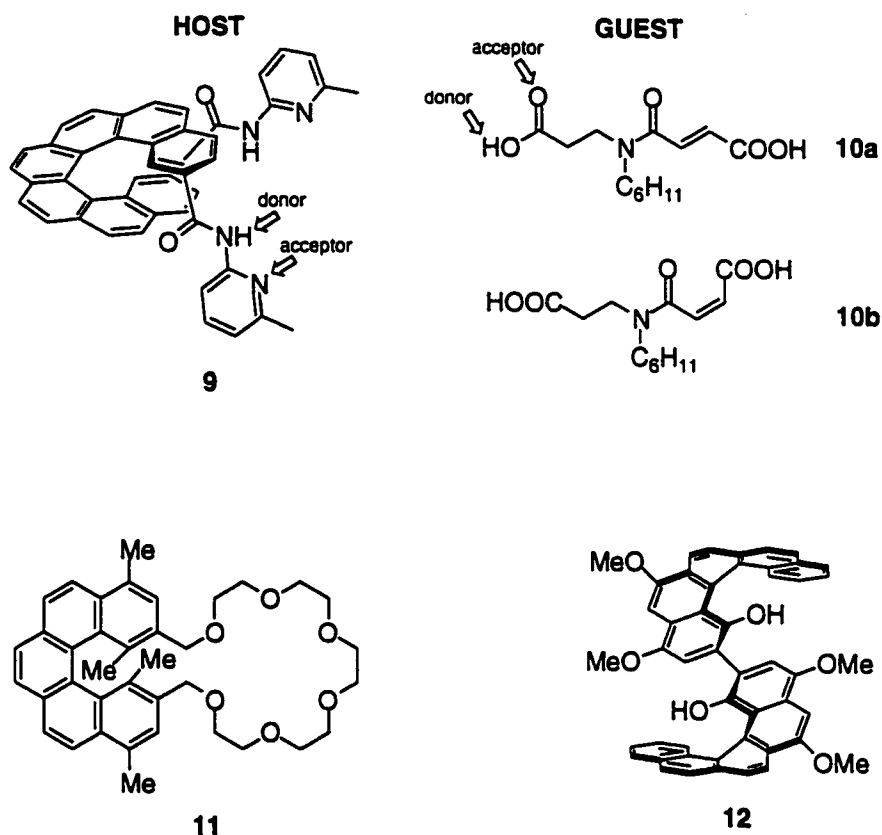


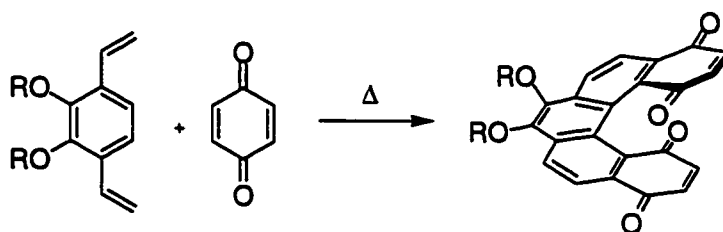
Figure 4. Examples of functional helicenes.

3.2.3 Synthesis of the Helicene

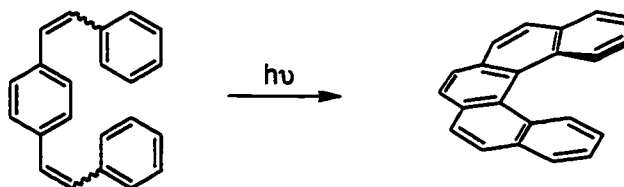
There are two common strategies used to obtain helicene scaffolds. One is the recently developed Diels-Alder reaction of bis-enol ether derivatives with *p*-benzoquinone (Equation 3).¹⁹ This approach, supplemented by an efficient procedure for obtaining optical resolution, has provided large quantities of optically pure simply functionalized helicenes and thus has opened the door for exploring the usefulness of helicenes in such projects as catalysis. The second is a pericyclic reaction of stilbene

derivatives (Equation 4).²⁰ Improved methodology that uses stoichiometric amounts of I_2 , in an inert atmosphere, to effect the oxidation and propylene oxide to act as an HI scavenger, has increased overall yields from a discouraging 20% to upwards of 80%. Here, the absence of air prevents photooxidative side reactions, while propylene oxide prevents HI from photoreducing the double bonds.

Equation 3



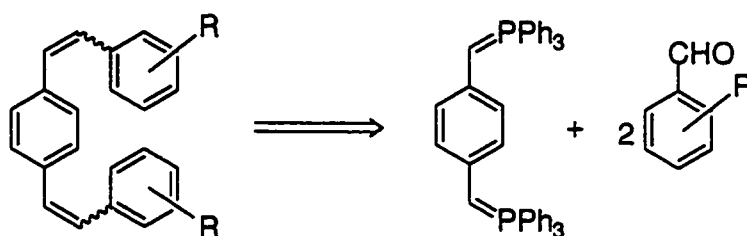
Equation 4



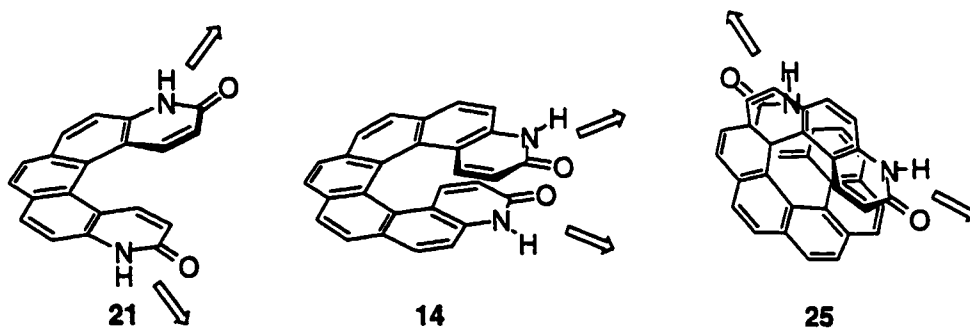
The electrocyclic cyclization of stilbenes is the method of choice for the preparation of highly functionalized helicenes. The two molecular requirements for the stilbene precursor are an easily obtainable ylid and a general aldehyde as shown in Equation 5. The appeal of this method stems from its generality and versatility, as this strategy allows

access to a variety of functionalized helicenes, including heterocycles, by simply varying the aldehyde while keeping the structure of the ylid constant.

Equation 5



3.2.4 Design of Specific Helicene Scaffolds



Three novel racemic helicenes **14**, **21** and **25** bearing pyridinone hydrogen bond sites on the ends of the twisted backbone were synthesized. The self-complementary nature of these molecular recognition elements and their position on the different helical scaffolds should allow for several possible stereochemical products of the self-assembly reaction.

The synthesis and results of the [7]-helicene scaffold will be presented first, as the solution and solid-state studies for this model have been the most successful, followed by a discussion of the other helical scaffolds.

3.3 [7]-Helicene: Results and Discussion

In this section, the synthesis and characterization of three novel racemic [7]-helicenes **14a-c** bearing pyridinone hydrogen bond sites on the ends of the twisted backbone will be described. The self-complementary nature of these molecular recognition elements and their position on the helical scaffold allows for several possible stereochemical products of the self-assembly reaction. This reaction can follow two general pathways and generate two topologically distinct supramolecular architectures as illustrated in Figure 5. One pathway leads to a fiber composed of alternating *M* and *P* stereoisomers as shown in the bottom of the figure. Alternatively, cooperative hydrogen bonding drives the building blocks into four stereochemically unique dimers with respect to the R-group as shown in the top of the figure. It will be shown that the self-assembly reaction takes the latter pathway both in solution and in the solid-state. In solution, helicenes **14b** and **14c** undergo a discrimination process that selects for only the dimeric topology. In the crystal, a second level of geometric discrimination occurs resulting in only two of the four possible dimers illustrated in Figure 5.

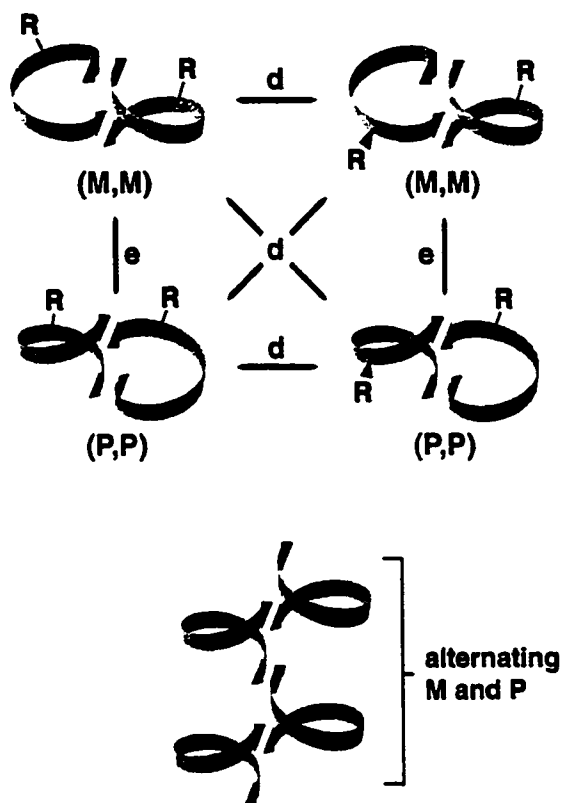


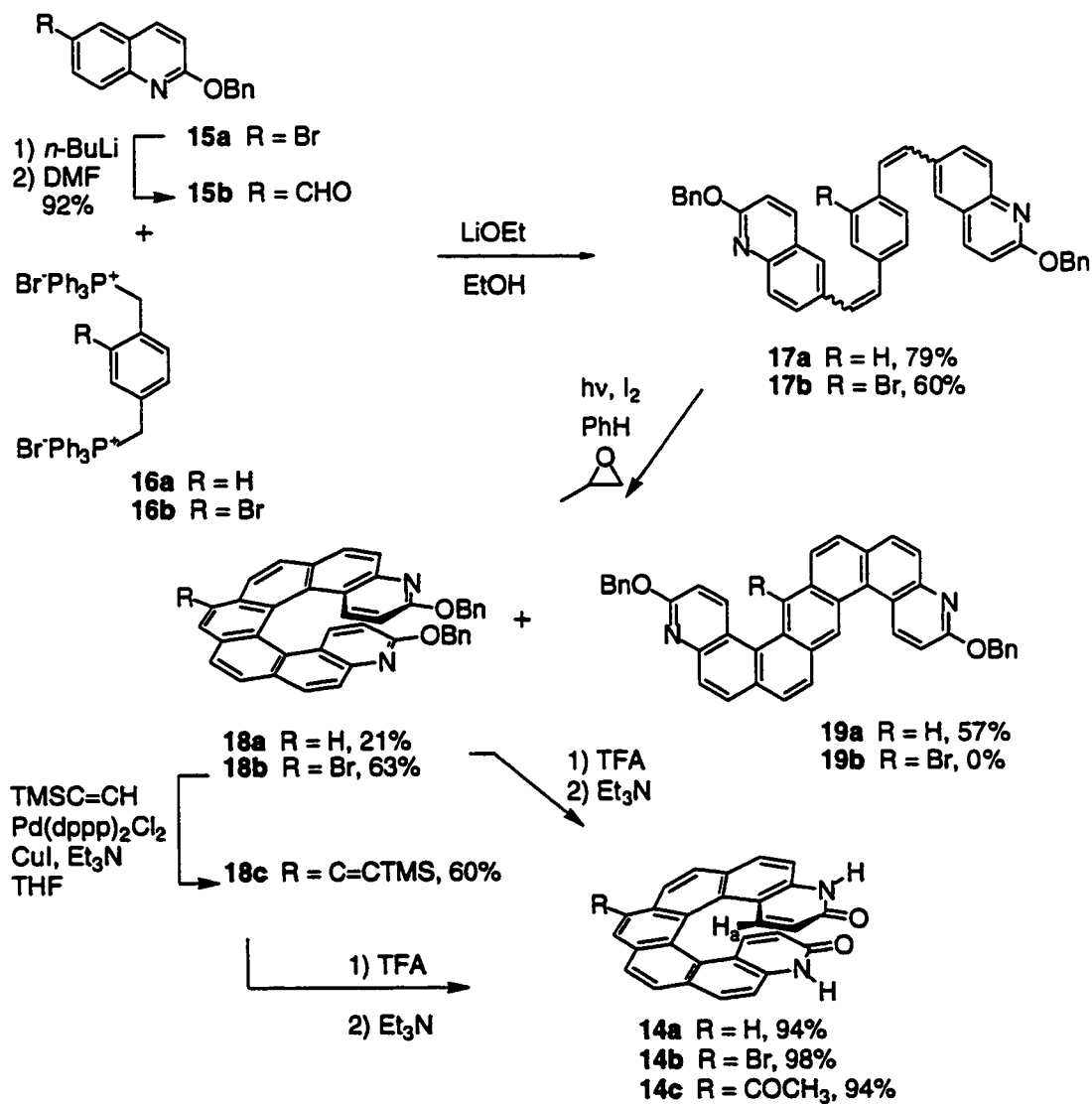
Figure 5. Schematic representations of all possible hydrogen-bonded assemblies of [7]-helicenes **14b** and **14c**. Enantiomeric (e) and diastereomeric (d) relationships between the dimers are highlighted in the top set of architectures. For clarity, the position of the side-groups ('R') in the stereochemically heterogeneous fiber are not shown (bottom architecture).

3.3.1 Synthesis

All [7]-helicenes were prepared as outlined in Scheme 1. The synthesis of parent helicene **14a** began with the condensation of 2-benzyloxy-6-quinolinecarboxaldehyde (**15b**)²² with *p*-xylenenebis(triphenylphosphonium bromide) (**16a**) to afford a mixture of *cis,cis*-, *cis,trans*- and *trans,trans*-**17a**. Irradiation of this isomeric mixture in the presence of iodine as an oxidizing agent and propylene oxide as a HI scavenger generated the desired [7]-helicene **18a** but in only minor amounts. Instead, the major product was the extended aromatic **19a**.²³ Removal of the benzyl groups from **18a** with trifluoroacetic

acid cleanly afforded pyridinone **14a** as a yellow solid. However, the insolubility of **14a** in all common solvents, as well as the large amounts of the undesirable *S*-isomer **19a** forced us to pursue alternative functional [7]-helicenes.

Scheme 1



The incorporation of a bromine atom onto the central benzene ring of the [7]-helicene as reported by Katz²⁰ conveniently addressed these critical issues. Here, the bromine plays two roles: (1) it minimizes the photo-induced cyclization to form structure **19** and (2) it provides a site to introduce solubilizing functional groups. Brominated [7]-helicene **14b** was synthesized starting from bis(phosphonium salt) **16b** in an analogous manner to that of **14a** (Scheme 1). It was immediately found that the bromine atom greatly improved the solubility of the helicene in typical organic solvents such as chloroform, DMSO and THF allowing the stereodiscrimination process to be assessed in solution.

3.3.2 Solution-State Studies Using ¹H NMR Analysis

All of the signals in the ¹H NMR spectrum of **14b** in CDCl₃ were assigned based on chemical shifts, coupling constants and G-COSY experiments. These experiments allowed the broad singlet at 13.70 ppm to be unambiguously identified as that corresponding to the N-H protons. It is significant that this signal resides downfield ($\Delta\delta = 1.5$ ppm) from where it appears in the ¹H NMR spectrum in the more competitive solvent DMSO-*d*₆. This downfield shift can only be a result of the presence of strong non-covalent interactions between [7]-helicenes and suggests the presence of cooperative hydrogen bonding. The significant upfield shift ($\Delta\delta = -0.97, 6 \times 10^{-3}$ M) of the signal corresponding to the N-H proton of 2-quinolinone **20** (see Figure 6), which can be considered to represent one of the hydrogen bond surfaces in **14b**, when the solvent is changed from DMSO-*d*₆ to CDCl₃ supports the involvement of cooperative hydrogen bonds in the association of **14b**.

^1H NMR studies of **14b** in CDCl_3 and $\text{THF-}d_8$ show the N-H resonance to be concentration independent ($\Delta\delta$ is unchanged over a 10^{-4} – 10^{-1} M range). Changing to a solvent such as pyridine- d_5 that competes more effectively for hydrogen bonds shows the N-H resonance to be concentration dependent. The data from the dilution experiment correlates well with calculated curves using a dimer binding model (although, as expected, it fits equally well to a polymer binding model) giving an association constant (K_a) of 207 M^{-1} (Figure 6). This value of K_a is much higher than would be expected if the two recognition surfaces are acting independently. More importantly, the association constant is also significantly higher than that calculated for the analogous dilution titration of 2-quinolinone **20** ($K_a < 1$). The position of the N-H resonance in the ^1H NMR spectrum ($\delta = 12.91\text{ ppm}$) for **20** is unchanged over a 10^{-4} – 10^{-2} M range and close to the chemical shift recorded for the most dilute solution of helicene **14b** ($\delta = 13.09\text{ ppm}$ at less than 10^{-5} M). The large discrepancy between the chemical shifts and the values of K_a for **14b** compared to **20** clearly indicates that cooperativity is the driving force for self-assembly.

These experimental observations would only result if **14b** exist as a dimer sewn together by four non-covalent bonding interactions. Molecular modeling shows that in order for **14b** to exist in this form, the building blocks within each dimer must be of the same helicity (*M* with *M* and/or *P* with *P*). This implies that there is enantiospecificity with respect to the building blocks and the possibility that the racemic fiber exists in solution can be eliminated. These observations, however, do not imply stereoselectivity and any of the proposed dimers in Figure 5 are reasonable under these conditions.

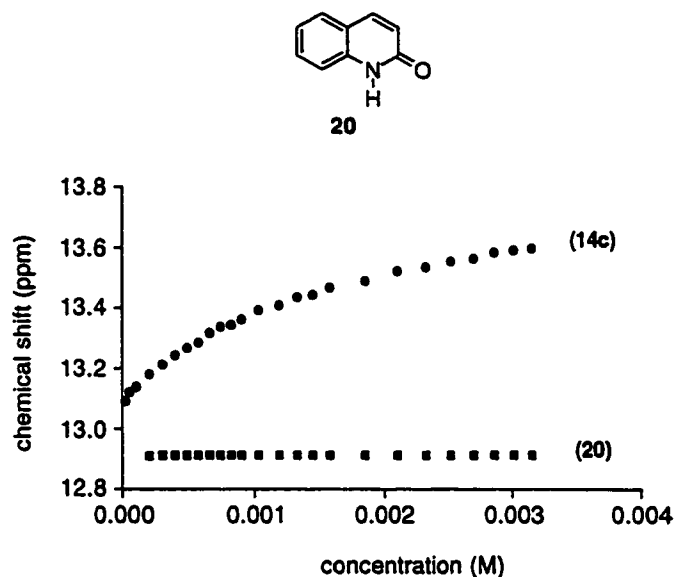


Figure 6. Concentration dependency of the chemical shift for the N-H proton in the ¹H NMR spectrum of [7]-helicene 14b and quinolinone 20 in pyridine-*d*₅.

3.3.3 X-ray Crystallographic Analysis

Single crystals of 18b suitable for X-ray crystallographic analysis were obtained by slow evaporation of a chloroform solution. The crystal structure reveals that racemate 18b exists in two conformations, where the benzyl groups are either convergent (top) or divergent (bottom) (Figure 7). Structural data for the helical scaffold of these two conformations is similar (Appendix II) and therefore will be discussed simultaneously. The bond lengths, bond torsional angles and intermolecular distances closely resemble those found in crystal structures of other [7]-helicenes.^{15c,24} The distortion from planarity influences double bond character and hence double bond length. The outer bonds (C(9)-C(10), C(6)-C(7), C(15)-C(16) and C(18)-C(19)) are shortened to 1.343-1.361 Å (standard aromatic bond length in benzene is 1.39 Å) while the inner bonds (C(24)-C(25) and C(28)-C(1)) are lengthened to 1.428–1.464 Å. The torsional angles along the inner

helical rim varies from $\approx 18^\circ$ for C(2)-C(1)-C(28)-C(27) to $\approx 27^\circ$ for C(25)-C(26)-C(27)-C(28). This deviation from planarity is confirmed by analysis of the ^1H NMR spectrum. Here, the protons on interior of the helicene (C2(23) $\delta = 5.90$) resonate at higher field than the protons on the exterior of the helicene ($\delta \approx 7.80$), suggesting that the interior protons are in the shielding zone exerted by helicene.

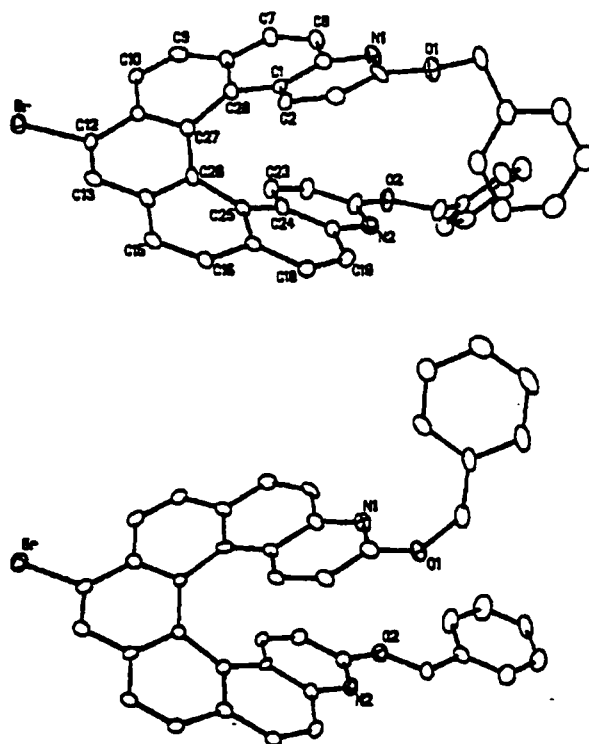


Figure 7. X-ray crystal structure of the two conformations of protected [7]-helicene **18b**.

X-ray crystallographic structure determination of the deprotected helicenes could not be accomplished as crystals of **14b** showed twinning, rendering this particular

helicene inappropriate for investigating the stereodiscrimination in the solid-state. We, therefore, focused our attention on replacing the bromine in helicene **14b** with a more utilitarian side group. Palladium and CuI co-catalyzed coupling of TMS-acetylene with **18b** yielded the ethynyl helicene **18c** (Scheme 1). Treatment of **18c** with trifluoroacetic acid cleanly liberated the pyridinone hydrogen bond sites and simultaneously deprotected the TMS-acetylene moiety generating methylketone derivative **14c** in nearly quantitative yield.

X-ray quality single crystals of **14c** were isolated by slowly diffusing pentane into a chloroform solution of the [7]-helicene. The crystal structure reveals what was already observed in the solution experiments of **14b**, analogue **14c** exists solely as a dimer (Figure 8). What is more significant is that a diastereoselective recognition process has taken place and only homochiral dimers where the R-groups exist exclusively in a *cis*-relationship appear in the crystal. These enantiomerically pure dimers are held together by four strong intermolecular hydrogen bonds (N...O distance of 2.740 and 2.829 Å) between the two pyridinone residues.

The dimers are similar in nature to one previously observed by Tanaka and co-authors.^{15d} These authors describe a bifunctional [7]-helicene that contains a terminus hydroxythiophene ring and a terminus pyridine ring. The crystal structure reveals a pair of intermolecular hydrogen bonds between the hydroxy group of one helicene to the pyridine nitrogen atom of an adjacent molecule. Here, the crystals were enantiomerically pure because the starting solution was also enantiomerically pure.

The bond lengths, bond torsional angles and intermolecular distances of **14c** closely resemble those found in the crystal structure of protected [7]-helicene **18b**. Once

again, significant C,C-bond alternation is observed in the helicene. The outer bonds (C(9)-C(10), C(6)-C(7), C(15)-C(16) and C(18)-C(19)) are shortened to 1.340-1.352 Å while the inner bonds (C(24)-C(25) and C(28)-C(1)) are lengthened to 1.427-1.458 Å. The torsional angles along the inner helical rim range from 20.8(16)° for C(2)-C(1)-C(28)-C(27) to 27.9(16)° for C(25)-C(26)-C(27)-C(28). The overlapping terminal rings in **14c** are separated by greater than van der Waal's half-radii of an aromatic ring on the outside of the helicene (C(22)-C(5) = 3.807(15) Å; C(20)-C(3) = 3.859(15) Å) but come into close contact on the interior of the helicene (C(23)-C(1) = 3.149(15) Å; C(24)-C(2) = 3.185(15) Å).

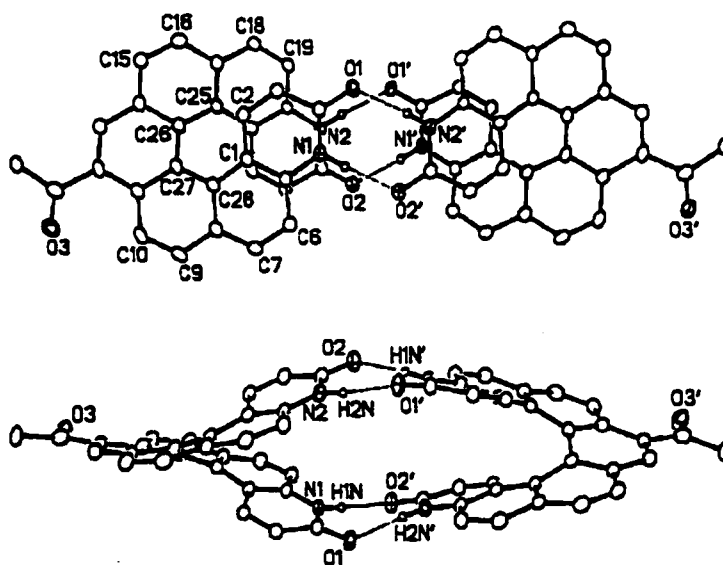


Figure 8. Two views of the X-ray diagram of one of the enantiomerically pure hydrogen-bonded dimers.

The packing diagram of **14c** shows that the homochiral dimers arrange into offset racemic columns where the benzene rings of the *P* and *M* diastereomers are orientated in

a face-to-face type orientation with an average distance of 3.64 Å between aromatic rings (Figure 9). The fact that the crystal is composed of racemic dimers reveals that the stereodiscrimination occurs at the molecular and not at the macroscopic level.

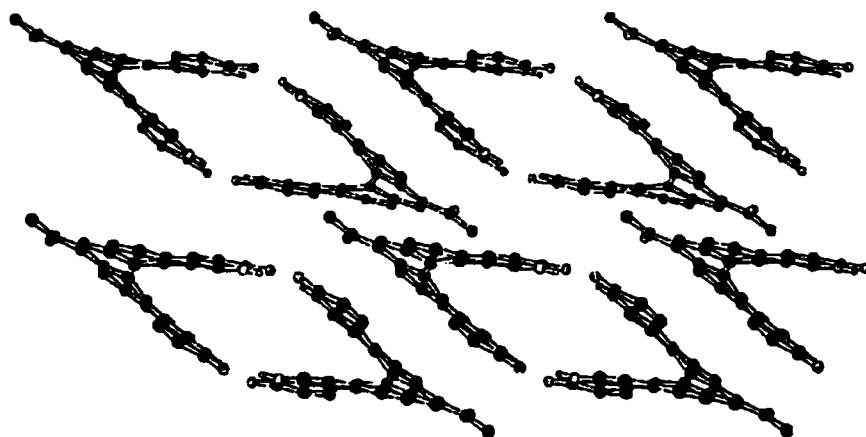


Figure 9. Packing diagram of [7]-helicene **14c**.

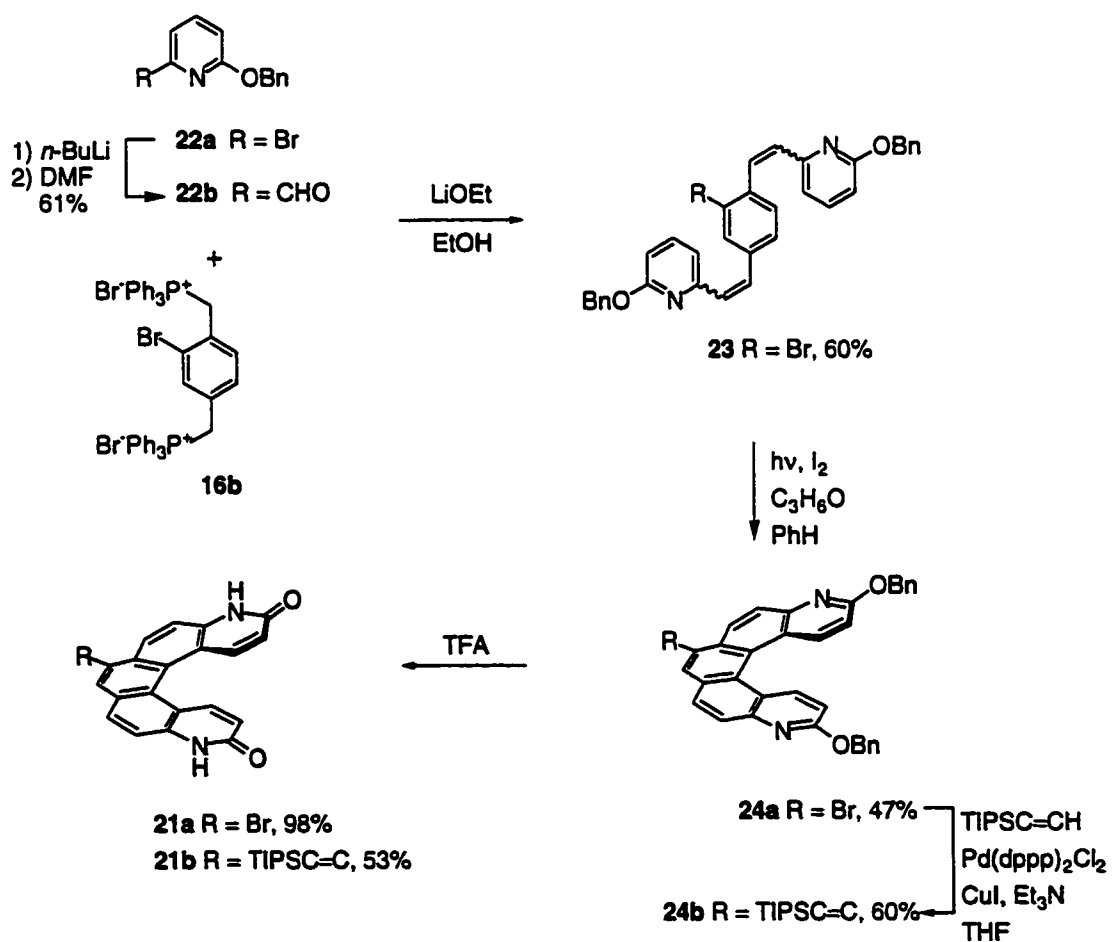
3.4 [5]- and [9]-Helicene: Results and Discussion

3.4.1 Synthesis

The concept of controlling the structure and function of heterocyclic helicenes was further investigated in derivatives **21** and **25**, which bear different orientations of the hydrogen bond vectors, by varying the number of aromatic rings. These compounds were prepared in an analogous manner to [7]-helicene **14** as depicted in Schemes 2 and 3. The route to **21** began with a Wittig reaction between phosphonium salt **16b** and 6-benzyloxy-2-pyridinecarboxaldehyde **22b** to afford an isomeric mixture of **23** (Scheme 2). Irradiation of the isomeric mixture of **23** in the presence of iodine led to protected [5]-helicene **24a**,

whose structure was confirmed by X-ray crystallography (see section 3.4.3 for analysis). Deprotection with neat TFA gave sparingly soluble [5]-helicene **21a**. Because of solubility concerns, we sought to replace the bromine with a more suitable side group. Palladium- and CuI- co-catalyzed coupling of TIPS-acetylene with **24a** gave **24b**. Treatment of **24b** with TFA cleanly freed the lactam hydrogen bonding sites while leaving the solubilizing TIPS-acetylene group unscathed to produce soluble [5]-helicene **21b**.

Scheme 2

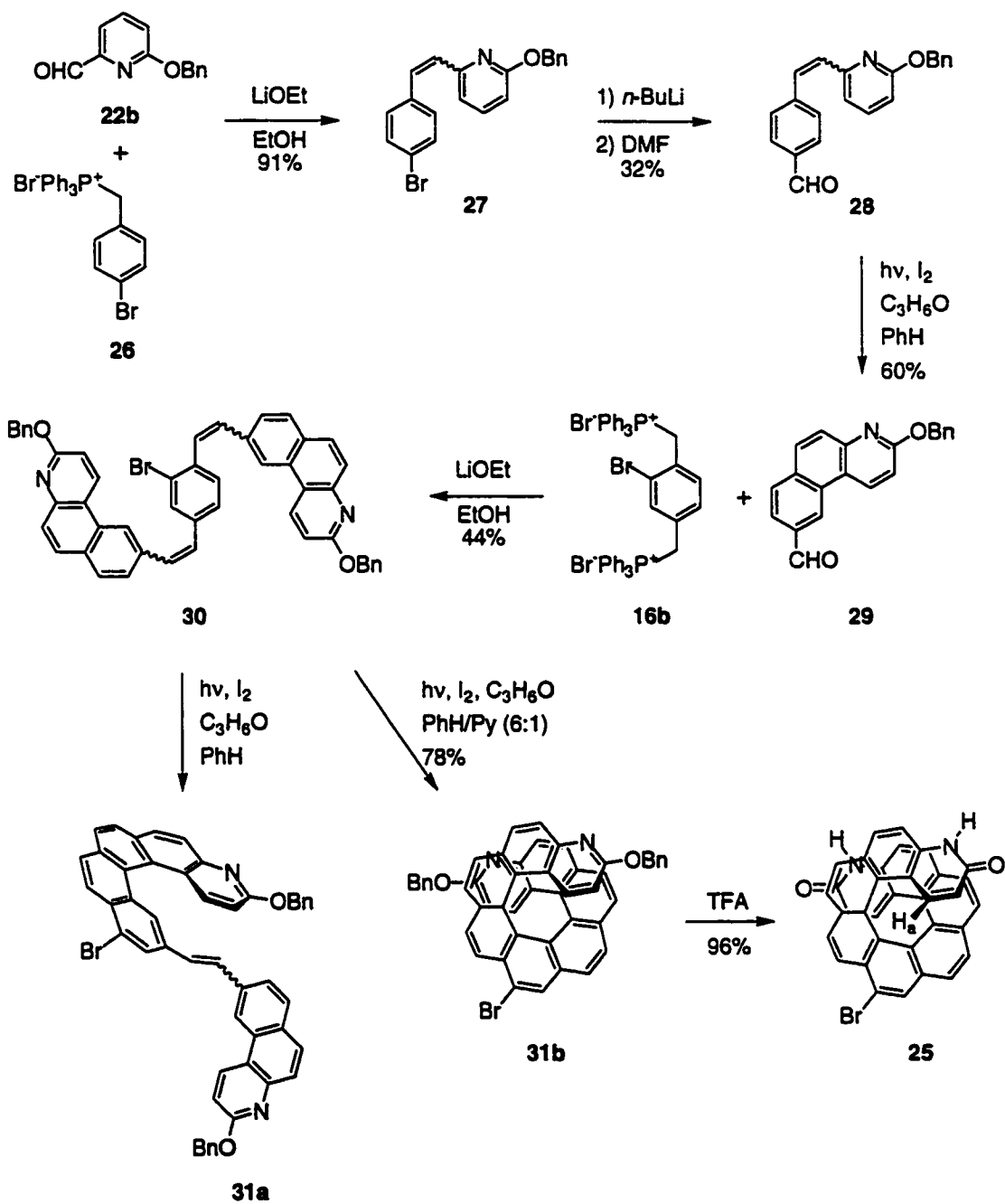


[9]-helicene **25** was prepared in a similar manner, with two photocyclization reactions used as key steps in the synthesis (Scheme 3). Condensation of aldehyde **22b** with mono-phosphonium salt **26** led to a mixture of *cis*- and *trans*-**27**. Bromide **27** was transformed into aldehyde **28** by lithium–halogen exchange with *n*-BuLi followed by formylation with dry DMF. The photocyclodehydrogenation of **28** in the presence of iodine and propylene oxide gave [3]-helicene **29**. Treatment of **29** with ylid **16b** afforded **30** as a mixture of isomers. Interestingly, photocyclization of **30**, in benzene, gave only partially cyclized product **31a**. We attribute the lack of complete photocyclodehydrogenation to the low solubility of **31a**. Changing the solvent system to 6:1 (benzene/pyridine) cleanly afforded the desired double photocyclization reaction to result in **31b**. Deprotection of the benzyl moiety on **31b** with TFA produced target [9]-helicene **25** in 13% overall yield.

3.4.2 Solution-State Studies Using ¹H NMR Analysis

The formation of all the helicenes in Schemes 2 and 3 was easily confirmed by the characteristic upfield chemical shifts in the ¹H NMR spectra. The ¹H NMR signal for the H_a protons of helicenes **14b** and **25** show particularly large upfield shifts (5.63 and 5.88 ppm, respectively) compared to the corresponding resonances in the olefinic precursors (6.96 and 7.16 ppm) or in helicene **21b** (6.45 ppm). These results indicate that helicenes **14b** and **25** have a full turn of a helix, since chemical shifts for the protons of the terminal aromatic rings are dependent on the degree of overlapping of the two terminal rings. In other words, the helical structure orients the protons directly into the

Scheme 3



shielding anisotropic regions of the aromatic rings and hence these protons experience shielding of the terminal rings.

Determination of the self-assembling behavior of **21b** and **25** was attempted using ¹H NMR spectrometry dilution studies. Unfortunately, both **21b** and **25** were only sparingly soluble in non-competitive solvents such as chloroform, thereby allowing access to only a very small part of the dilution curve. However, these studies do indicate that binding between synthons is occurring as confirmed by the upfield shift of the signal corresponding to the N-H proton upon dilution. Changing to a more competitive solvent such as pyridine-*d*₅ shows the N-H resonance to be concentration independent. These results are analogous to the dilution titration of 2-quinolinone **20** (Figure 6) suggesting that pyridine is effectively competing for the hydrogen bonding sites and hence renders the analysis of the self-assembly process in this solvent system futile.

Vapor-phase osmometry (VPO) and electrospray mass spectrometry (ES-MS) could provide some insight into the stoichiometry of these aggregates, but to date the results have not been promising. The hydrogen bond surfaces have proven to be too weak to maintain the aggregates' composition during the electrospray process while limited solubility has hampered VPO studies.

3.4.3 X-ray Crystallographic Analysis

X-ray quality single crystals of **24a** were isolated by slow evaporation of a chloroform solution of protected [5]-helicene. Standard parameters used to evaluate helical molecules (bond lengths, bond torsional angles and intermolecular distances) show that the crystal structure of **24a** closely resembles that of other crystal structures of [5]-helicenes, and confirms the main structural features of the receptor (Figure 10).²⁵ Further analysis reveals that the angles between the two planes varies from 22° (C(3)-

C(4)-C(9)-C(9')) to 25° (C(4)-C(9)-C(9')-C(4')), indicating that the strain is located in the inner aromatic rings. Hence, the outer bonds C(6')-C(7'), C(10')-C(10) and C(6)-C(7) are shortened to 1.352 (3) Å whereas the inner bonds distances C(3)-C(4), C(4)-C(9) and C(9)-C(9') are lengthened to 1.409-1.451 Å.

The packing diagram of racemate **24a** shows that the helicenes stack into enantiomerically pure columns, which are arranged into, offset racemic columns (Figure 10). The benzyl rings of the *P* and *M* enantiomers are orientated in a manner that maximizes π - π interactions (average distance between aromatic rings is 3.69 Å).

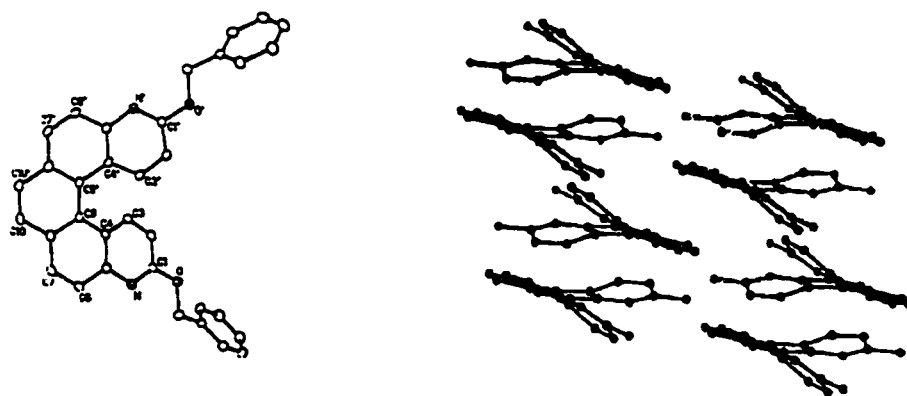


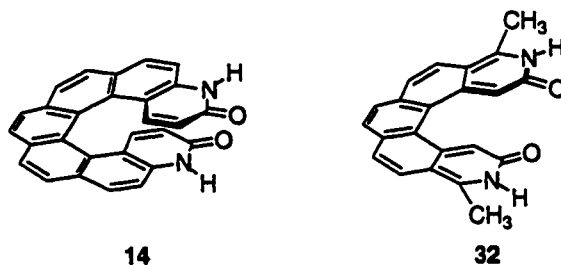
Figure 10. X-ray crystal structure and packing diagram of [5]-helicene **24a**. Hydrogen atoms and benzyl protecting groups in the packing diagram have been removed for clarity.

To date, X-ray quality crystals of either deprotected [5]-helicene **21a** or **21b** or [9]-helicene **25** have not been attainable. It is possible, though, to envisage these compounds self-associating in order to maximize all interactions such as hydrogen bonding and π - π stacking which may result in the organized helical conformations.

3.5 Alternate Helicenes

Controlling the formation of different helical aggregates can be achieved by manipulating the directionality of the hydrogen bond vectors. In helicenes **14**, **21** and **25** this was accomplished by varying the number of aromatic rings. An alternative approach is to alter the recognition elements' placement on the helicene scaffold.

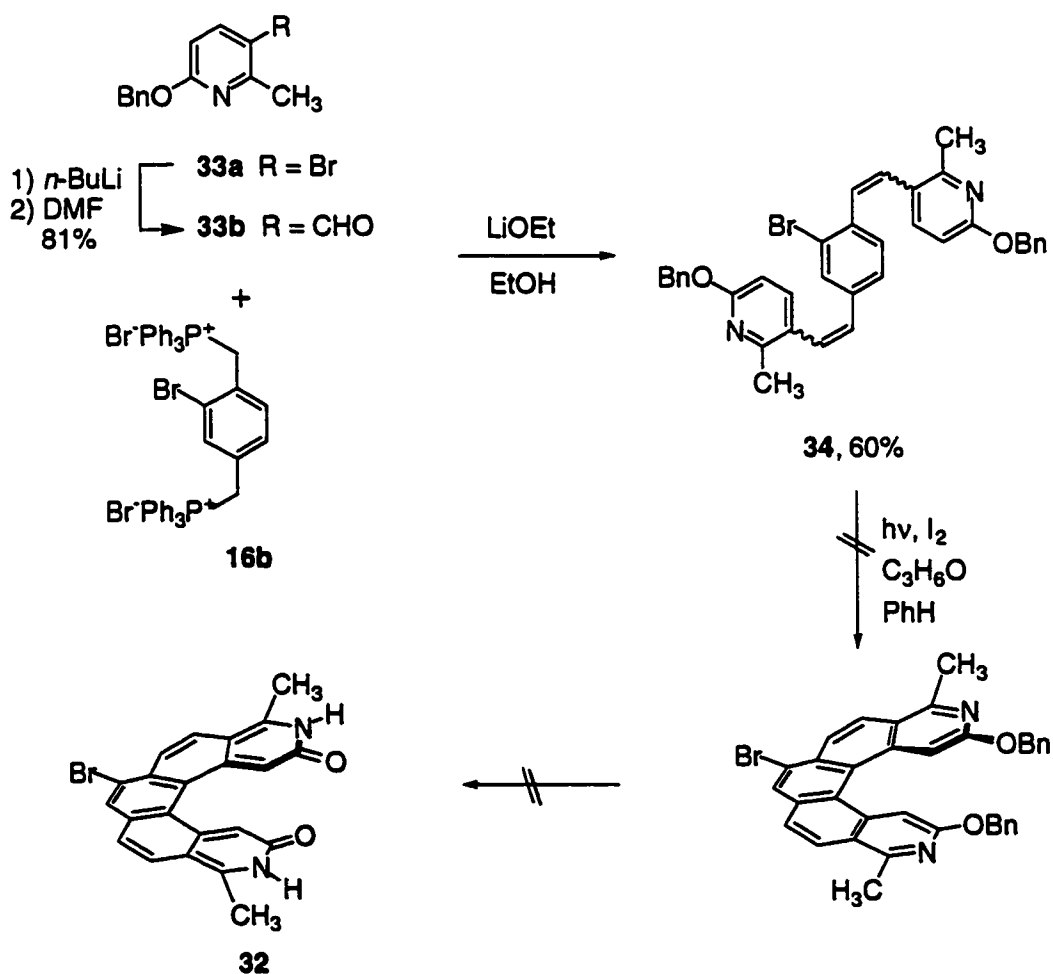
Moving the two lactam recognition sites from the *ortho* positions as seen in the previous helicenes to the *meta* position as depicted in target helicene **32**, greatly alters the hydrogen bonding directional vectors and should result in supramolecular aggregates with very different structural characteristics.



Synthesis of **32** began with a Wittig reaction between phosphonium salt **16b** and synthon **33** (Scheme 4) to afford an isomeric mixture of bis-stilbene **34**. Aldehyde **33** was chosen for two key reasons. First, the design incorporates the proper placement of the protected lactam recognition sites so that on cyclization the substituents will be in the desired *meta* position. Second, the introduction of the methyl substituent onto the 2 position effectively blocks one cyclization pathway to promote the formation of desired helicene **32**. Irradiation of bis-stilbene **34** in the presence of iodine, however, did not result in target molecule **32**. Instead a large mixture of unidentifiable products,

presumable due to degradation, was observed. We attribute the lack of desired photocyclized product to electronic effects. In the same manner that the inductively electron withdrawing bromine substituent prohibits ring systems from cyclizing to its adjacent *ortho* carbon sites,²⁰ an electron withdrawing nitrogen atom in a heterocycle forbids ring systems from cyclizing to the carbon atoms that are *ortho* or *para* to it, hence preventing the above pericyclic reaction from occurring.

Scheme 4



3.6 Diazahelicenes as Helical Catalysts

Recently, Fu and co-workers have developed a series of metal complexes that bear π -bound nitrogen heterocycles (Figure 11).²⁶ These complexes serve as effective nucleophilic catalysts for a range of processes, including the acylation of alcohols with diketene and the ring opening of azalactones. In this molecule it is the heterocyclic nitrogen, not the metal, that is acting as the catalyst. To achieve asymmetric catalysis, though, the nitrogen must be in a chiral environment. This was accomplished by differentiating the left side of the heterocycle from the right side and the top from the bottom. These key features are highlighted in Figure 11.

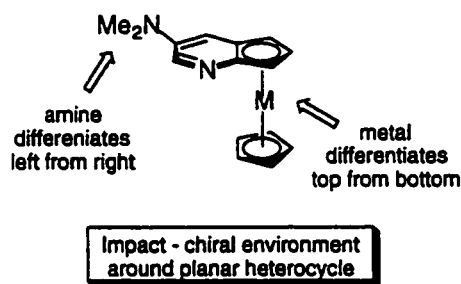


Figure 11. Key structural features required for nucleophilic catalyst

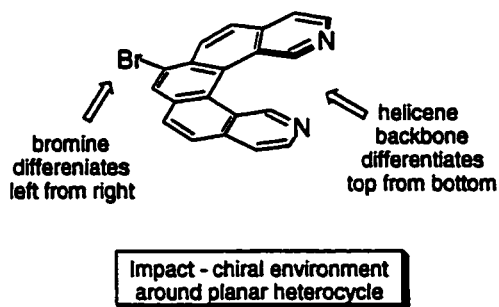


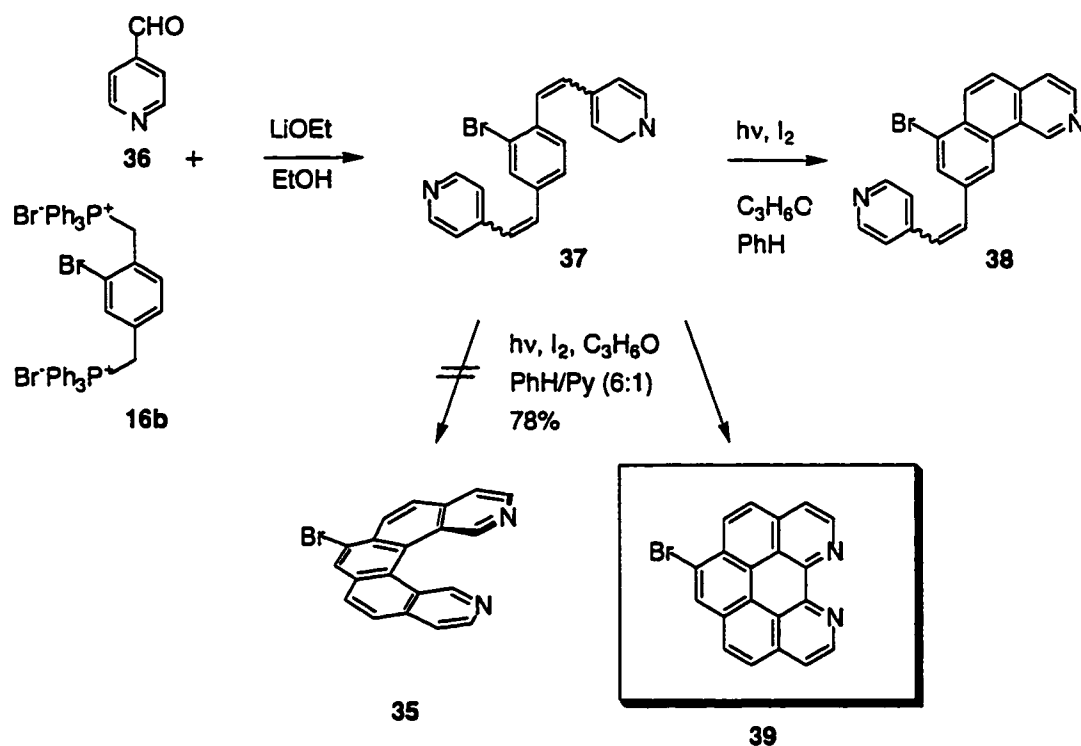
Figure 12. Structural features present in diaza[5]-helicene

Intrigued by this body of work, we envisioned designing a simple planar nucleophilic catalyst based on 3,12-diaza[5]-helicene backbones such as compound **35** (Figure 12). Molecule **35** was designed for this study because of ease of synthesis as well as its potential to promote asymmetric catalysis via the rigid chiral helicene scaffold as depicted in Figure 12.

3.6.1 Synthesis

The attempted synthesis of parent diazahelicene **35** began with the condensation of commercially available 4-pyridinecarboxaldehyde **36** with **16b** to give an isomeric mixture of bis-stilbene **37** (Scheme 5). Irradiation of **37**, in benzene, only gave partially cyclized product **38** as confirmed by the characteristic upfield chemical shifts of the remaining olefinic protons in the ^1H NMR spectrum. Once again, the lack of complete photocyclodehydrogenation can be attributed to the low solubility of **38** in benzene. Changing the solvent to 6:1 (benzene/pyridine) did not afford the desired diazahelicene **35** but instead produced over oxidized **39**. The identity of this product was confirmed by ^1NMR spectroscopy and high resolution mass spectrometry. In both spectra, the loss of two protons is clearly evident which led to the conclusion that the photocyclization product was compound **39**. Altering reaction conditions such as amount and type of oxidizing agent along with varying irradiation times (1-6 h) did not change the outcome. This type of over oxidization has been seen before²⁷ and is most common in electron deficient [5]-helicenes (such as **39**). It has been suggested that during the readily occurring racemization process the planar electron deficient transition state is ideal to promote a second dehydrogenation reaction.

Scheme 5



3.7 Conclusions

The design of molecules that self-assemble into predictable stereochemically pure supramolecular architectures has long been a goal of chemists. To achieve this goal a number of design criteria must be including choice of recognition elements used to guide the formation of polynuclear aggregates and choice of scaffold upon which to place the recognition elements. To this end, the above studies show that the conformational rigidity of helicene backbones is ideal to induce selective recognition. The pronounced asymmetric character provided by helical chirality coupled with limited racemization of the larger helicene scaffold results in a scrupulous receptor. Further, the lactam-lactam interaction provided by the two pyridinone heterocycles affords a strong bonding pattern.

that is required for aggregation. Unfortunately, attempts to study the effects of altering the hydrogen bonding vectors, by changing directionality and number of aromatic rings, on the self-assembly process were unsuccessful. The major disadvantages of this approach can be grouped into two areas, the first being solubility. The contrast of water soluble hydrogen bonding arrays to organic soluble aromatic surfaces is too great. A perfect example of this is shown in the [5]-helicene model. Replacement the bromine substituent with a triisopropyl (TIPS) moiety did increase the observed solubility of **14** in organic solvents, but the solubility was limited at best. The second design feature that must be addressed to make helicenes viable as selective supramolecular receptors in the solid-state is to uncover the forces that govern the crystal packing of helicenes. In all of the crystals structures presented in this chapter, the helicenes packed into enantiomerically pure columns, mostly likely as a result of favorable π - π stacking, but the columns always pack laterally as a racemate. Clearly, there is little or no selective recognition taking place in that direction of crystal growth. Perhaps tailoring the easily functionalized bromine moiety with another recognition element will promote autoresolution at both the molecular and supramolecular level.

3.8 Experimental

For a general description of apparatus, materials and methods see Chapter 2.

General procedure for photocyclizations.

The photoreactor was a 1.0 L cylindrical Pyrex vessel with an immersion well connected through a standard taper 50/60 ground glass joint. Attached to the upper part of the reaction vessel were gas-inlet and outlet joints, with the gas outlet leading to a silicon oil bubbler. There also was a third joint attached to the upper part of the vessel for monitoring of samples. The vessel was flat-bottomed to allow a magnetic stirring bar to rotate. The immersion well was a double-walled Pyrex tube cooled by water and contained a Hanovia 450-W high-pressure quartz Hg-vapor lamp.

Procedure for photoirradiation in the presence of propylene oxide.

Argon was bubbled through the stirred solution of the appropriate stilbene derivative and iodine in benzene for 20-30 min before excess propylene oxide was added. The lamp was then turned on and the argon flow was decreased but maintained throughout the procedure. The photoirradiation was monitored by the disappearance of the iodine color achieved by taking aliquots via the third joint. This typically took 8–12 h. The resulting solutions were then evaporated under pressure to dryness.

3.8.1 Synthesis of [7]-Helicene (14)

2-Benzyloxy-6-bromoquinoline (15a). A suspension of 6-bromoquin-2-ol (2.7 g, 12 mmol), silver carbonate (7.0 g, 25 mmol) and benzyl bromide (2.7 g, 16 mmol) in chloroform was stirred in the dark for 48 h. The silver salts were filtered off and the filtrate was purified by normal phase chromatography over silica gel (9:1 hexane/EtOAc) to afford 3.0 g (79%) of a pure white solid. mp 79–80 °C; ¹H NMR (300 MHz, CDCl₃) δ:

7.89 (d, $J = 9.0$ Hz, 1H), 7.85 (d, $J = 2.0$ Hz, 1H), 7.71 (s, 1H), 7.68 (d, $J = 2.0$ Hz, 1H), 7.50 (m, 2H), 7.35 (m, 3H), 6.95 (d, $J = 9.0$ Hz, 1H), 5.51 (s, 2H); ^{13}C NMR (300 MHz, CDCl_3) δ : 162.12, 145.26, 137.83, 137.09, 132.79, 129.55, 129.06, 128.55, 128.36, 128.04, 126.45, 117.33, 114.32, 67.92; FT-IR (microscope): 3030, 2938, 2876, 1612, 1598, 1299 cm^{-1} ; ES-MS m/z : calcd for $\text{C}_{16}\text{H}_{12}\text{BrNO}$ 315, found 316.0 $[\text{M} + \text{H}]^+$.

2-Benzoyloxy-6-quinolinecarboxaldehyde (15b). A solution of *n*-BuLi in hexanes (1.4 mL, 3.5 mmol) was added dropwise to a solution of **15a** (840 mg, 2.7 mmol) in dry THF (35 mL) at -78 °C. After 1 h, dry DMF (0.27 mL, 3.5 mmol) was added and the mixture was stirred at -78 °C for 45 min and then allowed to warm to room temperature. The reaction was quenched with NH_4Cl (50 mL), extracted with ether (3 x 30 mL), dried over MgSO_4 and evaporated to dryness. Purification by normal phase chromatography over silica gel (16:1 hexane/EtOAc) afforded 290 mg (42%) of the product as a white solid. ^1H NMR (300 MHz, CDCl_3) δ : 10.11 (s, 1H), 8.21 (d, $J = 2.0$ Hz, 1H), 8.11 (d, $J = 8.7$ Hz, 2H), 7.94 (d, $J = 8.7$ Hz, 1H), 7.49 (m, 2H), 7.34 (m, 3H), 7.03 (d, $J = 8.7$ Hz, 1H), 5.57 (s, 2H); ^{13}C NMR (300 MHz, CDCl_3) δ : 191.48, 163.85, 150.27, 139.86, 136.80, 132.70, 132.54, 128.60, 128.44, 128.18, 127.70, 124.66, 114.68, 68.26; FT-IR (microscope): 3039, 2893, 1734, 1689, 1621 cm^{-1} ; ES-MS m/z : calcd for $\text{C}_{17}\text{H}_{13}\text{NO}_2$ 263, found 264.0 $[\text{M} + \text{H}]^+$.

Bis-stilbene (17a). To a solution of *t*-BuO $^-\text{K}^+$ (500 mg, 4.4 mmol) in methanol (100 mL) was added *p*-xylylenebis(triphenylphosphonium bromide) **16a** (460 mg, 0.58 mmol).

After stirring at room temperature for 20 min, a solution of **15b** (290 mg, 1.1 mmol) in methanol (20 mL) was added and the reaction was stirred for 12 h. After the mixture was stirred overnight, the *trans, trans* product was filtered off and the filtrate was evaporated to dryness, dissolved in CHCl₃, washed with water (2 x 10 mL), brine (2 x 10 mL), dried over MgSO₄ and evaporated to dryness. Purification by normal phase chromatography over silica gel (9:1 hexane/EtOAc) afforded 210 mg (64%) of pure product as a yellow solid, as a mixture of isomers. ¹H NMR (300MHz, DMSO-*d*₆) δ : 8.20 (dd, *J* = 9.1, 18.1 Hz, 1H), 8.16 (dd, *J* = 9.1, 9.1 Hz, 1H), 7.98 (m, 2H), 7.81–7.26 (m, 14H), 7.12 (s, 2H), 7.05 (m, 2H), 6.70 (m, 3H), 5.49 (s, 2H), 5.46 (s, 2H); FT-IR (microscope): 3060, 3031, 2963, 1616, 1600 cm⁻¹; ES-MS *m/z*: calcd for C₄₂H₃₂N₂O₂ 596, found 597.2 [M + H]⁺.

3,16-Dibenzyloxy-4,15-diaza[7]-helicene (18a). A solution of **17a** (140 mg, 0.24 mmol) and iodine (120 mg, 0.47 mmol) in dry benzene (600 mL) was degassed with argon for 1/2 h. Propylene oxide (5 mL) was added and the mixture was irradiated with a 400 W mercury lamp, while under an argon atmosphere, for 12 h. The mixture was evaporated to dryness and purified by normal phase column chromatography over silica gel (9:1 hexane/EtOAc). The isolated compounds were then purified again over silica gel (0.25% MeOH/CH₂Cl₂) to afford 80 mg (58%) of the product as a white solid. ¹H NMR (300 MHz, CDCl₃) δ : 9.44 (d, *J* = 9.0 Hz, 2H), 9.37 (s, 2H), 8.08 (s, 2H), 8.05 (d, *J* = 9.4 Hz, 2H), 7.86 (d, *J* = 9.0 Hz, 2H), 7.65 (m, 2H), 7.48 (m, 3H), 7.21 (d, *J* = 9.0 Hz, 2H), 5.67 (s, 4H); ¹³C NMR (300 MHz, CDCl₃) δ : 161.51, 147.45, 138.38, 137.40, 136.59, 131.73,

130.53, 129.68, 128.60, 128.51, 128.45, 128.04, 127.80, 127.64, 127.51, 127.34, 121.94, 117.03, 112.25, 67.89; ES-MS m/z : calcd for $C_{42}H_{28}N_2O_2$ 591.0, found 592.2 $[M + H]^+$.

4,15-Diaza[7]helicene-3,16-dione (14a). A solution of protected [7]-helicene **18a** (130 mg, 0.3 mmol) in TFA (5 mL) was stirred at room temperature for 12 h. Evaporation of the trifluoroacetic acid followed by trituration with Et_3N , in acetone, afforded quantitative yields of the deprotected [7]-helicene. 1H NMR (300 MHz, $CDCl_3$) δ : 9.29 (s, 2H), 9.15 (d, $J = 10.0$ Hz, 2H), 8.16 (d, $J = 9.0$ Hz, 2H), 8.13 (d, $J = 9.0$ Hz, 2H), 7.85 (d, $J = 9.0$ Hz, 2H), 7.69 (d, $J = 9.0$ Hz, 2H), 6.78 (d, $J = 9.0$ Hz, 2H).

1-Bromo-2,5-bis-(bromomethyl)benzene. A suspension of 2-bromo-*p*-xylene (15 g, 81 mmol) and NBS (30 g, 166 mmol) in benzene (1.5 L) was degassed with argon for 1 h. Maintaining the stream of argon the mixture was irradiated using a 200 W UV light for 2 h. After the reaction was complete the mixture was evaporated to dryness, dissolved in CH_2Cl_2 , washed with water (3 x 150 mL), dried over $MgSO_4$, and the succinamide side product was removed through a small plug of silica gel (9:1 hexane/EtOAc). The product was further purified by column chromatography over silica gel (hexane) to afford 17.0 g (62%) of a pure white solid. 1H NMR (300 MHz, $CDCl_3$) δ : 7.60 (d, $J = 2.1$ Hz, 1H), 7.41 (d, $J = 7.8$ Hz, 1H), 7.30 (dd, $J = 2.1, 7.8$ Hz, 1H), 4.56 (s, 2H), 4.39 (s, 2H).

(2-Bromo-1,4-phenylene) bis(methylene) bis(triphenylphosphonium) dibromide (16b). To a solution of 1-bromo-2,5-bis-(bromomethyl)benzene (6.3 g, 18 mmol) in DMF

(200 mL) was added triphenylphosphine (10 g, 39 mmol) and the reaction was brought to reflux for 48 h. The solution was cooled and the addition of ether (250 mL) precipitated a solid. The solid was filtered and recrystallized from $\text{CHCl}_3/\text{Et}_2\text{O}$ to afford 22.3 g (54%) of a pure white solid. mp 260 °C; ^1H NMR (300 MHz, CDCl_3) δ : 7.67 (m, 30H), 7.27 (dd, J = 2.4, 8.7 Hz, 1H), 6.89 (d, J = 2.4 Hz, 1H), 6.87 (d, J = 8.4 Hz, 1H), 5.63 (d, J = 14.0 Hz, 2H), 5.42 (d, J = 14.0 Hz, 2H).

Bis-stilbene (17b). *n*-BuLi in hexanes (0.67 mL, 2.5M, 1.7 mmol) was added under argon dropwise to cold (-78 °C) dry ethanol (10 mL). After it had been warmed to room temperature and stirred until homogeneous, the solution was transferred by cannula to a slurry of 2-benzyloxy-6-quinolinecarboxaldehyde **15b** (200 mg, 0.8 mmol) and (2-bromo-1,4-phenylene)bis(methylene)bis(triphenylphosphonium) dibromide **16b** (360 mg, 0.4 mmol) in dry EtOH (20 mL) under argon. After the mixture was stirred overnight, the *trans, trans* product was filtered off (20 mg, 8%) and the filtrate was evaporated to dryness, dissolved in CHCl_3 , washed with water (2 x 10 mL), brine (2 x 10 mL), dried over MgSO_4 and evaporated to dryness. Purification by normal phase chromatography over silica gel (3:1 hexane/EtOAc) afforded 184 mg (72%) of pure product as a yellow solid, as a mixture of isomers (overall yield of 79%). ^1H NMR (300 MHz, CDCl_3) δ : 8.00 (d, J = 8.7 Hz, 1H), 7.98 (d, J = 8.7 Hz, 1H), 7.87–7.17 (m, 23H), 7.10 (d, J = 16.2 Hz, 1H), 6.96 (d, J = 8.7 Hz, 1H), 5.54, (s, 4H); ^{13}C NMR (300 MHz, CDCl_3) δ : 162.16, 146.60, 146.58, 142.60, 142.56, 140.10, 140.08, 138.90, 138.84, 138.32, 137.28, 136.00, 133.09, 132.87, 131.06, 131.00, 130.73, 130.62, 129.55, 129.40, 128.55, 128.37, 128.00,

127.88, 127.83, 127.64, 127.34, 127.11, 126.84, 126.61, 126.29, 126.21, 125.67, 125.42, 124.68, 123.89, 120.11, 113.80, 67.85; FT-IR (microscope): 3063, 3032, 2930, 2885, 1724, 1600, 1277 cm^{-1} ; EI-HRMS m/z : calcd for $\text{C}_{42}\text{H}_{31}\text{BrN}_2\text{O}_2$ 676.15485, found 676.15413 $[\text{M}]^+$.

9-Bromo-3,16-dibenzyloxy-4,15-diaza[7]-helicene (18b). A solution of bis-stilbene **17b** (120 mg, 0.18 mmol) and iodine (90 mg, 0.36 mmol) in dry benzene (600 mL) was degassed with argon for 1/2 h. Propylene oxide (5 mL) was added, and the solution was irradiated for 12 h. After irradiation, the solution was evaporated to dryness and purified by normal phase chromatography over silica gel (9:1 hexane/EtOAc) to afford 112 mg (63% yield) of a pure yellow solid. ^1H NMR (300 MHz, CDCl_3) δ : 8.38 (d, $J = 8.7$ Hz, 1H), 8.30 (s, 1H), 7.98 (d, $J = 8.7$ Hz, 1H), 7.92 (d, $J = 8.7$ Hz, 1H), 7.89 (d, $J = 8.4$ Hz, 2H), 7.80 (d, $J = 8.4$ Hz, 2H), 7.70 (d, $J = 8.7$ Hz, 1H), 7.68 (d, $J = 8.7$ Hz, 1H), 7.40 (m, 8H), 7.10 (d, $J = 8.7$ Hz, 2H), 5.90 (d, $J = 9.0$ Hz, 2H), 5.37 (d, $J = 12.3$ Hz, 2H), 5.30 (d, $J = 12.3$ Hz, 2H); ^{13}C NMR (300 MHz, CDCl_3) δ : 161.20, 137.43, 134.65, 134.38, 132.40, 132.31, 130.48, 129.92, 129.53, 129.32, 128.51, 128.40, 127.96, 127.82, 127.63, 126.54, 125.24, 125.20, 124.90, 109.36, 102.42, 67.38; FT-IR (microscope): 3062, 3029, 2944, 1608, 1593, 1268 cm^{-1} ; EI-HRMS m/z : calcd for $\text{C}_{42}\text{H}_{27}\text{BrN}_2\text{O}_2$ 672.12354, found 672.11916 $[\text{M}]^+$.

9-Bromo-4,15-diaza[7]-helicene-3,16-dione (14b). A solution of protected [7]-helicene **18b** (130 mg, 0.3 mmol) in TFA (5 mL) was stirred at room temperature for 12 h,

evaporated to dryness, dissolved in CHCl_3 , washed with NaHCO_3 (2 x 6 mL), brine (2 x 6 mL), dried over MgSO_4 to afford 128 mg (98% yield) of a pure yellow solid. ^1H NMR (300 MHz, $\text{DMSO}-d_6$) δ : 13.45 (s, 2H), 8.52 (s, 1H), 8.38 (d, $J = 8.7$ Hz, 1H), 8.13 (d, $J = 8.7$ Hz, 2H), 8.08 (d, $J = 8.7$ Hz, 1H), 8.04 (d, $J = 8.4$ Hz, 1H), 7.96 (d, $J = 8.4$ Hz, 1H), 7.55 (d, $J = 8.4$ Hz, 1H), 7.52 (d, $J = 8.4$ Hz, 1H), 6.80 (d, $J = 9.6$ Hz, 1H), 6.79 (d, $J = 9.6$ Hz, 1H), 5.63 (d, $J = 9.9$ Hz, 2H); ^{13}C NMR (500 MHz, $\text{THF}-d_8$) δ : 163.03, 162.97, 140.04, 139.87, 136.55, 136.37, 133.82, 132.27, 132.09, 131.84, 131.84, 131.77, 129.82, 129.47, 129.44, 127.69, 127.69, 127.55, 126.87, 125.33, 124.73, 124.54, 122.65, 118.79, 118.71, 118.58, 115.43, 115.27; FT-IR (CH_2Cl_2 cast): 3052, 2923, 1652, 1455, 1122, 667 cm^{-1} ; ES-MS m/z : 491.1, 982.1; EI-HRMS m/z : calcd for $\text{C}_{28}\text{H}_{15}\text{BrN}_2\text{O}_2$ 492.02963, found 492.02954 $[\text{M}]^+$.

9-Trimethylsilylethynyl-3,16-dibenzyloxy-4,15-diaza[7]-helicene (18c). A solution of protected [7]-helicene **18b** (42 mg, 0.06 mmol) in $\text{Et}_3\text{N}/\text{THF}$ (10 + 3 mL) was degassed with argon for 45 min. TMS-acetylene (70 mg, 0.10 mL, 0.6 mmol) was added and the solution was degassed for another 15 min, after which $\text{Pd}(\text{PPh}_3)_2\text{Cl}_2$ (5 mg, 5% mol) and CuI (1 mg, 2.5% mol) were added and the reaction was allowed to stir at 90°C , under argon, for 72 h. The solution was evaporated to dryness, dissolved in CHCl_3 (15 mL), washed with water (3 x 5 mL), brine (5 mL), dried over MgSO_4 and evaporated to dryness. Purification by normal phase chromatography over silica gel (13:1 hexane/ EtOAc) afforded 26 mg (60% yield) of a pure yellow solid. ^1H NMR (300 MHz, CDCl_3) δ : 8.51 (d, $J = 8.4$ Hz, 1H), 8.27 (s, 1H), 8.01 (d, $J = 8.1$ Hz, 1H), 7.95 (d, $J = 9.0$

Hz, 1H), 7.91 (m, 4H), 7.69 (d, $J = 9$ Hz, 1H), 7.67 (d, $J = 9.0$ Hz, 1H), 7.35 (m, 8H), 7.19, (d, $J = 9.3$ Hz, 1H), 7.15 (d, $J = 9.3$ Hz, 1H), 5.91 (d, $J = 9$ Hz, 2H), 5.36 (d, $J = 12.3$ Hz, 2H), 5.29 (d, $J = 12.3$ Hz, 2H), 0.40 (s, 9H); ^{13}C NMR (500 MHz, CDCl_3) δ : 161.10, 161.04, 146.01, 137.38, 134.65, 134.39, 131.96, 131.88, 131.27, 130.25, 129.83, 129.48, 128.43, 128.04, 127.97, 127.90, 127.88, 127.74, 127.45, 125.85, 124.89, 124.22, 120.97, 120.91, 119.84, 109.20, 109.13, 102.87, 100.55, 67.31, 0.125; FT-IR (CHCl_3 cast): 3030, 2956, 2145, 1593, 1521, 1269 cm^{-1} ; EI-MS m/z : calcd for $\text{C}_{47}\text{H}_{36}\text{N}_2\text{O}_2\text{Si}$ 688.25458, found 688.25367 $[\text{M}]^+$.

9-Acetyl-4,15-diaza[7]helicene-3,16-dione (14c). A solution of protected TMS- [7]-helicene **18c** (12 mg, 1.7×10^{-5} mol) in TFA (6 mL), was stirred at room temperature for 12 h, evaporated to dryness, redissolved in CHCl_3 , washed with NaHCO_3 (2 x 6 mL), brine (2 x 6 mL), dried over MgSO_4 to afford 7.5 mg (94% yield) of a pure yellow solid. ^1H NMR (300 MHz, CDCl_3) δ : 13.70 (s, 2H), 8.87 (d, $J = 9.0$ Hz, 1H), 8.49 (s, 1H), 7.99 (m, 5H), 7.61 (d, $J = 9.0$ Hz, 1H), 7.59 (d, $J = 9.0$ Hz, 1H), 6.83 (d, $J = 9.0$ Hz, 1H), 6.76 (d, $J = 9.0$ Hz, 1H), 5.74 (dd, $J = 1.8, 9.3$ Hz, 2H), 2.97 (s, 3H); ^{13}C NMR (400 MHz, CDCl_3) δ : 201.57, 164.13, 138.53, 138.44, 136.61, 136.33, 135.20, 131.10, 130.91, 130.82, 130.45, 129.98, 129.91, 129.26, 128.67, 128.47, 128.37, 128.23, 126.58, 126.50, 126.45, 125.77, 125.11, 123.04, 118.74, 118.31, 117.72, 117.51, 115.11, 30.22; FT-IR (CHCl_3 cast): 2922, 2850, 1958, 1652 cm^{-1} ; ES-MS m/z : 455.1, 909.3; EI-HRMS m/z : calcd for $\text{C}_{30}\text{H}_{19}\text{N}_2\text{O}_3$ 455.13956 found 455.139213 $[\text{M}]^+$.

3.8.2 Synthesis of [5]-Helicene (21)

6-Bromo-2-benzyloxy pyridine (22a). A solution of benzyl alcohol (5.0 g, 46 mmol) in THF (10 mL) was added dropwise to a suspension of NaH (1.5 g, 42 mmol) in THF (250 mL). The mixture was allowed to stir at room temperature for 15 min, then 2,6-dibromopyridine (10 g, 63 mmol) was added and the reaction was brought to reflux for 12 h. The solution was poured into 5% NaHCO₃ (250 mL), extracted with ether (3 x 30 mL), dried with MgSO₄ and evaporated to dryness. Purification by column chromatography through silica gel (13:1 hexane/EtOAc) afforded 8.8 g (80%) of the product as yellow oil. ¹H NMR (300 MHz, CDCl₃) δ : 7.42 (d, J = 8.7 Hz, 1H), 7.35 (d, J = 8.7 Hz, 1H), 7.30 (d, J = 8.7 Hz, 2H), 7.28 (d, J = 8.7 Hz, 1H), 6.82 (d, J = 8.7 Hz, 2H), 5.30 (s, 2H).

6-Benzyloxy-2-pyridinecarboxaldehyde (22b). A solution of *n*-BuLi, in hexanes, (9.9 mL, 2.5 M, 16 mmol) was added dropwise to a solution of **22a** (3.8 g, 14 mmol) in dry THF (120 mL) at -78 °C. After 1 h, dry DMF (1.2 mL, 16 mmol) was added and the mixture was allowed to stir at -78 °C for 45 min and then allowed to warm to room temperature. The reaction was quenched with NH₄Cl (200 mL), extracted with ether (3 x 30 mL), dried over MgSO₄ and evaporated to dryness. Purification by column chromatography through silica gel (13:1 hexane/EtOAc) afforded 4.3 g (61%) of the product as a white solid. ¹H NMR (300 MHz, CDCl₃) δ : 9.96 (s, 1H), 7.71 (t, J = 8.0 Hz, 1H), 7.57 (d, J = 1.0 Hz, 1H), 7.55 (d, J = 1.0 Hz, 2H), 7.37 (m, 3H), 7.04 (d, J = 9.0 Hz, 1H), 5.47 (s, 2H).

Bis-stilbene (23). *n*-BuLi in hexanes (1.3 mL, 2.5M, 3.1 mmol) was added under argon dropwise to cold (-78 °C) dry ethanol (20 mL). After it had been warmed to room temperature and stirred until homogeneous, the solution was transferred by cannula to a slurry of 2-benzyloxy-6-pyridinecarboxaldehyde **22b** (600 mg, 2.8 mmol) and of (2-bromo-1,4-phenylene)bis(methylene)bis(triphenylphosphonium) dibromide **16b** (1.3 g, 1.5 mmol) in dry EtOH (100 mL) under argon. After the mixture was stirred overnight, the *trans, trans* product was filtered off (20 mg, 6%) and the filtrate was evaporated to dryness, dissolved in CHCl₃, washed with water (2 x 10 mL), brine (2 x 10 mL), dried over MgSO₄ and evaporated to dryness. Purification by normal phase chromatography over silica gel (18:1 hexane/EtOAc) afforded 460 mg of pure product as a yellow solid, as a mixture of isomers (overall yield of 60%). ¹H NMR (300 MHz, CDCl₃) δ : 7.84 (d, *J* = 8.4 Hz, 2H), 7.77 (d, *J* = 8.7 Hz, 2H), 7.70 (d, *J* = 1.5 Hz, 2H), 7.67 (d, *J* = 8.4 Hz, 2H), 7.48–7.15 (m, 9H), 6.78 (d, *J* = 16.2 Hz, 2H), 6.68 (d, *J* = 5.7 Hz, 2H), 6.65 (d, *J* = 6.0 Hz, 2H), 5.39 (s, 4H); FT-IR (CH₂Cl₂): 3067, 3033, 2945, 1632, 1571, 1447, 1294 cm⁻¹; EI-HRMS *m/z*: calcd for C₃₄H₂₇BrN₂O₂ 574.12561, found 574.12528 [M]⁺.

7-Bromo-3,12-dibenzyloxy-4,11-diaza[5]-helicene (24a). A solution of bis-stilbene **23** (230 mg, 0.40 mmol) and iodine (200 mg, 0.80 mmol) in dry benzene (600 mL) was degassed with argon for 1/2 h. Propylene oxide (5 mL) was added, and the solution was irradiated for 12 h. After irradiation, the solution was evaporated to dryness and purified by normal phase chromatography over silica gel (18:1 hexane/EtOAc) to afford 116 mg

(47% yield) of a pure yellow solid. ^1H NMR (300 MHz, CDCl_3) δ : 8.55 (d, $J = 9.0$ Hz, 1H), 8.44 (d, $J = 9.0$ Hz, 1H), 8.39 (d, $J = 9.0$ Hz, 1H), 8.16 (s, 1H), 8.09 (d, $J = 9.0$ Hz, 1H), 8.02 (d, $J = 8.6$ Hz, 1H), 7.97 (d, $J = 8.7$ Hz, 1H), 7.69 (m, 2H), 7.53 (m, 6H), 7.38 (m, 6H), 6.77 (d, $J = 9.0$ Hz, 2H), 5.62 (s, 2H), 5.60 (s, 2H); ^{13}C NMR (300 MHz, CDCl_3) δ : 167.79, 162.27, 161.90, 146.75, 139.20, 138.82, 137.20, 137.15, 132.53, 131.15, 130.91, 130.05, 129.13, 129.06, 128.91, 128.85, 128.58, 128.48, 128.07, 125.71, 122.04, 121.64, 121.12, 110.68, 68.21, 67.98, 67.93; FT-IR(microscope): 3064, 3031, 2955, 2872, 1726, 1596, 1561 cm^{-1} ; EI-HRMS m/z : calcd for $\text{C}_{34}\text{H}_{23}\text{BrN}_2\text{O}_2$ 570.09430, found 570.09617 $[\text{M}]^+$.

7-Bromo-4,11-diaza[7]helicene-3,12-dione (21a). A solution of protected [5]-helicene **24a** (30 mg, 0.06 mmol) in TFA (5 mL) was stirred at room temperature for 12 h, evaporated to dryness and triturated with Et_3N /acetone (1:3) to afford 22 mg (98% yield) of a pure yellow solid. ^1H NMR (300 MHz, $\text{DMSO}-d_6$) δ : 12.21 (s, 2H), 8.39 (d, $J = 9.3$ Hz, 1H), 8.27 (s, 1H), 8.14 (d, $J = 8.7$ Hz, 1H), 8.01 (d, $J = 9.6$ Hz, 1H), 7.98 (d, $J = 9.9$ Hz, 1H), 7.79 (d, $J = 9.0$ Hz, 1H), 7.69 (d, $J = 8.7$ Hz, 1H), 6.46 (d, $J = 10.0$ Hz, 1H), 6.45 (d, $J = 9.9$ Hz, 1H); ES-HRMS m/z : calcd for $\text{C}_{20}\text{H}_{11}\text{BrN}_2\text{O}_2$ 390.24, found 391.0 $[\text{M} + \text{H}]^+$.

7-Triisopropylsilyl ethynyl-3,12-dibenzyloxy-4,11-diaza[5]-helicene (24b). A solution of protected [5]-helicene **24a** (83 mg, 0.15 mmol) in Et_3N /THF (15 + 6 mL) was degassed with argon for 45 min. TIPS-acetylene (270 mg, 0.3 mL, 1.5 mmol) was added

and the solution was degassed for another 15 min, after which Pd(PPh₃)₂Cl₂ (5 mg, 5% mol) and CuI (1 mg, 2.5% mol) were added and the entire mixture was allowed to stir at 90°C, under argon, for 72 h. The solution was evaporated to dryness, dissolved in CHCl₃ (15 mL), washed with water (3 x 5 mL), brine (5 mL), dried over MgSO₄ and evaporated to dryness. Purification by normal phase chromatography over silica gel (18:1 hexane/EtOAc) afforded 51 mg (60% yield) of a pure yellow solid. ¹H NMR (300 MHz, CDCl₃) δ: 8.72 (d, *J* = 9.0 Hz, 1H), 8.46 (d, *J* = 9.0 Hz, 1H), 8.43 (d, *J* = 9.0 Hz, 1H), 8.11 (s, 1H), 8.10 (d, *J* = 9.0 Hz, 1H), 8.03 (d, *J* = 9.0 Hz, 1H), 8.00 (d, *J* = 9.0 Hz, 1H), 7.56 (m, 4H), 7.39 (m, 6H), 6.78 (d, *J* = 9.0 Hz, 2H), 5.63 (s, 2H), 5.62 (s, 2H), 1.24 (m, 21H); ¹³C NMR (300 MHz, CDCl₃) δ: 161.98, 147.14, 146.75, 139.05, 138.95, 137.92, 137.24, 131.69, 130.61, 130.24, 129.79, 128.57, 128.52, 128.49, 128.18, 128.05, 126.62, 126.35, 121.97, 121.89, 199.78, 110.50, 110.37, 96.77, 67.93, 67.90, 18.88, 18.62, 17.81, 11.91, 11.53, 11.37, 11.15; FT-IR (CDCl₃ cast): 2941, 2863, 2148, 1596, 1270 cm⁻¹; EI-HRMS *m/z*: calcd for C₄₅H₄₄N₂O₂Si 672.31720, found 672.31809 [M]⁺.

7-Triisopropylsilylethynyl-4,11-diaza[7]helicene-3,12-dione (21b). A solution of TIPS-[5]-helicene **24b** (30 mg, 0.06 mmol) in TFA (5 mL) was stirred at room temperature for 12 h, evaporated to dryness and triturated with Et₃N/Et₂O (1:1) to afford 12 mg (53% yield) of a pure yellow solid. ¹H NMR (500 MHz, CDCl₃) δ: 8.65 (d, *J* = 9.0 Hz, 1H), 8.16 (d, *J* = 10.0 Hz, 1H), 8.13 (d, *J* = 10.0 Hz, 1H), 8.01 (d, *J* = 10.0 Hz, 1H), 8.00 (s, 1H), 7.70 (d, *J* = 9.0 Hz, 1H), 7.63 (d, *J* = 9.0 Hz, 1H), 6.58 (d, *J* = 10.0 Hz, 2H), 1.17 (m, 21H); ¹³C NMR (500 MHz, CDCl₃) δ: 161.23, 144.44, 141.29, 141.28, 141.14,

141.13, 139.02, 138.90, 131.66, 131.42, 131.15, 130.10, 129.93, 128.08, 125.78, 122.67, 118.99, 118.97, 118.83, 118.81, 117.83, 117.71, 116.09, 111.67, 110.83, 18.78, 11.49; FT-IR (CHCl₃ cast): 2942, 2864, 2148, 1671 cm⁻¹; EI-HRMS *m/z*: calcd for C₃₁H₃₂N₂O₂Si 492.22330, found 492.22226 [M]⁺.

3.7.3 Synthesis of [9]-Helicene (25)

Stilbene (27). *n*-BuLi in hexanes (5.6 mL, 2.5M, 14 mmol) was added under argon dropwise to cold (-78 °C) dry ethanol (25 mL). After it had been warmed to room temperature and stirred until homogeneous, the solution was transferred by cannula to a slurry of 6-benzyloxy-2-pyridinecarboxaldehyde **22b** (1.50 g, 7.0 mmol) and of *p*-bromobenzyltriphenylphosphonium bromide **26** (4.0 g, 7.7 mmol) in dry EtOH (100 mL) of under argon. After the mixture was stirred overnight the solution was evaporated to dryness, dissolved in CHCl₃, washed with water (2 x 30 mL), brine (2 x 30 mL), dried over MgSO₄ and evaporated to dryness. Purification by normal phase chromatography over silica gel (9:1 hexane/EtOAc) afforded 2.4 g (91%) of the product as a yellow solid. mp 115–120 °C; ¹H NMR (300 MHz, CDCl₃) δ: 7.58 (d, *J* = 16.2 Hz, 1H), 7.52 (m, 4H), 7.47 (m, 4H), 7.03 (d, *J* = 16.2 Hz, 1H), 6.87 (d, *J* = 7.7 Hz, 1H), 6.67 (d, *J* = 8.4 Hz, 1H), 5.46 (s, 2H); ¹³C NMR (300 MHz, CDCl₃) δ: 163.10, 152.62, 139.41, 137.51, 135.84, 131.91, 128.63, 128.56, 128.15, 127.94, 121.00, 116.12, 110.38, 67.74; FT-IR (microscope): 3032, 1634, 1589, 1572 cm⁻¹; EI-HRMS *m/z*: calcd for C₂₀H₁₆BrNO 375.04153, found 365.04252 [M]⁺.

Stilbene-carboxaldehyde (28). A solution of *n*-BuLi, in hexanes, (2.8 mL, 2.5 M, 7.1 mmol) was added dropwise to a solution of **27** (2.4 g, 6.4 mmol) in dry THF (50 mL) at -78 °C. After 1 h, dry DMF (0.74 mL, 9.6 mmol) was added and the mixture was stirred at -78 °C for 45 min and then allowed to warm to room temperature. The reaction was quenched with NH₄Cl (50 mL), extracted with ether (3 x 30 mL), dried over MgSO₄ and evaporated to dryness. Purification by normal phase chromatography over silica gel (13:1 hexane/EtOAc) afforded 640 mg (32%) of the product as a white solid. mp 93–94 °C; ¹H NMR (300 MHz, CDCl₃) δ: 9.99 (s, 1H), 7.86 (d, *J* = 8.1 Hz, 2H), 7.72 (d, *J* = 16.2 Hz, 1H), 7.69 (d, *J* = 8.1 Hz, 1H), 7.58–7.51 (m, 3H), 7.42–7.32 (m, 3H), 7.18 (d, *J* = 16.2 Hz, 1H), 6.92 (d, *J* = 7.2 Hz, 1H), 6.72 (d, *J* = 8.1 Hz, 1H), 5.49 (s, 2H); ¹³C NMR (300 MHz, CDCl₃) δ: 191.65, 163.23, 152.20, 143.04, 139.23, 137.57, 135.76, 131.00, 130.90, 130.25, 128.54, 128.14, 127.92, 127.54, 116.82, 111.10, 67.59; FT-IR (microscope): 3024, 2858, 2761, 1686, 15999, 1565 cm⁻¹; EI-HRMS *m/z*: calcd for C₂₁H₁₇NO₂ 315.12592, found 315.12645 [M]⁺.

3-Benzyloxy-4-azaphenanthridine-9-carboxaldehyde (29). A solution of **28** (160 mg, 0.5 mmol) and iodine (130 mg, 0.5 mmol) in dry benzene (700 mL) was degassed with argon for 1/2 h. Propylene oxide (5 mL) was added and the solution was irradiated for 12 h. After irradiation, the solution was evaporated to dryness and purified by normal phase chromatography over silica gel (13:1 hexane/EtOAc) afforded 94 mg (60%) of the product as a yellow solid. ¹H NMR (300 MHz, CDCl₃) δ: 10.22 (s, 1H), 8.93 (s, 1H), 8.83 (d, *J* = 9.0 Hz, 2H), 8.00 (d, *J* = 9.0 Hz, 2H), 7.96 (s, 2H), 7.54 (m, 2H), 7.38 (m,

3H), 7.15 (d, $J = 9.0$ Hz, 1H), 5.58 (s, 2H); ^{13}C NMR (300 MHz, CDCl_3) δ : 192.23, 162.80, 146.70, 137.18, 134.53, 134.46, 133.66, 130.46, 130.16, 129.73, 129.65, 128.56, 128.35, 128.04, 126.42, 124.43, 121.42, 112.94, 67.98; FT-IR (microscope): 3375, 3060, 3027, 2923, 2853, 1695, 1595 cm^{-1} ; EI-HRMS m/z : calcd for $\text{C}_{21}\text{H}_{15}\text{NO}_2$ 313.11029, found 313.11010 $[\text{M}]^+$.

Bis-stilbene (30). *n*-BuLi in hexanes (1.0 mL, 1.6M, 1.5 mmol) was added under argon dropwise to cold (-78 °C) dry ethanol (10 mL). After it had been warmed to room temperature and stirred until homogeneous, the solution was transferred by cannula to a slurry of **29** (300 mg, 1.0 mmol) and (2-bromo-1,4-phenylene)bis(methylene)bis-(triphenylphosphonium) dibromide **16b** (430 mg, 0.5 mmol) in dry EtOH (40 mL) under argon. After the mixture was stirred overnight the solution was evaporated to dryness, dissolved in CHCl_3 , washed with water (2 x 20 mL), brine (2 x 20 mL), dried over MgSO_4 and evaporated to dryness. Purification by normal phase chromatography over silica gel (9:1 hexane/EtOAc) afforded 350 mg (44%) of pure product as a mixture of isomers. ^1H NMR (300 MHz, CDCl_3) δ : 9.07 (d, $J = 8.4$ Hz, 2H), 8.78 (d, $J = 6.6$ Hz, 2H), 8.00–7.28 (m, 25H), 7.16 (d, $J = 9.0$ Hz, 2H), 5.60 (s, 4H); FT-IR (microscope): 3060, 3022, 1617, 1594, 1275 cm^{-1} ; EI-HRMS m/z : calcd for $\text{C}_{43}\text{H}_{28}\text{BrN}_2\text{O}_2$ 683.13342, found 683.12872 $[\text{M} - \text{Br}]^+$; ES-MS m/z : 777.2 $[\text{M} + \text{H}]^+$.

11-Bromo-3,20-dibenzyloxy-4,19-diaza[9]-helicene (31b). A solution of **30** (100 mg, 0.13 mmol) and iodine (70 mg, 0.27 mmol) in benzene/pyridine (6:1) was degassed by

bubbling argon through for 1 h. Propylene oxide (5 mL) was added and the mixture was irradiated with a 400 W mercury lamp, while under an argon atmosphere, for 12 h. Purification by normal phase chromatography over silica gel (9:1 hexane/EtOAc) afforded 80 mg (78%) of pure yellow product. ^1H NMR (300 MHz, CDCl_3) δ : 8.25 (s, 1H), 8.24 (d, J = 8.7 Hz, 1H), 7.71 (d, J = 8.4 Hz, 1H), 7.60–7.38 (m, 16H), 7.17 (d, J = 9.3 Hz, 1H), 7.09 (d, J = 9.0 Hz, 1H), 7.08 (d, J = 8.4 Hz, 2H), 6.88 (d, J = 8.1 Hz, 1H), 6.86 (d, J = 8.4 Hz, 1H), 5.88 (d, J = 9.3 Hz, 1H), 5.86 (d, J = 9.0 Hz, 1H), 5.63 (d, J = 12.0 Hz, 1H), 5.61 (d, J = 12.0 Hz, 1H), 5.33 (dd, J = 1.2, 12.0 Hz, 2H); ^{13}C NMR (300 MHz, CDCl_3) δ : 160.65, 160.62, 145.75, 145.67, 137.93, 137.89, 133.56, 133.45, 132.62, 132.54, 131.39, 129.92, 129.80, 129.74, 129.68, 129.26, 129.20, 128.47, 128.01, 127.94, 127.88, 127.81, 127.52, 126.60, 125.88, 125.57, 124.77, 124.50, 124.38, 123.98, 121.45, 118.66, 118.60, 108.96, 108.90, 67.25, 67.23; FT-IR (microscope): 3030, 2941, 1610, 1595, 1265 cm^{-1} ; EI-HRMS m/z : calcd for $\text{C}_{50}\text{H}_{31}\text{BrN}_2\text{O}_2$ 772.15485, found 772.15790 $[\text{M}]^+$.

11-Bromo-4,19-diaza[9]helicene-3,20-dione (25). A solution of protected [9]-helicene **31b** (130 mg, 0.3 mmol) in TFA (5 mL) was stirred at room temperature for 12 h, evaporated to dryness, dissolved in CHCl_3 , washed with NaHCO_3 (2 x 6 mL), brine (2 x 6 mL), dried over MgSO_4 to afford 128 mg (90% yield) of a pure yellow solid. ^1H NMR (300 MHz, $\text{DMSO}-d_6$) δ : 11.42 (s, 2H), 8.57 (s, 1H), 8.29 (d, J = 8.7 Hz, 1H), 8.06 (d, J = 8.7 Hz, 1H), 7.94 (d, J = 8.4 Hz, 1H), 7.93 (d, J = 8.4 Hz, 1H), 7.82 (d, J = 8.4 Hz, 1H), 7.47 (d, J = 10.0 Hz, 2H), 7.44 (d, J = 9.9 Hz, 2H), 7.37 (d, J = 7.5 Hz, 1H), 7.35 (d, J =

7.5 Hz, 1H), 7.03 (d, $J = 7.7$ Hz, 1H), 7.00 (d, $J = 7.7$ Hz, 1H), 6.59 (d, $J = 9.9$ Hz, 1H), 6.52 (d, $J = 9.9$ Hz, 1H), 5.33 (d, $J = 8.7$ Hz, 2H); FT-IR (microscope): 2942, 2864, 2148, 1671 cm^{-1} ; EI-HRMS m/z : calcd for $\text{C}_{36}\text{H}_{20}\text{N}_2\text{O}_2\text{Br}$ 591.071662, found 591.070814 $[\text{M}]^+$.

3.8.4 Synthesis of [5]-Helicene (32)

6-Benzoyloxy-2-methyl-3-pyridine carboxaldehyde (33b). A solution of *n*-BuLi, in hexanes, (2.8 mL, 7.1 mmol) was added dropwise to a solution of known molecule 6-benzyl-3-bromo-2-methylpyridine (2.4 g, 6.4 mmol) in dry THF (50 mL) at -78 °C. After 1 h, dry DMF (0.74 mL, 9.6 mmol) was added and the mixture was stirred at -78 °C for 45 min and then allowed to warm to room temperature. The reaction was quenched with NH_4Cl (50 mL), extracted with ether (3 x 30 mL), dried over MgSO_4 and evaporated to dryness. Purification by normal phase chromatography over silica gel (13:1 hexane/EtOAc) afforded 1.9 g (84%) of the product as a white solid. ^1H NMR (300 MHz, CDCl_3) δ : 10.18 (s, 1H), 7.97 (d, $J = 8.4$ Hz, 1H), 7.47–7.35 (m, 4H), 6.70 (d, $J = 8.4$ Hz, 1H), 5.46 (s, 2H), 2.78 (s, 3H); ^{13}C NMR (300 MHz, CDCl_3) δ : 189.70, 165.26, 160.88, 140.30, 136.60, 128.41, 128.34, 128.16, 128.00, 127.90, 124.18, 109.23, 68.34, 22.10; FT-IR (neat film): 3032, 2953, 1648, 1592, 1314 cm^{-1} ; ES-MS m/z : calcd for $\text{C}_{14}\text{H}_{13}\text{NO}_2$ 227.30, found 228.1 $[\text{M} + \text{H}]^+$.

Bis-stilbene (34). *n*-BuLi in hexanes (1.0 mL, 1.6 M, 1.5 mmol) was added under argon dropwise to cold (-78 °C) dry ethanol (10 mL). After it had been warmed to room temperature and stirred until homogeneous, the solution was transferred by cannula to a

slurry of **33** (300 mg, 1.0 mmol) and of (2-bromo-1,4-phenylene)bis(methylene)bis-(triphenylphosphonium) dibromide **16b** (430 mg, 0.5 mmol) in dry EtOH (40 mL) under argon. After the mixture was stirred overnight the solution was evaporated to dryness, dissolved in CHCl₃, washed with water (2 x 20 mL), brine (2 x 20 mL), dried over MgSO₄ and evaporated to dryness. Purification by normal phase chromatography over silica gel (9:1 hexane/EtOAc) afforded 300 mg (71%) of pure product as a mixture of isomers. mp 133–135 °C; ¹H NMR (300 MHz, CDCl₃) δ: 7.84–6.65 (m, 21H), 5.39 (s, 4H), 2.58 (s, 6H); ¹³C NMR (300 MHz, CDCl₃) δ: 162.37, 153.81, 138.35, 137.51, 136.21, 136.08, 135.81, 130.66, 128.44, 128.16, 127.82, 127.08, 127.06, 126.78, 126.57, 125.78, 125.55, 124.52, 124.42, 124.27, 108.86, 67.65, 22.40; FT-IR (cast): 3024, 2922, 1590, 1314 cm⁻¹; EI-HRMS *m/z*: calcd for C₃₆H₃₁BrN₂O₂ 604.15485, found 604.15595.

3.8.5 Synthesis of Diaza[5]-Helicene (**35**)

Bis-stilbene (37). *n*-BuLi in hexanes (2.0 mL, 2.5M, 5.2 mmol) was added under argon dropwise to cold (-78 °C) dry ethanol (10 mL). After it had been warmed to room temperature and stirred until homogeneous, the solution was transferred by cannula to a solution of 4-pyridinecarboxaldehyde **36** (0.5 g, 4.7 mmol) and *p*-phosphonium bromide **16b** (2.3 g, 2.6 mmol) in dry EtOH (20 mL) under argon. After the mixture was stirred overnight the solution was evaporated to dryness, dissolved in CHCl₃, washed with water (2 x 30 mL), brine (2 x 30 mL), dried over MgSO₄ and evaporated to dryness. Purification by normal phase chromatography over silica gel (10% MeOH/CHCl₃) afforded 0.6 g (64%) of the product as a yellow oil. ¹H NMR (300 MHz, CDCl₃) δ:

8.62–8.45 (m, 4H), 7.80–6.5 (m, 11H); ^{13}C NMR (300 MHz, CDCl_3) δ : 150.41, 150.09, 149.92, 143.96, 133.03, 133.07, 131.74, 131.67, 131.26, 131.21, 130.99, 130.92, 130.53, 129.35, 129.30, 129.23, 127.66, 123.42, 123.36, 121.10, 120.94; FT-IR (neat film): 3019, 2967, 1633, 1596, 754, 664 cm^{-1} ; ES-MS m/z : calcd for $\text{C}_{20}\text{H}_{15}\text{BrN}_2$ 363.3, found 363.0.

3,12-Diaza[3]-helicene (38). A solution of **37** (85 mg, 0.24 mmol) and iodine (120 mg, 0.47 mmol) in benzene (600 mL) was degassed by bubbling argon through for 1 h. Propylene oxide (5 mL) was added and the mixture was irradiated with a 400 W mercury lamp, while under an argon atmosphere, for 12 h. Purification by normal phase chromatography over silica gel (10% MeOH/ CHCl_3) afforded 20 mg (23%) of pure yellow product. ^1H NMR (300 MHz, CDCl_3) δ : 8.73 (d, $J = 6.6$ Hz, 1H), 8.72 (s, 1H), 8.71 (d, $J = 6.6$ Hz, 2H), 8.07 (d, $J = 1.5$ Hz, 1H), 8.01 (d, $J = 8.4$ Hz, 1H), 7.88 (d, $J = 6.6$ Hz, 1H), 7.87 (d, $J = 6.6$ Hz, 2H), 7.80 (d, $J = 8.4$ Hz, 1H), 7.76 (d, $J = 1.5$ Hz, 1H), 7.56 (d, $J = 16$ Hz, 1H), 7.48 (d, $J = 16$ Hz, 1H),

3,12-Diaza[3]-helicene (39). A solution of **37** (85 mg, 0.24 mmol) and iodine (120 mg, 0.47 mmol) in benzene/pyridine (6:1) was degassed by bubbling argon through for 1 h. Propylene oxide (5 mL) was added and the mixture was irradiated with a 400 W mercury lamp, while under an argon atmosphere, for 12 h. Purification by normal phase chromatography over silica gel (10% MeOH/ CHCl_3) afforded 20 mg (21%) of pure yellow product. ^1H NMR (300 MHz, $\text{DMSO}-d_6$) δ : 9.46 (d, $J = 5.1$ Hz, 1H), 9.44 (d, $J = 5.7$ Hz, 1H), 9.16 (s, 1H), 8.80 (d, $J = 9.0$ Hz, 1H), 8.62 (d, $J = 9.0$ Hz, 1H), 8.55 (d, $J =$

9.0 Hz, 1H), 8.51 (d, $J = 4.8$ Hz, 1H), 8.46 (d, $J = 4.8$ Hz, 1H), 8.44 (d, $J = 9.0$ Hz, 1H); ES-MS m/z : calcd for $C_{20}H_9BrN_2$ 356.8, found 356.9.

3.8.6 X-ray crystallographic analysis

X-ray crystallography of compound 18b.

Crystal Data: $C_{42}H_{27}BrN_2O_2$ ($M = 671.57$); crystal dimensions 0.37 x 0.22 x 0.02 mm, monoclinic, space group $Pca2_1$ (No. 29) $a = 8.2130(6)$, $b = 43.512(4)$, and $c = 17.2151(15)$ Å, $V = 6152.1(9)$ Å³, $Z = 8$, $\rho_{\text{calc}} = 1.450$ g cm⁻³, $\mu = 1.379$ mm⁻¹, $T = -80^\circ\text{C}$; Bruker P4/RA/SMART 1000 CCD; Mo $K\alpha$ radiation ($\lambda = 0.71073$ Å), scan method ϕ and ω ; 27382 data measured; 11576 independent reflections. The crystal structure was solved using direct methods (SHELXS-86) and refined by full-matrix least squares on F^2 (SHELXL-93). All hydrogens were generated in idealized positions according to the sp^2 or sp^3 -hybridized geometries of their attached carbon and nitrogen atoms. Final $R_1(F) = 0.0534$ (for 11576 data with $F_o^2 \geq 2\sigma(F_o^2)$), $wR_2(F^2) = 0.1350$ (on all 11576 unique data), and $S = 0.825$ for 847 parameters varied. The largest difference peak and hole in the final difference Fourier map had intensities of 0.463 and -0.534 e Å⁻³, respectively.

X-ray crystallography of compound 14c.

Crystal Data: $C_{30}H_{18}N_2O_2 \cdot 1/2H_2O$ ($M = 463.47$); crystal dimensions 0.36 x 0.19 x 0.10 mm, monoclinic, space group $C2/c$ (No. 15) $a = 13.4205(13)$, $b = 17.6403(15)$, and $c = 18.4087(17)$ Å, $\beta = 94.4865(16)^\circ$, $V = 4344.8(7)$ Å³, $\rho_{\text{calc}} = 1.417$ g cm⁻³, $\mu = 0.094$ mm⁻¹, $T = -80^\circ\text{C}$; Bruker P4/RA/SMART 1000 CCD; Mo $K\alpha$ radiation ($\lambda = 0.71073$ Å), scan

method ϕ and ω ; 12007 data measured; 4451 independent reflections. The crystal structure was solved using direct methods (SHELXS-86) and refined by full-matrix least squares on F^2 (SHELXL-93). All hydrogens were generated in idealized positions according to the sp^2 or sp^3 -hybridized geometries of their attached carbon and nitrogen atoms. Final $R_1(F) = 0.0736$ (for 1941 data with $F_o^2 \geq 2\sigma(F_o^2)$), $wR_2(F^2) = 0.2497$ (on all 4451 unique data), and $S = 0.942$ for 325 parameters varied. The largest difference peak and hole in the final difference Fourier map had intensities of 0.840 and $-0.283 \text{ e } \text{\AA}^{-3}$, respectively.

X-ray crystallography of compound 24a.

Crystal Data: $C_{34}H_{23}BrN_2O_2$ ($M = 571.23$); crystal dimensions $0.38 \times 0.20 \times 0.10 \text{ mm}$, monoclinic, space group $C2/c$ (No. 15) $a = 21.822(5)$, $b = 9.075(2)$, and $c = 12.393(3) \text{ \AA}$, $\beta = 92.265(5)^\circ$, $V = 2452.4(10) \text{ \AA}^3$, $\rho_{\text{calc}} = 1.334 \text{ g cm}^{-3}$, $\mu = 0.083 \text{ mm}^{-1}$, $T = -80^\circ\text{C}$; Bruker P4/RA/SMART 1000 CCD; Mo $K\alpha$ radiation ($\lambda = 0.71073 \text{ \AA}$), scan method ϕ and ω ; 6391 data measured; 2347 independent reflections. The crystal structure was solved using direct methods (SHELXS-86) and refined by full-matrix least squares on F^2 (SHELXL-93). All hydrogens were generated in idealized positions according to the sp^2 or sp^3 -hybridized geometries of their attached carbon and nitrogen atoms. Final $R_1(F) = 0.0416$ (for 2347 data with $F_o^2 \geq 2\sigma(F_o^2)$), $wR_2(F^2) = 0.0968$ (on all 2347 unique data), and $S = 0.951$ for 172 parameters varied. The largest difference peak and hole in the final difference Fourier map had intensities of 0.169 and $-0.205 \text{ e } \text{\AA}^{-3}$, respectively.

3.9 References

1. (a) T. J. Katz, *Angew. Chem. Int. Ed.* **2000**, *39*, 1921 and references therein; (b) L. A. Cuccia, J. -M. Lehn, J.-C. Homo, M Schmutz, *Angew. Chem. Int. Ed. Engl.* **2000**, *39*, 233; (c) K. Deshayes, R. D. Broene, I. Chao, C. B. Knobler, F. Diederich, *J. Org. Chem.* **1991**, *56*, 6787; (d) M. Mazik, D. Bläser, R. Boese, *Tetrahedron Lett.* **1999**, *40*, 4783; (e) M. S. Gin, J. S. Moore, *Org. Lett.* **2000**, *2*, 135.
2. H. J. Schnieder, R. K. Juneja, S. Simora, *Chem. Ber.* **1989**, *122*, 1211.
3. S. Scheiner, *Acc. Chem. Res.* **1994**, *27*, 402.
4. M. Mammen, E. E. Simanek, G. M. Whitesides, *J. Am. Chem. Soc.* **1996**, *118*, 12614.
5. S. C. Zimmerman, P. S. Corbin in *Molecular Self-Assembly – Organic versus Inorganic Approaches*, Ed. M. Fujita, Springer-Verlag Berlin Heidelberg, New York, 2000.
6. J. Pranata, S. G. Wierschke, W. L. Jorgensen, *J. Am. Chem. Soc.* **1991**, *113*, 2810.
7. S. C. Zimmerman, M. Mrksich, M. Baloga, *J. Am. Chem. Soc.* **1989**, *111*, 8528.
8. J. A. Zerkowski, C. T. Seto, G. M. Whitesides, *J. Am. Chem. Soc.* **1992**, *114*, 5473.
9. (a) C. T. Seto, G. M. Whitesides, *J. Am. Chem. Soc.* **1993**, *115*, 905; (b) L. J. Prins, J. Huskens, F. de-Jong, P. Timmerman, D. N. Reinhoudt, *Nature* **1999**, *398*, 498.
10. (a) O. Ermer, *Angew. Chem. Int. Ed. Engl.* **1988**, *27*, 829; (b) O. Ermer, L. Lindenberg, *Helv. Chim. Acta.* **1991**, *74*, 825.
11. R. K. Castellano, D. M. Rudkevich, J. Jr Rebek, *Proc. Natl. Acad. Sci. USA*, **1997**, *94*, 7132.

12. (a) M. Suárez, N. R. Branda, J. -M. Lehn, *Helv. Chim. Acta.* **1998**, *81*, 1; (b) M. J. Brienne, J. Gabard, M. Leclercq, J. -M. Lehn, M. Chéve, *Helv. Chim. Acta.* **1997**, *80*, 856; (c) M. Simard, D. Su, J. D. Wuest, *J. Am. Chem. Soc.* **1991**, *113*, 4696.
13. R. H. Janke, G. Haufe, E. -U. Würthwein, J. H. Borkent, *J. Am. Chem. Soc.* **1996**, *118*, 6031.
14. I. Kuzmenko, I. Weissbuch, E. Gurovich, L. Leiserowitz, M. Lahav, *Chirality* **1998**, *10*, 415.
15. For other studies that use rigid polyazaclefts, helicopodands or bifunctional helicenes for hydrogen-bonding recognition, see: (a) D. M. Perreault, X. Chen, E. V. Anslyn, *Tetrahedron* **1995**, *51*, 353; (b) C. -Y. Huang, V. Lynch, E. V. Anslyn, *Angew. Chem. Int. Ed. Engl.* **1992**, *31*, 1244; (c) L. Owens, C. Thilgen, F. Diederich, C. B. Knobler, *Helv. Chim. Acta.* **1993**, *76*, 2757; (d) K. Tanaka, Y. Kitahara, *J. Chem. Soc. Chem. Comm.* **1998**, 1141; (e) K. Tanaka, Y. Shogase, H. Osuga, H. Suzuke, W. Nakanishi, K. Nakamura, Y. Kawai, *J. Chem. Soc. Chem. Comm.* **1995**, 1873; (f) K. Tanaka, Y. Kitahara, H. Suzuki, H. Osuga, Y. Kawai, *Tetrahedron Lett.* **1996**, *37*, 5925.
16. For a review on self-assembling helices, see: A. E. Rowan, R. J. M. Nolte, *Angew. Chem. Int. Ed. Engl.* **1998**, *37*, 63.
17. K. Yamamoto, T. Ikeda, T. Kitsubki, Y. Okamoto, H. Chikamatsu, M. Nakazaki, *J. Chem. Soc. Perkin Trans. 1* **1990**, 271.
18. M. T. Reetz, E. W. Beuttenmüller, R. Goddard, *Tetrahedron Lett.* **1997**, *83*, 3211; (b) A. Terfort, H. Görls, H. Brunner, *Synthesis* **1997**, 79; (c) S. D. Dreher, T. J. Katz, K. C. Lam, A. L. Rheingold, *J. Org. Chem.* **2000**, *65*, 815.

19. T. J. Katz, L. Liu, N. D. Willmore, J. F. Fox, A. L. Rheingold, S. Shi, C. Nuckolls, B. H. Rickman, *J. Am. Chem. Soc.* **1997**, *119*, 10054.
20. L. Liu, B. Yang, T. J. Katz, M. K. Poindexter, *J. Org. Chem.* **1991**, *56*, 3769.
21. For a description of *M* and *P* nomenclature and how it is used to describe the stereochemistry of helicenes, see: E. L. Eliel, S. H. Wilen, *Stereochemistry of Organic Compounds*; Wiley: New York, 1994; Chapter 14, pages 1121, 1163-1166.
22. The precursor to **15b** was prepared as described for the methyl ether: A. G. Osborne, L. A. D. Miller, *J. Chem. Soc. Perkin Trans. 1* **1993**, 181.
23. ¹H NMR of **19a** (R = H) shows a resonance peak at 9.22 ppm, characteristic of the *S*-isomer. T. J. Katz, A. Sudhakar, M. F. Teasley, A. M. Gilbert, W. E. Geiger, M. P. Robben, M. Wuensch, M. D. Ward, *J. Am. Chem. Soc.* **1993**, *115*, 3182.
24. J. Navaza, G. Toucaris, G. Le Bas, A. Navazade, C. de Rango, *Bull. Soc. Chim. Belg.* **1979**, *88*, 863.
25. R. H. Martin, *Angew. Chem. Int. Ed. Engl.* **1974**, *13*, 649.
26. (a) B. L. Hodous, J. C. Ruble, G. C. Fu, *J. Am. Chem. Soc.* **1999**, *121*, 2637 and references cited therein; (b) R. Rios, J. Liang, M. M. C. Lo, G. C. Fu, *Chem. Commun.* **2000**, *5*, 377.
27. C. Goedicke, H. Stegemeyer, *Tetrahedron Lett.* **1970**, *12*, 937.

Chapter 4 – Dative Bonding, Hydrogen Bonding and Molecular Squares

There is presently considerable interest in molecules capable of acting as selective hosts for guest species for applications in areas such as catalysis and transport.¹ Self-assembly represents a powerful means for the spontaneous and programmed generation of these often large, complex architectures. Designing synthons which are capable of participating in self-assembly processes demands the consideration of the type of intramolecular interactions that can be used such that the self-assembly synthesis and the resulting aggregate display their unique properties. In Chapter 2, the strength and directionality of dative bonds were exploited for the production of stable optically pure helicates. While in Chapter 3, the reversibility of hydrogen bonds were utilized to induce a stereoselective discrimination process, which resulted in the formation of homochiral dimers.

This chapter will explore the utility of the combination of dative and hydrogen bonds for the fabrication of large cyclic supramolecular arrays for applications in inclusion-complex chemistry such as host-guest transport systems and catalysis. First, the design principles behind making large complex arrays will be discussed, and then the utility of this methodology will be highlighted with selected examples.

4.1 Dative Bonds and Molecular Squares

Metal ions play a prominent role in supramolecular chemistry because of their ability to organize organic ligands through dative bonds and to provide a feature of directionality as a consequence of their particular coordination geometry. The groups of Fujita² and Stang³ pioneered a rational and predictable approach to spontaneous self-assembled molecular squares by utilizing *cis*-protected square-planar metals such as platinum(II) as the angular components and diatomic ligands such as 4,4'-bipyridine as the linear components (Figure 1). Variations in both metal and ligand geometry has led to a wealth of two and three-dimensional cyclic arrays, some of which are shown in Table 1.

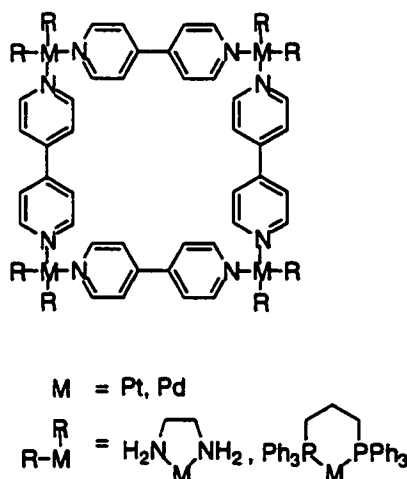




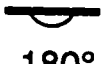



















Figure 1. Self-assembly of molecular square.

Knowledge in this area (commonly referred to as metal-directed self-assembly) has grown from the design and synthesis of predictable supramolecular architectures to the incorporation of these useful structures for function in such areas as host-guest chemistry,^{1b} chiral recognition^{1c} and catalysis.^{1a} For example, self-assembled nanocage **1** was found to promote the aerobic, aqueous oxidation of styrene to acetophenone with the

help of (en)Pd(NO₃)₂ in good yield (Scheme 1).^{1a} Initially, styrene, which is in the organic phase, is enclosed by cage 1 and transferred into the aqueous phase. The

Table 1. Molecular library of cyclic molecular arrays created by the systematic combination of ditopic building blocks of predetermined angles with ditopic metals.

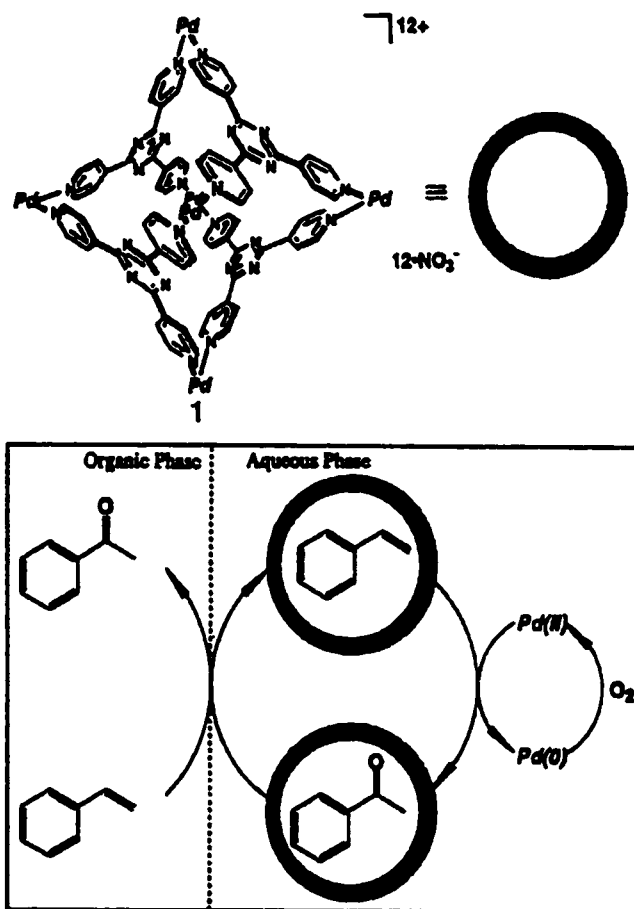
	 60°	 90°	 109.5°	 120°	 180°
 60°					
 90°					
 109.5°					
 120°					
 180°					

encapsulated styrene is then oxidized to acetophenone by the action of Pd(II) reagent.

Lastly, acetophenone (the less hydrophobic component) is replaced by unreacted styrene (the more hydrophobic component), where the differences in hydrophobicity promote smooth product-substrate replacement. This reaction maybe regarded as a double

catalysis system where **1** is the reverse phase-transfer catalyst and (en)Pd(NO₃)₂ is the oxidation catalyst.

Scheme 1



4.1.1 Dative and Hydrogen Bonds, and Molecular Squares

In recent years, alternative approaches to constructing molecular cyclic arrays have been developed. In these approaches, both hydrogen bonding and organometallic interactions have been employed.^{4,5} The introduction of functionality capable of hydrogen bonding adds a dynamic property (reversibility in binding and release) to the molecular array, a necessary requirement if these types of structures are to be used for applications in host-guest transport systems. The success of this approach hinges on

ligand design which must contain not only the necessary site for dative bonding but also retain its complementary hydrogen bonding capabilities upon metal complexation. An important design concept must be considered, however, as the number and arrangement of hydrogen bonding donor (D) and acceptor (A) sites, with respect to one another, can significantly influence the stability of the supramolecular complex (see Chapter 1).

Studies by Lippert⁴ show that the replacement of a proton in a hydrogen bonded nucleobase pair by a *trans*-protected Pt(II) moiety affords a stable ‘metal-modified’ base pair. The modified base pair displays a donor, acceptor sequence for hydrogen bonding of DADA, making it self-complementary and thus promoting it to crystallize as a dimer, hence, as a dimetalated base quartet (Figure 2).

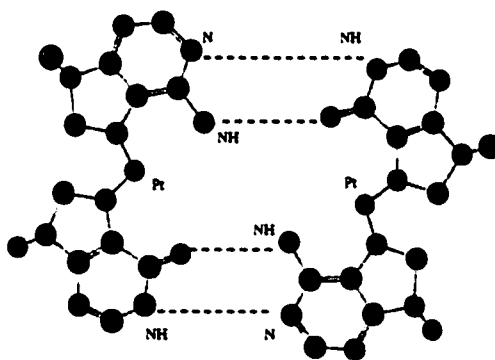
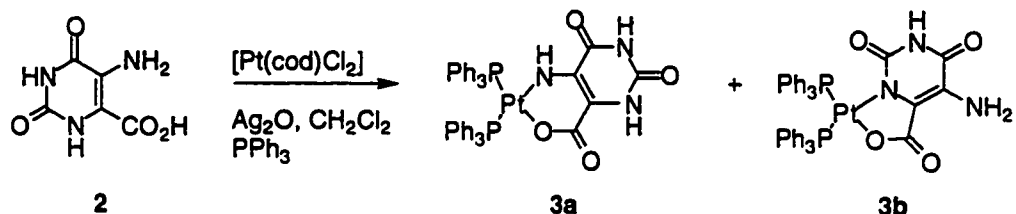


Figure 2. Base quartet formed by hydrogen bonds between two self-complementary base pairs.

Previous studies by Mingos and Burrows⁵ have also illustrated that deprotonated nucleobase derivatives such as 5-aminoorotic acid **2** will bind metals through a five- or six-membered chelate ring (Equation 1). The difference in coordination of the metal leads to a differentiation in the orientation of the hydrogen-bond donors and acceptors remaining on the ligand. This, in turn, results in different supramolecular complexes

being formed, dimers for **3a** and cyclic tetramers for **3b**. Limited cavity size of this example and the example shown in Figure 2, however, restricts their use in inclusion complex chemistry.

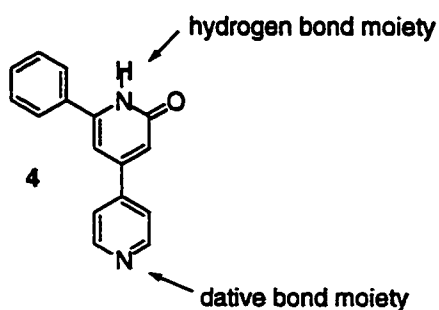
Equation 1



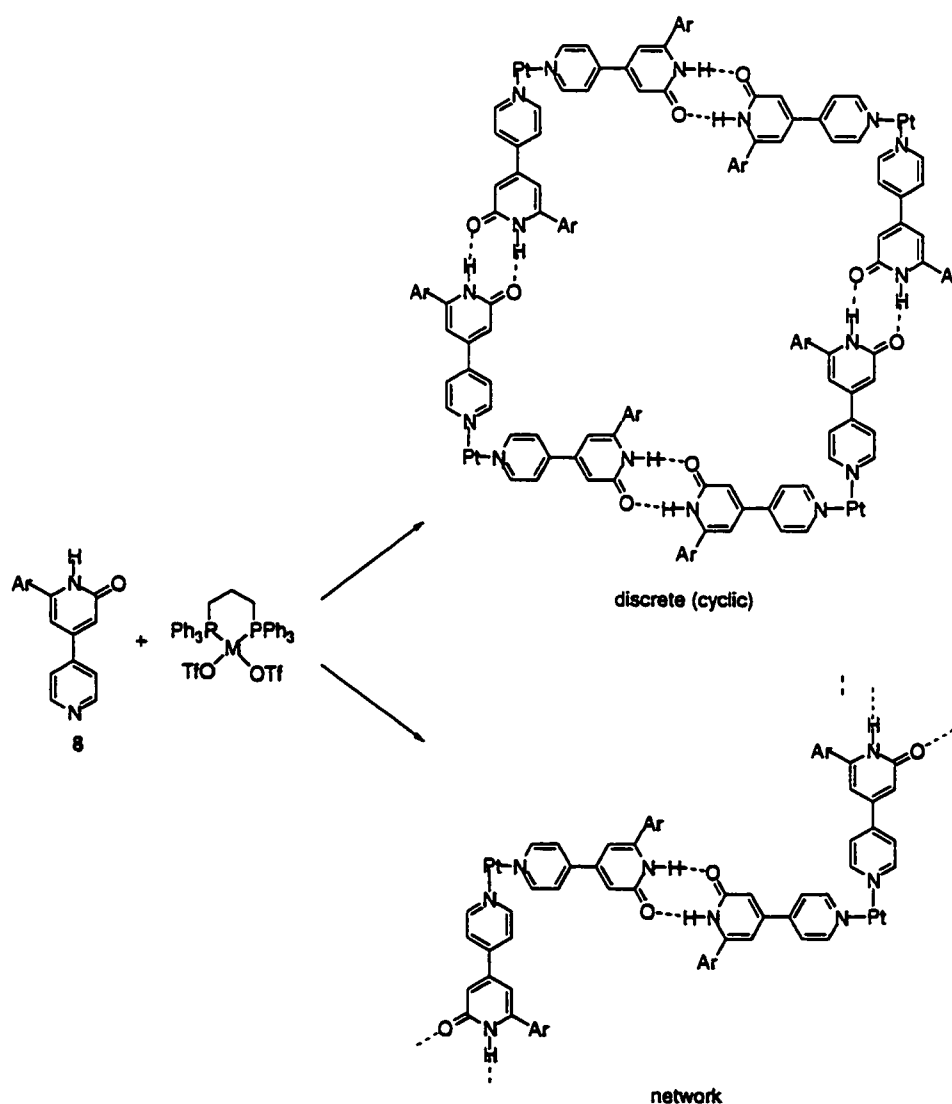
4.1.2 Design of a Bifunctional Synthron

Intrigued with the possibility of combining two or more different constructive recognition elements onto a single ligand that can spontaneously and selectively assemble into predictable architectures prompted us to investigate a unique ligand design which has two independently addressable recognition elements, dative and hydrogen bonds. The end goal of this project is the realization of a two-tier self-assembly processes which should result in large, well-defined molecular arrays.

Ligand **4** was designed for this study because of the ease of synthesis as well as its potential to form dative metal bonds (via the pyridine ring) and promote spontaneous self-assembly (through self-complementary hydrogen bonding recognition elements).



The combination of the linear bifunctional ligand **4** with cis-protected platinum(II) ions should form via a one-pot spontaneous self-assembly process novel platinum(II) complexes (Scheme 2). This process can follow two general pathways and generate two distinctly different supramolecular complexes. One pathway results in linear arrays of varying lengths. Alternatively, cooperative hydrogen bonding drives the self-assembly synthesis resulting in a cyclic array. It will be shown that, depending on the ligand and the reaction conditions, the self-assembly reaction can take both pathways.



Scheme 2. Some possible assemblies of linear ligand **4** and square planar metal Pt^{2+} .

4.2 Results and Discussion

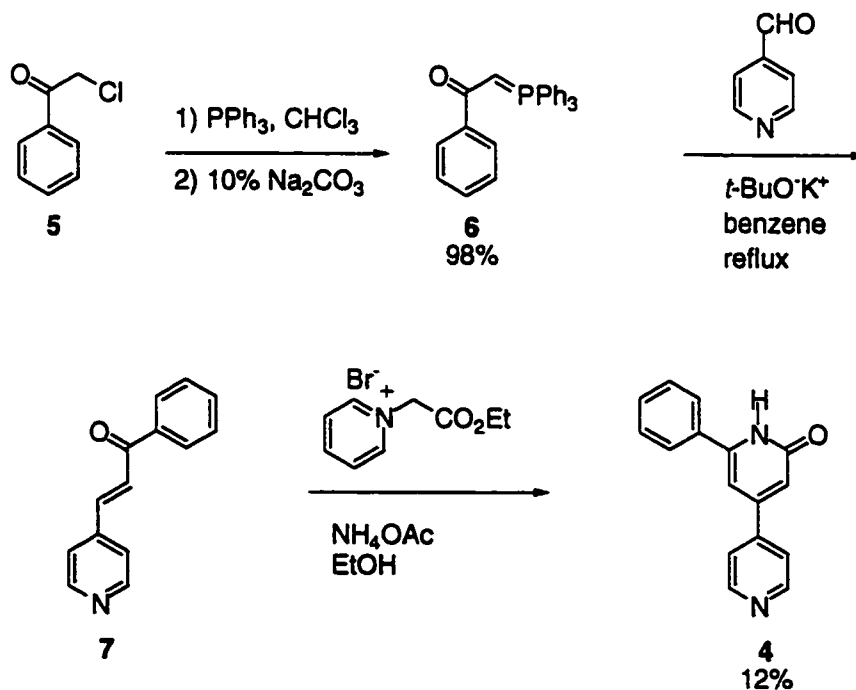
4.2.1 Synthesis of Ligands 4 and 8

Commercially available phenylacetyl chloride **5** was converted into pyridinone **4** in three steps following standard procedures developed by Kröhnke (Scheme 3).⁷ Treatment of chloride **5** with triphenylphosphine, followed by base afforded stabilized ylid **6**.

Condensation of **6** with pyridine-4-carboxaldehyde gave α,β -unsaturated ketone **7**.

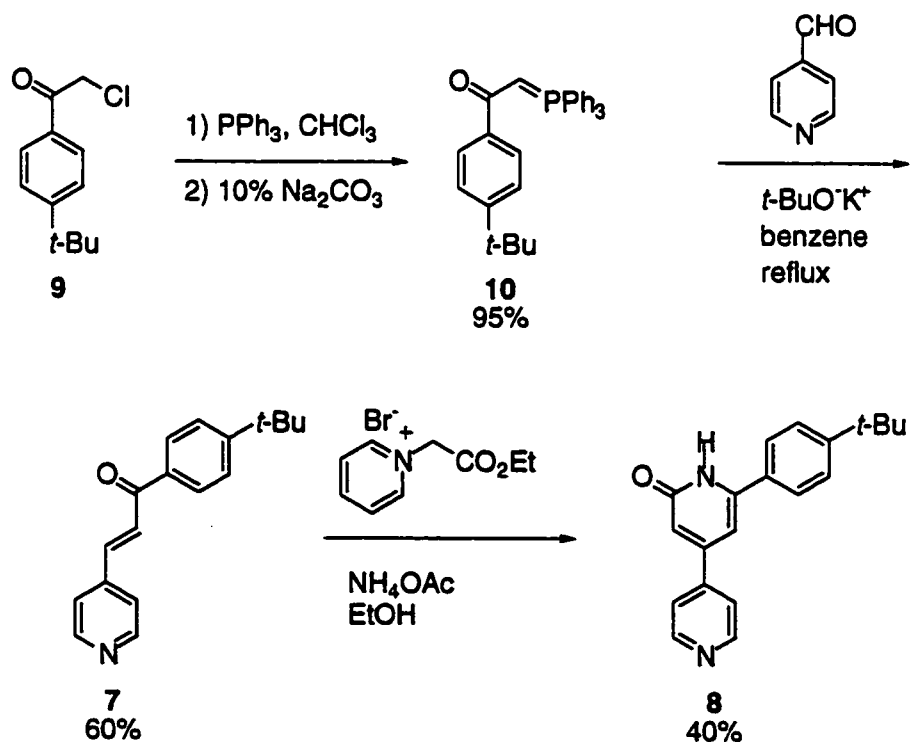
Treatment of **7** with a pyridinium salt and ammonium acetate resulted in ligand **4** in 12% overall yield. Unfortunately, low solubility of **4** in solvents suitable for hydrogen bonding studies (CHCl_3 , CH_2Cl_2 , for example) forced us to pursue alternative derivatives of **4**.

Scheme 3



Incorporation of a *t*-butyl group on the *para*-position of the phenyl ring readily resolved this issue. Following a similar procedure, *p*-*tert*-butylphenylacetyl chloride **9** was converted to substituted pyridine **8** in three steps (Scheme 4). Treatment of **9** with triphenylphosphine and subsequent addition of base gave activated ylid **10**. Condensation of **10** with pyridine-4-carboxaldehyde afforded α,β -unsaturated ketone **11**. Care was taken to isolate the ketone in order to avoid the low yields observed in Scheme 3. Reaction of ketone **11** with a pyridinium salt and ammonium acetate resulted in ligand **8** in 24% overall yield. All of the signals in the ^1H NMR spectra of **8** were assigned based on chemical shifts, coupling constants and G-COSY experiments.

Scheme 4



4.2.2 Self-Assembly Involving Ligand 8

Platinum(II) complexes were prepared by adding a 2:1 molar amount of ligand **8** in dry, acid free dichloromethane to platinum bistriflate complex (Pt(dppp)OTf₂) at room temperature for 1 hour (Scheme 2).⁸

4.2.2.1 Solution-State Studies Using ¹H NMR Analysis

Upon metal complexation, the number of signals in the ¹H NMR spectrum of **8** in CDCl₃ appear to remain constant (many of the peaks are masked by the signals from the triphenylphosphine functionality) but their positions shift significantly, indicating the formation of a symmetrical metal-ligand complex. The doublet corresponding to the α -pyridine hydrogens shifts downfield ($\Delta\delta = 0.5$) to 9.22 ppm. The proximity of the pyridyl ring to the deshielding metal center is the likely cause of the downfield shift.

Surprisingly, the signals of the two protons of the pyridinone ring are shifted upfield ($\Delta\delta = -0.3$) to 6.34, relative to the free ligand. This shift can be attributed to the shielding effects of the triphenylphosphine rings, which are in close proximity to these pyridinone protons. This explanation has been suggested previously¹ and is supported by molecular modeling.

¹H NMR spectrometry dilution studies in CDCl₃ were performed to determine the self-assembling behaviour of both the ligand alone and the platinum(II) complex (Figure 3). Both of these studies show the N-H resonance signals to be concentration dependent, with the signals moving significantly ($\Delta\delta \approx 3$ ppm) over a broad concentration range ($3 \times 10^{-2} \times 10^{-5}$ M). These results indicate that self-association between the components via

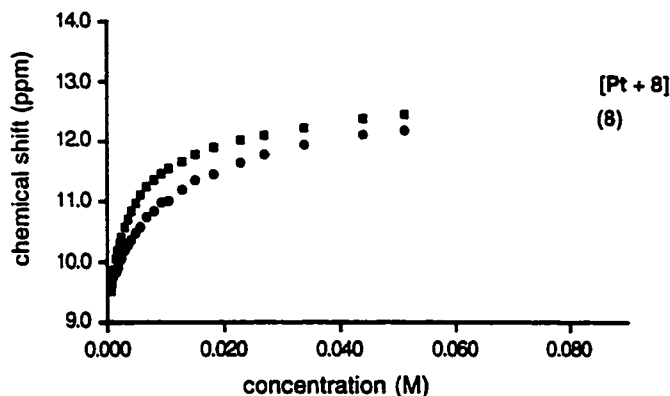


Figure 3. Concentration dependency of the chemical shift for the N-H proton in the ^1H NMR spectrum of ligand **8** alone and $[\text{Pt}(\text{dppp})\text{OTf}_2 + \mathbf{8}]$ in CDCl_3 .

hydrogen bonding is taking place. The data from the dilution experiment of the ligand alone correlates well with calculated curves using a dimer binding model, giving an association constant (K_a) of 43 M^{-1} . Conversely, a plot of platinum(II) complex does not give an analogous curve. This curve gives an association constant (K_a) of 243 M^{-1} . Because the association constant of the platinum complex is much larger than double the association constant of that of the ligand alone, which could be expected if two sets of dimer ligands were binding to a single Pt^{2+} ion ($\text{Pt}(\text{dppp})(\mathbf{8})_4$), larger aggregates must be formed. Furthermore, these larger aggregates are well-ordered as suggested by the simplicity of the ^1H NMR spectrum and the lack of peak broadening over this large concentration range. These results can best be explained by invoking the argument for the formation of discrete (cyclic) structures over random oligomers. At this time we are unable to fit this curve to an n-merization model as solubility problems, even with the $\text{R} = t\text{-butyl}$, have eluded the higher concentrations and the breaking of the dative bonds at

lower concentrations have eliminated the lower part of the curve. We, therefore, turned our attention to mass spectrometry analysis in order to elucidate the molecular weight, and hence the molecular composition, of the metal complexes that are being formed in solution.

4.2.2.2 Mass Spectrometry Analysis

Vapour-phase osmometry (VPO) experiments, which show the average molecular weight of the species present, were performed with a 10^{-4} M solution of the platinum(II) complex in dichlorobenzene. The average molecular weight was found to be 1242 ± 64 . This weight coincides with the prefabricated monomeric building component only (M_{calc} of $\text{Pt}(\text{dppp})(\text{8}_2)(\text{OTf})^{1+} = 1254$). This result is not surprising, though, as ^1H NMR studies, at similar concentrations, show that very little self-assembly via hydrogen bonding is taking place.

The low resolution electrospray mass spectrometry (ES-MS) spectrum of a dichloromethane solution of a freshly prepared mixture of ligand **8** and $\text{Pt}(\text{dppp})\text{OTf}_2$ shows a major peak at m/z 551 corresponding to the basic monomeric building block $(\text{Pt}(\text{dppp})(\text{8}_2))_n^{2n+}$. Also seen are peaks at m/z 903, 1253, 1722 and 1953 corresponding to trimeric and tetrameric species with varying amounts of the counter ion (OTf^1) (Figure 4). More importantly, the peaks at 1953, 1283 and 903 show successive loss of triflate ions from the trimeric species, which further strengthens the argument of presence of discrete over oligomeric aggregates. The isotopic abundance of each peak does not display the typical (1.0) peak separation of singly charged species confirming the presence of multi-charged species. Attempts at resolving the isotopic abundance of each

peak, which should give the exact charge of the peak in question, by using high resolution electrospray mass spectrometry were unsuccessful, presumably due to the “harshness” of the ionization technique of this particular high resolution electrospray mass spectrometer. To date, X-ray quality crystals of the platinum complexes have not been grown. We, therefore, turned our attention to synthesizing a ligand with a stronger hydrogen bond array, which should be able to maintain its hydrogen bonding capabilities during the electrospray process.

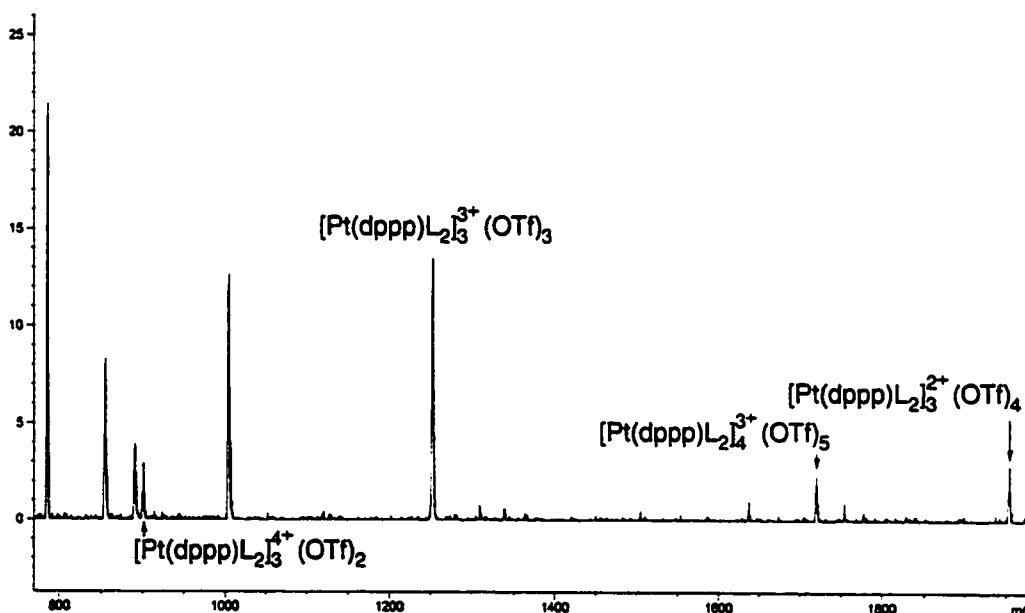
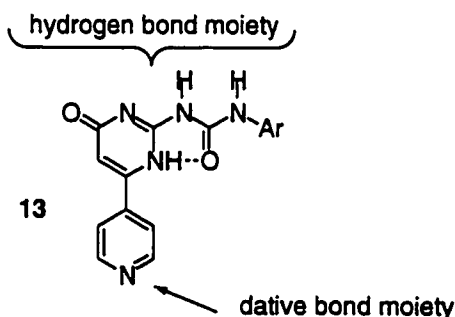


Figure 4. ES-MS spectrum of **8** and $Pt(dppp)OTf_2$ in CH_2Cl_2 , where L represents ligand **8**.

4.2.3 Synthesis of Ligand 13

Ligand **13** is an easily preparable synthon that contains the necessary site for dative bonding (the pyridine ring), and an enhanced self-complementary hydrogen bonding array, provided by a AADD motif.

Synthon **13** was prepared in two steps from known ethyl isonicotinoylacetate as outlined in Scheme 5. Initial condensation of β -keto ester **14** with guanidine afforded 6-substituted isocytosine **15**.⁹ Treatment of 3,5-di-*t*-butylbenzoic acid with di-phenylphosphoryl azide and isocytosine **15** in dry pyridine at reflux generated desired ligand **13** in 72% yield.



Depending on the conditions, pyridyl-substituted **13** can exist in two tautomeric forms, pyrimidinone **13a** and pyrimidinol **13b** (Scheme 5). One of the problems with using heteroaromatic synthons in self-assembly is controlling the tautomeric equilibrium (this issue is discussed in greater detail in Appendix 1). Initially, though, it was thought that the advantages of having a stronger hydrogen-bonding array would offset the diagnostic disadvantages encountered by having both tautomers present. This is a point that will be disproved in latter studies.

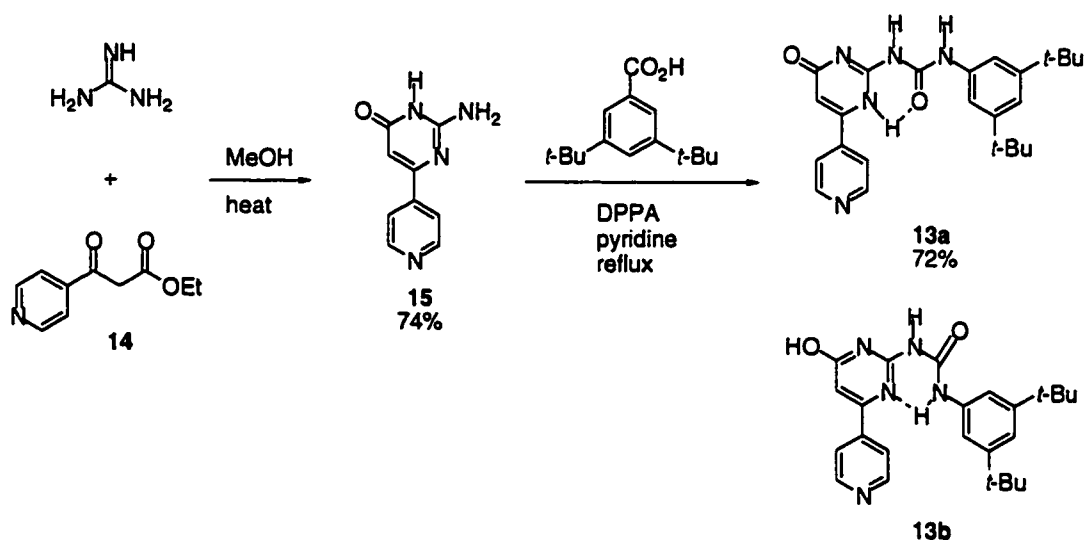
4.2.4 Self-Assembly Involving Ligand **13**

Initial studies on **13**, alone, were done to determine not only the association constant but also the ability of the dimer (**13**)₂ to maintain its integrity during the electrospray process. These studies were followed by experiments involving the

formation of platinum(II) complexes of **13** with Pt(dppp)(OTf)₂ in an analogous manner to experiments involving **8**.

All of the signals in the ¹H NMR spectrum of tautomers of **13** were assigned based on chemical shifts, coupling constants and G-COSY experiments, while the relative amounts of each tautomer were determined by comparing the integration values.

Scheme 5



4.2.4.1 Solution-State Studies For **13** Only

The ¹H NMR spectrum of **13** in CDCl₃ shows two sets of signals. One set of the N-H signals at 13.96, 12.30 and 11.90 ppm is assigned to the 4[1H]-pyrimidinone tautomer **13a**, while a second sets of peaks at 13.67, 12.09 and 11.34 ppm (abundance of 81%), is assigned to the pyrimidinol tautomer **13b**. This assignment was easily determined because the aromatic proton signal of **13b** resonates 0.38 ppm downfield of the alkylidene signal of the pyrimidinone tautomer **13a** (δ = 6.46 ppm).⁹ Changing the

solvent from CDCl_3 to CD_2Cl_2 further increases this population discrepancy, in favor of **13b**, from 81% to 86%. FT-IR spectra in both CHCl_3 and CH_2Cl_2 confirms the presence of both tautomers as indicated by the diagnostic absorption bands of the hydrogen-bonded OH of the pyrimidinol tautomer at 2500 cm^{-1} and the carbonyl CO of the pyrimidinone tautomer at 1670 cm^{-1} .

It is surprising that pyrimidinol tautomer **13b** is the predominant one, as it has a significantly lower dimer association constant as compared to the pyrimidinone tautomer **13a**. The dominance of **13b** is most likely due to the electron withdrawing effects of the 6-pyridyl substituent.⁹ The presence of the pyridyl moiety decreases the basicity of the carbonyl group (found in **13a**) but increases the acidity of the hydroxyl group, and hence, the hydrogen bond donor capabilities found in **13b**. This, in turn, should increase the stability of the dimer formed from **13b**.

^1H NMR dilution studies of **13** in CDCl_3 show the heteroatomic resonances (N-H and O-H) to be concentration independent (δ is unchanging over a 10^{-4} – 10^{-1} M^{-1}). A conservative estimate of less than 10% dissociation at 10^4 M^{-1} results in an association constant (K_a) that exceeds 10^5 M^{-1} . These results are similar to ones reported by Meijer and co-workers⁹ and suggest that the mode of self-association should be strong enough to maintain the integrity of dimer (**13**)₂ during the electrospray process.

Initial electrospray mass spectrometry studies of dichloromethane solutions of ligand **13**, alone, show peaks at 420.2 and 861.5 corresponding to free ligand **13** and dimer $\text{Na}(\text{13})_2$ respectively, with the ratio of dimer increasing when the solution is concentrated. It is unknown, though, if the sodium ion is coordinating without disrupting

the integrity of dimer (**13**)₂ (Figure 5a) or if it is acting as a bridge between the two ligands (Figure 5b), which breaks up the hydrogen bonding array. Surprisingly, no peaks corresponding to di-metalated species, Na₂(**13**)₂, are observed, which may support the formation of the coordination compound in Figure 5b.

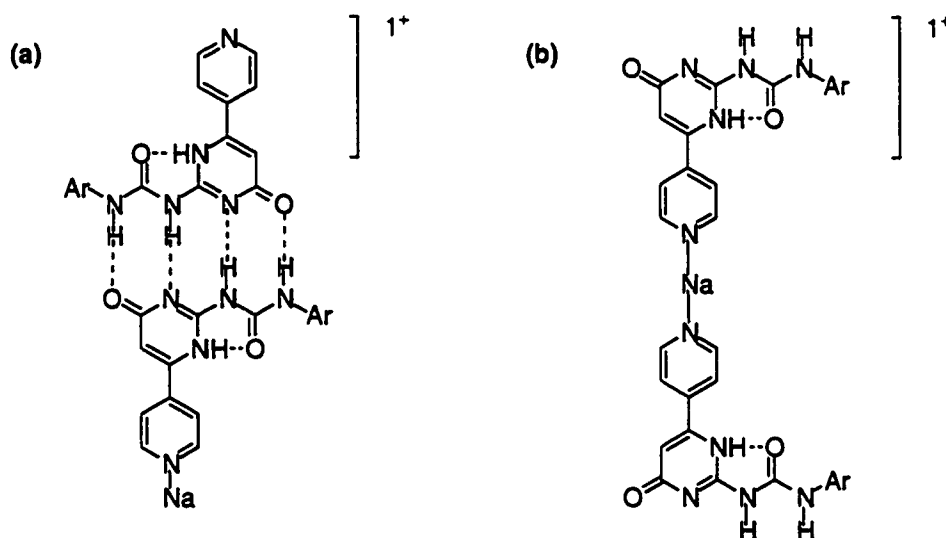


Figure 5. Two modes of **13** binding to a sodium ion.

4.2.4.2 Solution-State Studies For [Pt(dppp)OTf₂ + **13**]

The platinum(II) complexes were easily prepared by combining a 2:1 molar ratio of synthon **13** and Pt(dppp)OTf₂ in dry, acid-free dichloromethane.

The ¹H NMR spectrum of a solution of platinum(II) and ligand **13** is complex, which made analysis of this system difficult. Therefore, ³¹P NMR was used to ascertain the composition of the products of the self-assembly synthesis. The ³¹P NMR spectrum at

25°C has nine signals, which can be grouped into two sets, based on their chemical shifts (Figure 6a). It is significant that there are so many signals in the ^{31}P NMR spectrum, as it indicates that at room temperature there are many products of the self-assembled reaction, and may also help to explain why the ^1H NMR spectrum is so complex.

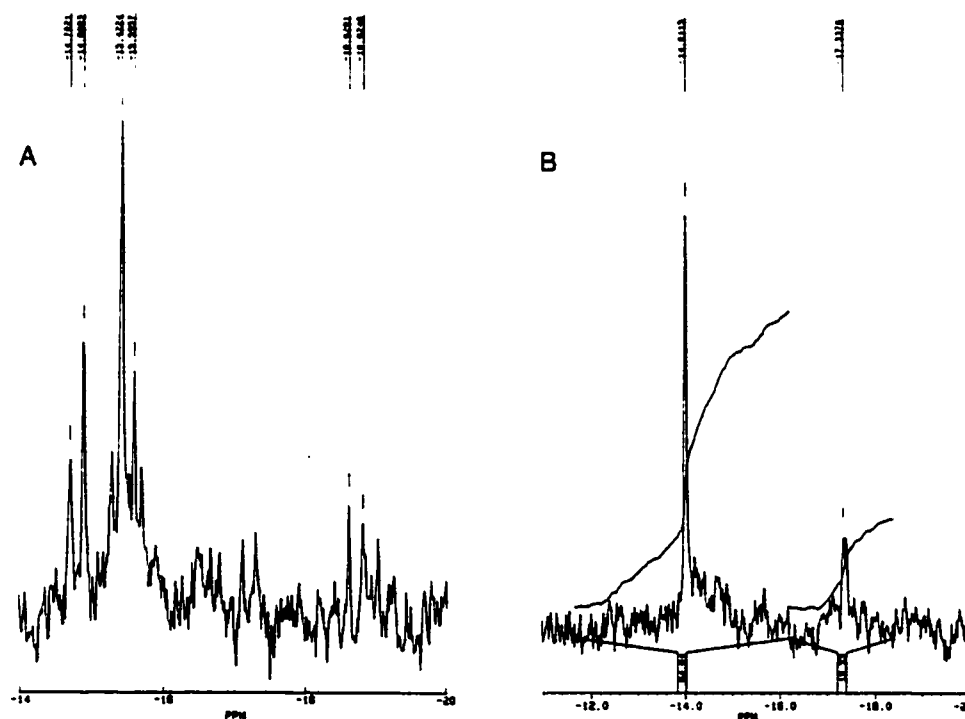


Figure 6. Temperature dependency of the platinum complex in the ^{31}P NMR spectra at: a) 25°C, and b) -80°C.

As mentioned in Appendix I, temperature has a dramatic effect on the tautomeric equilibrium. Therefore, variable temperature ^1H and ^{31}P NMR experiments were performed to help decipher the complex spectra obtained at room temperature. There are no observable changes in the ^1H and ^{31}P NMR spectra of **13** alone in CD_2Cl_2 over the temperature range evaluated (25°C to -80°C). However, the spectra of CD_2Cl_2 solutions

of $[\text{Pt}(\text{dppp})\text{OTf}_2 + \mathbf{13}]$ show dramatic changes over this temperature range, with the ^{31}P NMR spectra being most diagnostic. Upon cooling, the number of signals in the ^{31}P NMR spectrum change from 9 to 2 and their position shift slightly downfield ($\Delta\delta \approx 0.8$) (Figure 6b). Integration shows the relative signal intensities to be 3.5:1. This ratio is similar to the results found in the population abundance study of $\mathbf{13}$ alone. Based on these similarities, the largest signal, which is found furthest downfield (-15 ppm), is assigned to aggregates composed of pyrimidinol tautomer $\mathbf{13b}$. While the smaller signal, which is found further upfield (-19 ppm) is assigned to architectures containing tautomer $\mathbf{13a}$. While the ^{31}P NMR spectrum is consistent with the formation of a highly symmetric metal complex and shows large coordination shifts for the α -pyridyl protons, no information about the ratio of ligand to metal is available. We, therefore, turned our attention to mass spectrometry analysis in order to elucidate the molecular weight, and hence the molecular composition, of the metal complexes that are being formed in solution.

Initial low-resolution electrospray mass spectrometry studies of dichloromethane solutions of $[\text{Pt}(\text{dppp})\text{OTf}_2 + \mathbf{13}]$ (1:2 molar ratio) show a major peak at 773 (100%) corresponding to $[\text{Pt}(\text{dppp})\text{L}]^{2+}\text{Cl}^{-1}$. This peak, which is an impurity, is significant. The chlorine contaminate, which is not present in the original sample, presumably comes from the ES-MS machine and indicates the instability of the platinum complex when competitive ions capable of coordinating to the platinum are present.

Also, seen are peaks at 723 (20%) $\{[\text{Pt}(\text{dppp})\text{L}_2]^{2+}\}$, 1176 $\{[\text{Pt}(\text{dppp})\text{L}]^{2+}\text{OTf}^{-1}\}$ and 1595 $\{[\text{Pt}(\text{dppp})\text{L}_2]^{2+}\text{OTf}^{-1}\}$. No peaks corresponding to higher aggregates are seen. These results are similar to the ES-MS results of $\mathbf{13}$ alone and again it is unknown if the

platinum ion is coordinating without disrupting the integrity of dimer (13)₂ or if it is acting as a bridge between the two ligands as illustrated in Figure 5. Because no higher aggregates are seen, it is most likely that the platinum is coordinated by two ligands and the hydrogen bonds between ligands are broken (as dative bonds are stronger than hydrogen bonds). It is surprising that the integrity of dimer is lost during the electrospray process considering that the association constant of the dimer is estimated to be greater than 10⁵ M⁻¹. Perhaps, coordination of 13 to a metal (either sodium or platinum) alters the electronic properties of 13 such that the basicity of the acceptor sites (Npy and C(O)) is reduced and leads to a net decrease in H-bonding affinity between self-complementary ligands.¹⁰ To date, X-ray quality crystals of the platinum complexes have not been grown.

4.3 Conclusions

Hydrogen bonding and metal coordination are extensively used to control the formation of supramolecular aggregates. Hydrogen bonding is an efficient way to make reversible linkages. On the other hand, metal coordination is highly directional and forms strong dative bonds, and therefore is a powerful tool to make well-ordered aggregates. The combination of these two recognition elements onto one ligand provides an entry into the formation of large well-defined arrays under thermodynamic control, capable of solution dynamics provided by the hydrogen bonding functionality. However, it was seen that no matter what type of metal (main groups or transition metal; charge; hard- or soft-ness) its binding preference (mono- or multi-functional) or other ligands already bound to the metal ion a pronounced destabilization of the hydrogen bonding capabilities of the

ligand was observed. Whether this destabilization is due to electronic effects and/or steric is unknown. Eliminating the conjugation between pyridyl and pyridone rings could provide some insight to this problem and perhaps lead to the construction of large two- and three-dimensional assemblies for applications in inclusion complex chemistry such as host-guest transport and catalysis. Much improvement is required in the characterization of these complex arrays and the need for tailored ES-MS conditions is imperative.

4.4 Experimental

For a general description of apparatus, materials and methods see Chapter 2.

4.4.1 Synthesis

Pyridinone (4). To a solution of pyridine-4-carboxaldehyde (0.10 g, 0.8 mL, 9.3 mmol) in benzene was added ylid 6 (3.3 g, 9.3 mmol) and the entire mixture was heated at reflux for 4 hours. After 4 hours, ammonium acetate (1.2 g, 10 mmol) and 1-ethoxycarbonylmethylpyridinium bromide (2.8 g, 11 mmol) were added and the reaction was heated under reflux for 30 h. The solution was then evaporated under pressure and the residue was dissolved in CHCl_3 , washed with water (3 x 50 mL) and dried over MgSO_4 . Purification by column chromatography over silica gel (7% $\text{MeOH}/\text{CH}_2\text{Cl}_2$) afforded 0.20 g (10%) of a pale yellow solid. ^1H NMR (300 MHz, $\text{DMSO}-d_6$) δ : 11.76 (s, 1H), 8.72 (d, $J = 4.5$ Hz, 2H), 7.92 (d, $J = 4.5$ Hz, 2H), 7.82 (d, $J = 8.7$ Hz, 2H), 7.69 (m, 3H), 7.05 (s, 1H), 6.80 (s, 1H); ^{13}C NMR (300 MHz, $\text{DMSO}-d_6$) δ : 163.59, 150.32,

149.07, 144.53, 129.71, 128.68, 127.04, 121.36; FT-IR (microscope): 2922, 1623, 1595, 1561 cm^{-1} ; EI-HRMS m/z : calcd for $\text{C}_{16}\text{H}_{12}\text{N}_2\text{O}$ 248.09497, found 248.09527.

α,β -Unsaturated ketone (11). To a solution of pyridine-4-carboxaldehyde (0.9 g, 0.48 mL, 5.1 mmol) in benzene was added ylid **10** (2.0 g, 5.1 mmol) and the entire mixture was heated at reflux for 4 h. The solvent was evaporated under pressure and the residue was recrystallized from hexane/EtOAc (which precipitates out PPh_3O) to afford 0.8 g (60%) of a pure white solid. ^1H NMR (300 MHz, CDCl_3) δ : 8.67 (d, $J = 5.7$ Hz, 2H), 7.95 (d, $J = 8.1$ Hz, 2H), 7.66 (s, 2H), 7.51 (d, $J = 8.4$ Hz, 2H), 7.46 (d, $J = 4.5$ Hz, 2H), 1.35 (s, 9H); ^{13}C NMR (300 MHz, CDCl_3) δ : 189.39, 157.33, 150.63, 142.34, 141.11, 134.97, 128.67, 126.29, 125.83, 122.08, 35.27, 31.13; FT-IR (microscope): 3041, 2964, 1664, 1612, 1593 cm^{-1} ; EI-HRMS m/z : calcd for $\text{C}_{18}\text{H}_{18}\text{NO}$ 264.13882, found 264.13831.

Pyridinone (8). To a solution of **11** (1.2 g, 5.1 mmol), in absolute ethanol, was added ammonium acetate (0.8 g, 10 mmol) and 1-ethoxycarbonylmethylpyridinium bromide (1.5 g, 6.2 mmol) and the entire lot was heated under reflux for 30 h. The solution was then evaporated to dryness and the residue was dissolved in CHCl_3 , washed with water (3 x 50 mL) and dried over MgSO_4 . Purification by column chromatography over silica gel (5% MeOH/ CHCl_3) afforded 0.61 g (40%) of a pale yellow solid. ^1H NMR (300 MHz, $\text{DMSO}-d_6$) δ : 8.72 (dd, $J = 1.5, 4.5$ Hz, 2H), 7.61 (d, $J = 8.7$ Hz, 2H), 7.54 (d, $J = 8.7$ Hz, 2H), 7.49 (dd, $J = 1.5, 4.5$ Hz, 2H), 6.74 (d, $J = 1.8$ Hz, 1H), 6.64 (d, $J = 1.5$ Hz, 1H), 1.35 (s, 9H); ^{13}C NMR (300 MHz, $\text{DMSO}-d_6$) δ : 163.52, 152.59, 149.55, 148.44, 130.97,

128.62, 126.91, 126.82, 125.61, 125.51, 122.16, 34.49, 30.92; FT-IR (CH₂Cl₂ cast): 2922, 2852, 1741, 1651, 1605 cm⁻¹; EI-HRMS *m/z*: calcd for C₂₀H₂₀N₂O 304.15756, found 304.15732.

6-Pyridylisocytosine (15). To a boiling solution of guanidine carbonate (0.52 g, 2.9 mmol) in absolute ethanol (25 mL) was gradually added ethyl isonicinoylacetate **14** (0.50 g, 2.6 mmol). The mixture was heated under reflux for 12 h, after which the solution was cooled and treated with acetic acid until neutral. The precipitate was filtered and washed with diethyl ether to afford 360 mg (74%) of a pure pale yellow solid. ¹H NMR (300 MHz, DMSO-*d*₆) δ: 10.97 (s, 1H), 8.64 (dd, *J* = 1.5, 4.5 Hz, 2H), 7.86 (dd, *J* = 1.8, 4.5 Hz, 2H), 6.70 (s, 2H), 6.26 (s, 1H); ¹³C NMR (300 MHz, DMSO-*d*₆) δ: 163.12, 160.16, 156.01, 150.10, 144.53, 120.70, 99.18; FT-IR (microscope): 3426, 3330, 3197, 3067, 3038, 2657, 1672, 1631 cm⁻¹; EI-HRMS *m/z*: calcd for C₉H₈N₄O 188.06981, found 188.06945.

***N*-[[(*-3,5-tert-butyl*)phenylamino]carbonyl]-6-pyridylisocytosine (13).** To a solution of bis-3,5-*tert*-butylbenzoic acid (240 mg, 1.0 mmol) in dry pyridine was added DPPA (310 mg, 1.1 mmol) and the entire lot was allowed to stir at room temperature for 20 min. After 20 min **15** (95 mg, 0.5 mmol) was added and the suspension was heated under reflux for 12 h. The resulting solution was evaporated under pressure, dissolved in CHCl₃, washed with NaHCO₃, dried over MgSO₄. The residue was purified by column chromatography over silica gel (5% MeOH/CHCl₃) to afford 40 mg (20%) of a pure

white solid. ^1H NMR (300 MHz, CDCl_3) δ : (pyrimidinol tautomer) 13.67 (s, 1H), 12.09 (s, 1H), 11.34 (s, 1H), 8.80 (d, $J = 4.5$ Hz, 2H), 7.80 (d, $J = 4.5$ Hz, 2H), 7.44 (s, 2H), 7.21 (s, 1H), 6.83 (s, 1H), 1.34 (s, 18H); 19% of pyrimidinone tautomer at 13.98 (s, 1H), 12.30 (s, 1H), 11.87 (s, 1H), 7.51 (d, $J = 4.5$ Hz, 2H), 7.21 (d, $J = 4.5$ Hz, 2H), 6.46 (s, 1H) other peaks obscured by main tautomer; FT-IR (CHCl_3 solution): 3943, 3690, 3056, 2986, 2305, 1670 cm^{-1} ; ES-MS m/z : 420.2 $[\text{M} + \text{H}]^+$, 861.5 $[2\text{M} + \text{Na}]^+$, 877.5 $[2\text{M} + \text{K}]^+$.

4.5 References

1. (a) H. Ito, T. Kusakawa, M. Fujita, *Chem. Lett.* **2000**, 598; (b) T. N. Parac, D. L. Coulder, K. N. Raymond, *J. Am. Chem. Soc.* **1998**, *120*, 8003; (c) H. –J. Schneider, A. Yatsimirsky, *Principles and Methods in Supramolecular Chemistry*, John Wiley & Sons, England, **2000**; (d) D. B. Amabilino, J. F. Stoddart, *Chem. Rev.* **1995**, *95*, 2725; (e) R. V. Stone, D. I. Yoon, R. M. Calhoun, J. T. Hupp, *J. Am. Chem. Soc.* **1995**, *117*, 11813; (f) J. R. Hall, S. J. Loeb, G. K. H. Shimizu, G. P. A. Yap, *Angew. Chem. Int. Ed. Engl.* **1998**, *37*, 121.
2. M. Fujita in *Molecular Self-Assembly Organic versus Inorganic*, Edited by M. Fujita, Springer-Verlag Berlin Heidelberg, New York, **2000** and references therein.
3. S. L. Leininger, B. Olenyuk, P. J. Stang, *Chem. Rev.* **2000**, *100*, 853 and references therein.
4. I. B. Rother, E. Freisinger, A. Erxleben and B. Lippert, *Inorg. Chim. Acta*, **2000**, 300-302, 339.

5. A. D. Burrows, D. M. P Mingos, A. J. P. White, D. J. Williams, *J. Chem. Soc. Dalton Trans.* **1996**, 3805.
6. M. Albrecht, O. Blua, E. Wegelius, K. Rissanen, *New J. Chem.* **2000**, 667
7. F. Kröhnke, *Synthesis*, **1976**, 1.
8. (a) P. J. Stang, D. H. Cao, *J. Am. Chem. Soc.* **1994**, *116*, 4981; P. J. Stang, D. H. Cao, S. Saito, A. M. Arit, *J. Am. Chem. Soc.* **1995**, *117*, 6273.
9. F. H. Beijer, R. P. Sijbesma, H. Kooijman, A. L. Speck, E. W. Meijer, *J. Am. Chem. Soc.* **1998**, *120*, 6761.
10. B. Lippert, *J. Chem. Soc. Dalton Trans.* **1997**, 3971.

Appendix I – Tautomerism of 4-Hydroxypyridine

I.1 Introduction

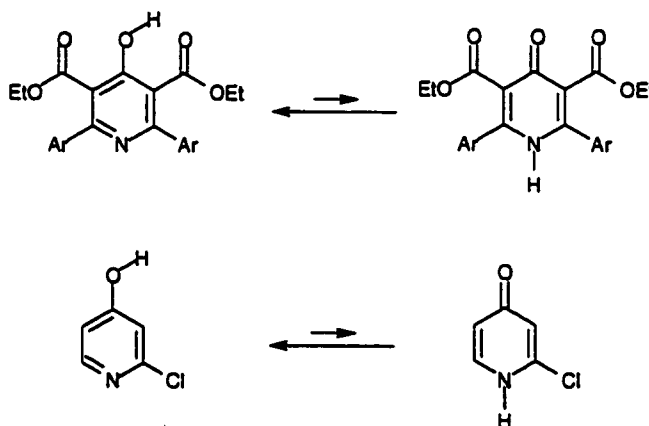
Heterocyclic compounds that can exist as a mixture of rapidly equilibrating tautomers, play interesting roles in both chemical and biochemical processes.¹⁻³ Tautomerism can provide a rationale for the structure-function relationships in nucleotides, the mechanism of enzyme catalysis and substrate-receptor interactions. The ability to accurately predict the position of the tautomeric equilibrium in such compounds is critical in order to create useful models for biochemical transformations, as well as when designing solution and solid-state supramolecular structures.

The factors that affect the position of tautomeric equilibria have been the subject of many studies. The interconversion between the keto and enol forms of 4-hydroxypyridine has received considerable attention.⁴⁻¹¹ In the gas phase, where solvent-assisted stabilization is absent, and in non-polar solvents such as cyclohexane, the enol isomer is the predominant species.^{10,11} It has also been shown that the keto form exists exclusively in polar solvents such as dimethylsulfoxide^{5,10,11} as well as in the solid-state¹²⁻¹⁸ where efficient solvation and intermolecular hydrogen bonding are key stabilizing factors, respectively.

Previous studies have also illustrated that incorporating secondary structural features into heterocycles can upset the position of the hydroxypyridine-pyridinone equilibrium. For example, the population of the less favorable hydroxy form is increased

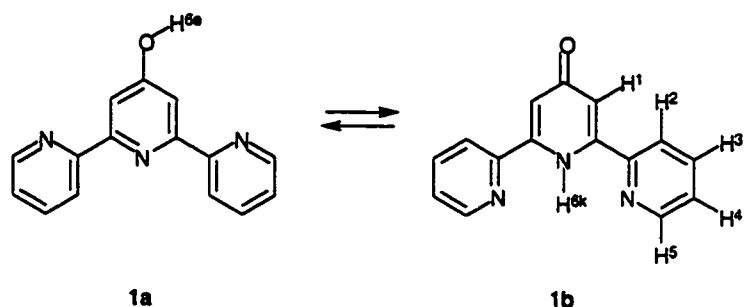
through: 1) intermolecular^{19,20} and intramolecular²¹⁻²⁸ hydrogen-bonding of the hydroxyl hydrogen and an appropriately placed hydrogen bond acceptor, or 2) a reduction in the proton affinity of the pyridine nitrogen atom through the incorporation of electron withdrawing groups and consequently a reduction in the efficacy of the nitrogen to act as a hydrogen bonding acceptor²⁹⁻³² (Scheme 1). These studies have successfully demonstrated the power of substituents and hydrogen bonding to govern the position of the tautomeric equilibrium.

Scheme 1



Numerous studies have taken advantage of 4-hydroxypyridine **1a** as a ligand to prepare coordination compounds.³³⁻³⁷ It appears that the choice of nomenclature is at the discretion of the authors as the terpyridine backbone appears in the literature in both its keto and enol forms. There has not been a study to date that rigorously investigates the influence of the environment on the tautomeric equilibrium in this interesting molecule. In this context, the effects of external species and the basic nitrogens positioned by the terminal pyridine rings to effectively stabilize electrostatic charge build-up must both be addressed. Here we study the question of how the populations of terpyridines **1a** and **1b**

vary when the environment is changed from the solid-, to the solution-, and finally to the gas-state. The use of X-ray crystallographic analysis, infrared spectroscopy, ^{13}C CPMAS and ^1H NMR spectroscopy to investigate the equilibrium is reported and discussed. The influence of temperature on the tautomeric population will also be described.



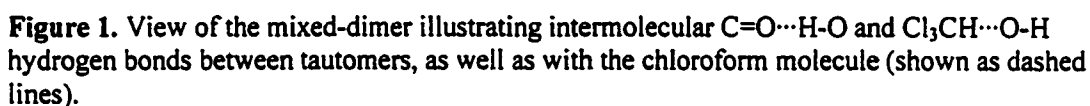
I.2 Results and Discussion

I.2.1 X-ray Crystallographic Analysis

Single crystals of **1** suitable for X-ray crystallographic analysis were obtained by slow evaporation of a chloroform solution. The crystal structure shows that **1** exists as a dimer comprised of an equimolar mixture of tautomers (Figure 1). This mixed-dimer is held together by a strong intermolecular hydrogen bond ($\text{OH}\cdots\text{O}$ distance of 1.702 Å) between the hydroxyl hydrogen of one tautomer and the carbonyl oxygen of the other [$\text{O}(1\text{A})\cdots\text{H}(1\text{OA})\cdots\text{O}(1\text{B})$]. The mixed-dimer we report here is analogous to one previously observed by Bradshaw and Izatt.²⁰ These authors describe a 4-pyridone system in which a crown ether appendage steers the nitrogen atom of aniline into a position where it can act as a strong hydrogen bond acceptor to the N-H hydrogen atom of the pyridone heterocycle. In this way, the 4-pyridone is forced to exist as the keto isomer.

The authors report the presence of one equivalent of the 4-hydroxypyridine isomer, which acts as a hydrogen bond donor in the same way as we describe for this system.

The identity of each tautomer was unambiguously determined by the location of the N-H and O-H hydrogen atoms in difference Fourier calculations and by C-N and C-O bond lengths (Table 1). One terpyridine species displays nitrogen-to-carbon bond lengths of 1.349(4) and 1.342(5) Å in the central ring [N(1A)-C(1A) and N(1A)-C(5A)] which are comparable to those found in standard aromatic pyridines (1.349 Å) and an oxygen-to-carbon bond length of 1.351(5) Å [O(1A)-C(3A)] which is consistent with a C-O single bond.⁴⁰ This species was assigned as the hydroxyl tautomer **1a**. In this species, the *trans-trans* orientation of the three nitrogen atoms with respect to each other eliminates any repulsive N...N lone pair interactions that would be present in the *cis-cis* conformation as well as maximizes weak electrostatic interactions between N(3A)...H(C4A) and N(2A)...H(C2A). This conformational preference plays a critical role in the ¹H NMR analysis as will be described in later sections. The second component of the mixed-dimer displays a significantly shorter oxygen-to-carbon bond length (1.279(4) Å) [O(1B)-C(3B)] which is comparable to those found in carbonyl C=O double bonds.⁴⁰ The nitrogen-to-carbon bond lengths in the central ring of this species [N(1B)-C(1B) and N(1B)-C(5B)] are slightly longer than those in isomer **1a** (1.362(4) and 1.357(5) Å) showing their increased single bond character. This species was assigned as the keto tautomer **1b**. In this case, the cisoid orientation of the three nitrogen atoms results in strong intramolecular NH...N hydrogen bonds (N(2B) and N(3B)...H(1NB) distances of 2.196 Å).



135

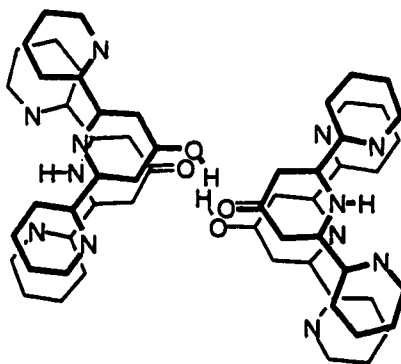
Table 1. Selected interatomic distances (Å) from the X-ray structure of **1**

Enol Tautomer 1a		Keto Tautomer 1b	
bond	distance (Å)	bond	distance (Å)
O1A-C3A	1.351(4)	O1B-C3B	1.279(4)
N1A-C1A	1.349(4)	N1B-C1B	1.362(4)
N1A-C5A	1.342(5)	N1B-C5B	1.357(5)
C1A-C2A	1.393(5)	C1B-C2B	1.356(5)
C2A-C3A	1.376(5)	C2B-C3B	1.420(5)
C3A-C4A	1.391(5)	C3B-C4B	1.432(5)
C4A-C5A	1.387(5)	C4B-C5B	1.363(5)
N2A-C11A	1.335(5)	N2B-C11B	1.341(5)
N2A-C15A	1.337(5)	N2B-C15B	1.337(5)
C11A-C12A	1.393(5)	C11B-C12B	1.381(5)
C12A-C13A	1.379(5)	C12B-C13B	1.375(5)
C13A-C14A	1.360(5)	C13B-C14B	1.375(5)
C14A-C15A	1.378(5)	C14B-C15B	1.380(5)

The packing diagram of **1** shows that the mixed-dimers arrange into parallel sheets stacked in a manner as to maximize favorable offset π - π stacking interactions (Figure 2a). The shortest distance between the π -stacked planes is 3.404 Å. These parallel sheets arrange in a “herringbone” fashion that extends throughout the crystal (Figure 2b). There are channels that run within the planes at the junction of each stacked sheet in the “herringbone” motif (not shown). It is within these channels that the ordered solvent

molecules reside. This sheds light onto the preference for the hydrogen atom of the chloroform to interact with the hydroxy oxygen of **1a**. The lone pair electrons of the oxygen in **1b** lie in the plane defined by the mixed-dimers and are thus less accessible than those for **1a** which point into the channels.

(a)



(b)



Figure 2. Cross section of the crystal packing diagram of the dimeric species **1** illustrating a) the offset π - π stacked parallel layers, and b) the herringbone arrangement of the parallel layers. Chloroform molecules have been removed for clarity.

1.2.2 Solid-State Analysis Using ^{13}C NMR Spectroscopy

Table 2. ^{13}C CPMAS DPD NMR data (δ) for terpyridine **1**^a

δ C3A	δ C3B	δ C1, C5 (A, B)	δ C11, C21 (A, B)
167.77	180.91	155.25	149.90

^aNumbering scheme corresponds to that described in the crystal structure (Fig. 1).

The solid-state ^{13}C CPMAS NMR results are consistent with the X-ray crystallographic analysis. In the ^{13}C NMR spectrum, there are nine signals, seven of which are broadened due to overlapping resonances of the two tautomers as well as partially unaveraged dipolar interactions between adjacent ^{13}C and ^{14}N atoms.⁴¹ The two furthest downfield signals (δ 180.91 and 167.77) were assigned as the carbonyl C=O (C3B) and the phenolic C-OH (C3A) carbons respectively. A dipolar dephasing (DPD) ^{13}C NMR experiment, which suppresses all signals except those that correspond to carbonyl and quaternary carbons, corroborates this assignment. As anticipated, this spectrum shows, in addition to the two downfield signals identified above, signals at δ 155.25 and 146.90 (Table 2). Integration shows the relative signal intensities of the four signals to be 1:1:4:4 which were assigned as C(3B), C(3A), C(1A, 5A) and C(1B, 5B), C(21A, 11A) and C(21B, 11B) respectively (see Figure 1 for atom labeling scheme). The resonance at δ 155.25 corresponds to the C1 and C5-carbon atoms and is identical for both tautomeric forms of **1**. This also holds true for the signal at δ 146.90, which represents carbons C11 and C21. This highlights the efficacy of ^{13}C CPMAS NMR as a diagnostic technique for quantifying solid-state tautomeric populations. This technique is utilitarian in the absence of a crystal suitable for X-ray analysis.^{42,43}

1.2.3 Infrared Spectroscopic Analysis

The gas phase FT-IR spectrum of **1** was obtained using coupled GC/FT-IR analysis. Only one major molecular species eluted as evidenced by a single sharp peak in the GC trace. The FT-IR spectrum of this species exhibits a sharp absorbance at $\bar{\nu}$ 3640, characteristic of an "isolated" hydroxy stretch (Figure 3a).⁴⁴ The spectrum also shows a very weak C=O stretching band at 1635 cm^{-1} . These observations suggest that the hydroxy tautomer **1a** may exist almost exclusively in the gas phase. It is not certain whether the predominance of **1a** using this technique can be attributed to a preference for the less polar enol tautomer.⁴⁵ It may also be an artifact of the column stationary phase, which may retain **1b**, or effect the preferential stabilization of **1a**.

The solution IR spectrum of **1** in CHCl_3 (Figure 3b) and CH_3OH (not shown) reveals the presence of an N-H stretch at $\bar{\nu}$ 3310 cm^{-1} and a C=O stretch at $\bar{\nu}$ 1630 cm^{-1} . These absorbances, combined with the absence of an O-H stretch indicate the presence of only the keto tautomer **1b** in these solvents. The solution IR spectrum of **1** in CH_2Cl_2 at 25 °C is similar to that of CHCl_3 , however, subsequent variable temperature ^1H NMR studies discussed in the following section argues the existence of the hydroxy tautomer as well. These results are in good agreement with previous experimental studies done on the 4-hydroxypyridine/pyridone system, where the tautomeric equilibrium favors the more polar keto tautomer in these solvents.¹⁰

The solid-state FT-IR spectrum of **1** (Figure 3c) contains a sharp absorption band at $\bar{\nu}$ 3280 cm^{-1} as well as a broad band centered at $\bar{\nu}$ 2400 cm^{-1} , both indicative of strong hydrogen bonding.^{9,46} The sharp band is due to an N-H stretch of **1b** which is

intramolecularly hydrogen-bonded to the nitrogen atoms of the terminal pyridine rings. The broad absorption band can be attributed to an O-H stretch of **1a**, which spans a wide range of absorption frequencies in the spectrum due to intermolecular hydrogen bonding to the carbonyl oxygen of **1b**. Both of these phenomena have already been observed in the crystal structure. This result differs from the simple 4-hydroxypyridine/pyridone system, in which the keto tautomer exists exclusively in the solid state as $\text{C}=\text{O}\cdots\text{H}-\text{N}$ intermolecularly hydrogen-bonded ribbons.¹³ In the 4-hydroxyterpyridine/pyridone system there exist two intramolecular hydrogen bonds between the central pyridone hydrogen (H_{6k}) of the keto tautomer and the two terminal pyridine nitrogen atoms. This shields the N-H hydrogen atom and prevents it from participating in intermolecular hydrogen bonding.

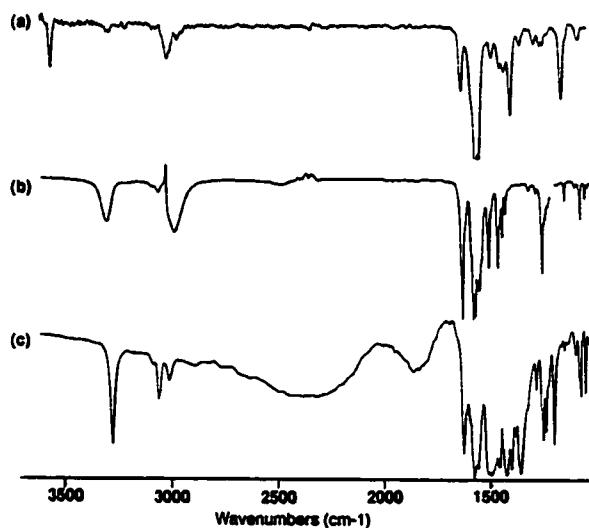


Figure 3. FT-IR spectrum of terpyridine **1** in (a) the vapor phase (190 °C), (b) CHCl_3 solution at 25 °C, (c) the solid-state.

The solid-state FT-IR spectrum of **3**, which cannot form intramolecular hydrogen bonds, also displays a broad absorbance from $\bar{\nu}$ 3000 to 2200 cm^{-1} , indicative of O-H...N intermolecular hydrogen bonding between the hydroxyl group with the pyridine nitrogens of the enol isomer. This observation, combined with the absence of N-H and C=O stretches, indicates the existence of only the hydroxy tautomer. The comparison of **1** and **3** clearly demonstrates the ability of the terminal pyridyl rings to alter the position of the tautomeric equilibrium through hydrogen bonding.

I.2.4 Solution-State Studies Using ^1H NMR Analysis

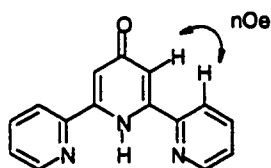
The ^1H NMR spectrum of **1** in CDCl_3 exhibits six resonances as expected for the symmetrical structure of either **1a** or **1b** (Table 3). We, however, argue that the keto isomer is the only species present in this solvent. The signals were assigned based upon coupling constants and T-ROESY experiments, which allowed the broad singlet at δ 11 to be unambiguously identified as the heteroatomic proton H(1NB) of the ketone. This assignment was based on ^1H NMR studies that show the N-H resonance to be solvent and concentration independent ($\Delta\delta$ less than 0.5 over a 0.1 mM to 0.1 M range). This observation can best be explained if the proton is intramolecularly hydrogen bound, and this is only possible for the keto tautomer. The protons of the terminal pyridine rings are clearly seen as four coupled resonances with peaks at δ 8.78, 7.91, 7.87 and 7.42 representing H₅, H₂, H₃ and H₄, respectively. The remaining resonance at δ 7.07 was assigned to H₁ of the central pyridone ring. This assignment was based on the presence of a nuclear Overhauser enhancement (n.O.e.) (Figure 4) from the resonance at δ 7.07 (H₁)

to that at δ 7.91 (H_2), and from a D_2O exchange experiment where this doublet at δ 7.07 collapses to a singlet upon the addition of D_2O .

Table 3. Proton NMR data (δ) for terpyridines **1**, **2** and **3** in $CDCl_3$

Com- pound	δH_1 (d)	δH_2 (dd)	δH_3 (dd)	δH_4 (dd)	δH_5 (dd)	δH_6 (s)
1 ^a	7.07	7.91	7.87	7.42	8.78	11.95
2 ^b	8.03	8.62	7.85	7.33	8.69	
3 ^c	7.51	8.72	8.09			

^a N-H at 11.93 ppm. ^b OCH₃ at 4.04 ppm. ^c Data in DMSO-*d*₆, O-H at 11.23 ppm.

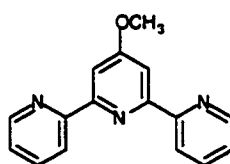


1a

Figure 4. N.O.e. assignments for **1** in $CDCl_3$ at 25 °C.

It is significant that this peak is shifted upfield ($\Delta\delta = -1$) with respect to unsubstituted 2,2':6',2''-terpyridine or the suitably O-methylated derivative **2**, which can be considered as a model for the hydroxy tautomer since it effectively locks the molecule into an analogous conformation. In solution, the keto tautomer **1b** can adopt a *cis-cis* conformation. This has two significant consequences: 1) it allows for the formation of

two strong intramolecular hydrogen bonds between the central pyridone N-H and the nitrogen atoms on the two adjacent pyridine rings, and 2) it results in an upfield shift of H_1 due to the lack of the weak intramolecular hydrogen bonds between the H_1 protons (δ 7.07) and the nitrogen atoms of the terminal pyridine rings. The positive n.O.e. between H_1 and H_2 strengthens the case of the existence of the cisoid conformer (Figure 4). Another probe for the tautomeric preference in solution is the notable feature that H_1 appears as a finely split doublet ($J = 1.8$ Hz). This splitting is not observed for compounds **2** and **3** (where **3** represents an electronically similar structure, that does not have the ability to form a bifurcated intramolecular $NH\cdots N$ hydrogen bond). This feature is particularly interesting as we believe it signifies *meta* coupling between H_1 and the heteroatomic proton H_{6k} , which explains the transformation of this doublet into a singlet upon the addition of D_2O . Again, this phenomenon can only hold true in the case of the keto isomer. It is important to note that the coupling of H_1 to the exchangeable proton H_{6k} eliminates the possibility that there exists a fast exchange process between the two tautomers, and provides additional proof for the presence of a single tautomer on the NMR time-scale.



2

Isomer **3** represents an interesting case where the less polar hydroxy tautomer is exclusively present in the solid state as well as in polar solvents (as diagnosed by FT-IR). The poor solubility of terpyridine **3** in most organic solvents limited its use as a model.

The ^1H NMR of **3** in $\text{DMSO}-d_6$ shows a positive n.O.e. between the heteroatomic hydrogen (-OH) at 11.23 and the hydrogen on the central ring (H_1) which appears at δ 7.51 (Figure 5). The most likely explanation for this tautomeric preference is that unfavourable steric interactions between the central N-H and the C-H atoms of the adjacent heterocycles force the three rings in **3** out of co-planarity when in the keto form.

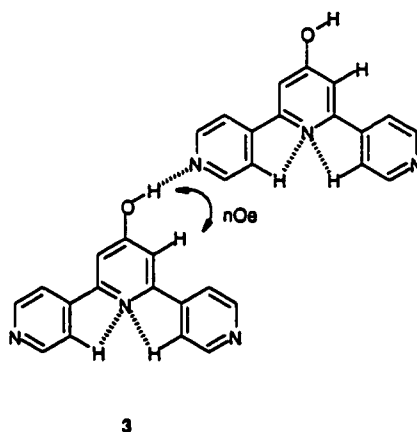


Figure 5. N.O.e. assignments for **3** in CDCl_3 at 25 °C.

Also, the steric bulk of the terminal pyridine rings hinders the approach of the carbonyl oxygen in another molecule of **3** to hydrogen bond with the "buried" N-H. The result is that **3** isomerizes to its enol form. Only now can all three rings adopt a co-planar geometry which maximizes $\text{C-H}\cdots\text{N}$ intramolecular as well as $\text{O-H}\cdots\text{N}$ intermolecular hydrogen bonding.

An effective illustration of the influence of environment on the tautomeric equilibrium in **1** is highlighted by the variable temperature ^1H NMR experiments. There are no observable changes in the ^1H NMR spectra of **1** in CDCl_3 over the temperature

range evaluated (25 °C to -80 °C).[†] On the other hand, the spectra of CD₂Cl₂ solutions display twelve resonances representing the existence of two species in a ratio of 6:1 at 25 °C. This ratio changes to 3:1 as the temperature is lowered (Figure 6). The six predominant signals at ambient temperature closely resemble those found in the CDCl₃ solution spectra and were assigned to the keto tautomer **1b**. The second set of signals at δ 13.51, 8.64, 8.61, 8.00, 7.86 and 7.33 were assigned to the hydroxy tautomer **1a** based on the coupling constants and by a comparison with the chemical shifts of the O-methylated isomer **2** (Fig. 6c). The significant downfield shifts ($\Delta\delta = 1$) of the singlet assigned to H₁ (δ 7.05 at 25 °C; δ 8.00 at -70 °C) and the doublet assigned to H₂ (δ 7.96 at 25 °C; δ 8.65 at -70 °C) clearly demonstrate that the terminal pyridine rings have rotated to adopt a transoid configuration in the enol form. These downfield shifts can be attributed to intramolecular hydrogen bonding between the acidic aromatic C-H protons and the basic nitrogen atoms. The broad singlet assigned to H_{6e} at δ 12.5 is shown to be temperature dependent and moves downfield ($\Delta\delta = 1.3$) to δ 13.8 as the solution is cooled from 25 °C to -80 °C. The other H_{6k} resonance at δ 12.3, assigned to the N-H of the keto tautomer, does not move over this temperature range. This indicates that H_{6e} is not intramolecularly hydrogen bound (as these types of protons are concentration and temperature independent) but intermolecularly hydrogen bound. We attribute the downfield shifts of H_{6e} to an increase in the strength of the hydrogen bond between isomers as the solution is cooled. Furthermore, the large steric interactions in the transoid rotamer of **1a** prevent H_{6e} from existing as a N-H pyridinone, thereby denoting the existence of the hydroxy tautomer **1a** and eliminating the existence of transoid rotamer of **1b**.

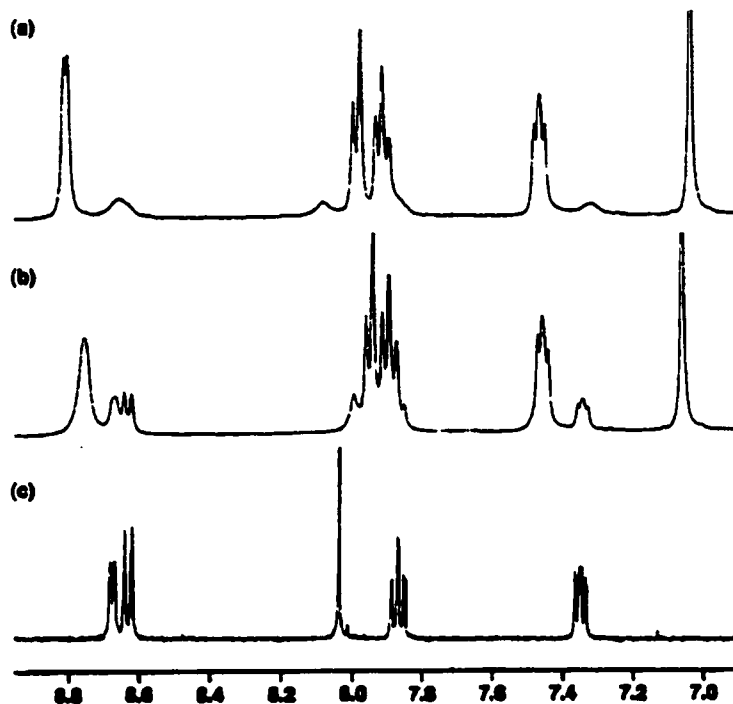


Figure 6. ^1H NMR spectra of CD_2Cl_2 solutions of **1** in CD_2Cl_2 at (a) 25°C , (b) -70°C , and (c) **2** at 25°C .

The dominance of the pyridone tautomer in CDCl_3 is most likely the result of both solvent effects (the stabilization of the more polar keto tautomer by the polar solvent) and substituent effects (the formation of strong intramolecular hydrogen bonds between $\text{N}\cdots\text{N}-\text{H}\cdots\text{N}$). It was unexpected that the hydroxy tautomer would increase in abundance (from 17% to 33%) as the temperature of the CD_2Cl_2 solution is lowered as it has been reported that the dielectric constant of dichloromethane increases upon cooling.⁴⁷ This implies that the more polar keto tautomer should exist exclusively at colder temperatures. However, we show that this is not the case for terpyridine **1**. We believe that the enol

tautomer **1a** exists in CD_2Cl_2 because this solvent is not as effective in stabilizing the electrostatic charge built up on the carbonyl group of **1b**, shifting the tautomeric equilibrium towards the hydroxy tautomer **1a** which can be better stabilized under these conditions. The existence of **1a** provides a suitable hydrogen bond donor (the O-H hydrogen atom), which can now stabilize the electrostatic demand of the keto tautomer through hydrogen bonding. We propose that as the temperature is lowered, the system in CD_2Cl_2 begins to resemble the mixed-dimer found in the crystal.

1.3 Conclusion

It has been shown that here are three major factors governing the population distribution of terpyridine **1**. The first one concerns the choice of solvent. As has been reported for the simple 4-hydroxypyridine derivative, the more polar keto tautomer is predominant if not exclusive in polar solvents. VT ^1H NMR experiments uncovered an exception to this generalization, where the population of the hydroxy isomer **1a** increased as CD_2Cl_2 solutions were cooled. We rationalize this observation with the selective destabilization of the keto form. The inability of CD_2Cl_2 to effectively solvate the basic carbonyl group of **1b** through intermolecular hydrogen bonding shifts the equilibrium towards the enol form **1a** which possesses a weaker hydrogen bond donor.

We have also shown that the tautomeric equilibrium can be upset by steric factors. This was clearly demonstrated by terpyridine **3**, which exists in the hydroxy form even in very polar solvents such as dimethylsulfoxide. In this form, the all three heterocyclic rings can adopt a conformation that is close to co-planar. There is an additional stabilization resulting from intramolecular C-H \cdots N hydrogen bonding. A shift to the keto

form would disrupt this co-planarity because of unfavourable steric interactions of the pyridone N-H and C-H protons, destabilizing the molecule, and resulting in a preference for the hydroxy tautomer.

The third factor concerns intra- and intermolecular hydrogen bonding.

Stabilization of the keto form **1a** in polar solvents is achieved by strong bifurcated intramolecular N-H...N hydrogen bonds. In the absence of a suitable hydrogen bond donor provided by either the solvent or solute, the tautomeric equilibrium shifts and the population of the less polar hydroxy isomer grows. This is evident in the solid state as well as in CD₂Cl₂ solutions. We believe the presence of this less favorable tautomer provides a suitable hydrogen bond donor (O-H) which is able to satisfy the electrostatic demand of the basic carbonyl of **1b**.

In summary, the present study show that solvent, hydrogen bonding and structural substituents all play a key role in affecting tautomeric distributions, illustrating the necessity to address all factors when designing species capable of rapid isomer interconversion.

I.4 Experimental

For a general description of apparatus, materials and methods see Chapter 2.

I.4.1 Preparation of 2,6-bis(2-pyridyl)-1H-4-pyridone (1), 2,6-bis(2-pyridyl)-4-methoxy-pyridine (2) and 2,6-bis(4-pyridyl)-1H-4-pyridone (3)

Parent compound **1** was prepared in two steps by condensation of ethyl picolinate and acetone under basic conditions.³⁶ The intermediate 1,5-bis(2'-pyridyl)pentane-1,3,5-trione was cyclized in the presence of excess ammonium acetate to afford multi-gram quantities of **1** in high yield.³⁷ The corresponding methoxy derivative **2** was prepared from **1** by treatment with iodomethane in acetone under basic conditions.³⁸ Isomer **3** was prepared in an analogous fashion as **1** from ethyl isonicotinate. The structures of **1**, **2** and **3** were verified by ¹H and ¹³C NMR spectroscopy, infrared spectroscopy and electrospray mass spectrometry (ES-MS).

I.4.2 ¹H and ¹³C NMR Spectroscopy

¹³C CP MAS NMR spectra were obtained at 25 °C on a Bruker AMR300 spectrometer. For this purpose a 7-mm Bruker DAB 7 probehead which achieves rotation frequencies up to 5 kHz was used. The standard CP pulse sequence was applied with a 6.8 μs ¹H-90° pulse width, 2 ms contact pulses, 2 s repetition time and a spectrum width of 35kHz. Chemical shifts are reported with respect to the spectrometer frequency, which was calibrated by the adamantane signal at 38.56 ppm. For ¹H NMR dilution experiments, a concentrated solution of **1** (1 M) was prepared in the appropriate solvent. A 500 μL aliquot of this solution was transferred to a NMR tube and subsequently diluted with the appropriate pure deuterated solvent. The procedure was repeated to sub-millimolar concentrations. Spectra were recorded with increasing acquisition times for diluted samples. ¹H NMR variable temperature (VT) spectra were obtained from 25 °C to -80 °C on a Bruker AM400 spectrometer, working at 400.13 MHz. Temperatures were calibrated with a copper/constantan thermocouple and are accurate to ±1 °C.

I.4.3 UV-Vis Spectroscopy

FT-IR measurements were performed using a Nicolet Magna-IR 750 (solution phase studies), Nicolet-Plan IR Microscope (solid-state studies) and Hewlett-Packard GC-IR fitted with an HP1 column (25Mx0.32mm idx0.52 μ film) for the gas phase studies.

I.4.4 X-ray Crystallographic Analysis

The crystal structure was solved using direct methods (SHELXL-86) and refined by full-matrix least squares on F^2 (SHELXL-93).³⁹ The hydrogen atoms attached to O(1A) and N(1B) were located from a difference Fourier map, then refined in idealized positions (H(1OA) as a hydroxyl proton hydrogen-bound to O(1B); H(1NB) as attached to an sp^2 -hybridized nitrogen atom); all other hydrogens were generated in idealized positions according to the sp^2 or sp^3 -hybridized geometries of their attached carbon atoms. $V(\text{\AA}^3)=2894.1(3)$, $Z=4$, final $R_1(F) = 0.0595$ (for 2748 data with $F_o^2 \geq 2 \sigma(F_o^2)$), $wR_2(F^2) = 0.1415$ (on all data), and $S = 1.059$ for 379 parameters varied. The largest difference peak and hole in the final difference Fourier map had intensities of 0.405 and $-0.469e \text{ \AA}^{-3}$, respectively.

I.4.5 Footnotes

† There was no observable change in the ^1H NMR spectrum when the CDCl_3 was deacidified with basic alumina.

I.5 References

1. A. R. Katritzky, *Handbook of Heterocyclic Chemistry*; Pergamon, Oxford, 1985.
2. J. Elguero, C. Marzin, A. R. Katritzky, P. Linda, *Adv. Heterocycl. Chem. Supp.*, 1 1976.
3. J. S. Kwaitkowski, B. Pullman, *Adv. Heterocycl. Chem.* 1975, 18, 199.
4. M. T. Chenon, R. J. Pugmire, D. M. Grant, R. P. Panzica, L. B. Townsend, *J. Am. Chem. Soc.* 1975, 97, 4636.
5. H. B. Schlegel, P. Gund, E. M. Fluder, *J. Am. Chem. Soc.* 1982, 104, 5347.
6. M. J. Scanlan, I. H. Hillier, A. A. MacDowell, *J. Am. Chem. Soc.* 1983, 105, 3568.
7. J. Wang, R. J. Boyd, *J. Phys. Chem.* 1996, 100, 16141.
8. M. J. Nowak, K. Szczepaniak, A. Barski, D. Shugar, *J. Mol. Struct.* 1980, 62, 47.
9. M. Yildiz, A. Kilic, T. Hokelek, *J. Mol. Struct.* 1998, 441, 1.
10. J. Gao, L. Shao, *J. Phys. Chem.* 1994, 98, 13772.
11. J. Frank, A. R. Katritzky, *J. Chem. Soc., Perkin Trans. 2* 1975, 1428.
12. D. M. L., Goodgame, M. Lalia-Kantouri, D. J. Williams, *J. Crystallogr. Spectrosc. Res.* 1993, 23, 373.
13. F. P. Boer, *Acta Crystallogr., Sect B* 1972, 28, 3200.
14. L. M. Toledo, J. W. Lauher, F. W. Fowler, *Chem. of Mater.* 1994, 6, 1222.
15. W. O. Nelson, T. B. Karpishin, S. J. Rettig, C. Orvig, *Can. J. Chem.* 1988, 66, 123.
16. F. Vogtle, J. Breitenbach, M. Nieger, *J. Chem. Soc., Chem. Comm.* 1991, 860.
17. J. S. Bradshaw, J. M. Gwynn, S. G. Wood, B. E. Wilson, N. K. Dalley, R. M. Izatt, *J. Heterocycl. Chem.* 1987, 24, 415.
18. W. Chu, S. Kamitori, M. Shinomiya, R. G. Carlson, F. Takusagawa, *J. Am. Chem. Soc.* 1994, 116, 2243.

19. Y. Nakatsuji, J. S. Bradshaw, P.-K. Tse, G. Arena, B. E. Wilson, N. K. Dalley, R. M. Izatt, *J. Chem. Soc., Chem. Comm.* **1985**, 751.
20. J. S. Bradshaw, M. L. Colter, Y. Nakatsuji, N. O. Spencer, M. B. Brown, R. M. Izatt, G. Arena, P.-K. Tse, B. E. Wilson, J. D. Lamb, N. K. Dalley, *J. Org. Chem.* **1985**, *50*, 4865.
21. E. Muller, R. Haller, K. W. Merz, *Chem. Ber.* **1966**, *99*, 445.
22. R. Haller, *Tetrahedron Lett.* **1965**, 3175.
23. G. P. Bean, M. J. Cook, T. M. Dand, A. R. Katritzky, J. R. Lea, *J. Chem Soc. (B)* **1971**, 2339.
24. D. N. Bailey, D. M. Hercules, T. D. Eck, *Analyt. Chem.* **1967**, *39*, 877.
25. H. J. Roth, *Arch. Pharm.* **1965**, *298*, 12; H. J. Roth, K. Jager, R. Brandes, *Arch. Pharm.* **1965**, *298*, 885.
26. S. Garcia-Granda, J. F. Van Der Maelen Uria, J. Barluenga, M. Tomas, A. Ballesteros, J.-S Kong, *Acta Crystallogr., Sect C* **1993**, *49*, 99.
27. S. Shiotani, H. Morita, M. Inoue, T. Ishida, Y. Iitaka, A. Itai, *J. Heterocycl. Chem.* **1984**, *21*, 725.
28. N. B. Perry, L. Ettouati, M. Litaudon, J. W. Blunt, M. H. G. Munro, S. Parkin, H. Hope, *Tetrahedron*, **1994**, *50*, 3987.
29. A. Gordon, A. R. Katritzky, S. K. Roy, *J. Chem Soc. (B)* **1968**, 556.
30. A. R. Katritzky, J. D. Rowe, S. K. Roy, *J. Chem Soc. (B)* **1967**, 758.
31. R. D. Chambers, J. Hutchinson, W. K. R. Musgrave, *J. Chem Soc.* **1964**, 5634.
32. F. P. Boer, J. W. Turley, F. P. Van Remoortere, *J. Chem. Soc., Chem. Comm.* **1972**, 573.

33. K. T. Potts, M. J. Cippullo, P. Ralli, G. Theodoridis, *J. Org. Chem.* **1982**, *47*, 3027.
34. R.-A. Fallahpour, E. C. Constable, *J. Chem. Soc., Perkin Trans. 1*, **1997**, 2263.
35. J. D. Holbrey, G. J. T. Tiddy, D. W. Bruce, *J. Chem. Soc., Dalton Trans. 1* **1997**, 2263.
36. K. T. Potts, D. Konwar, *J. Org. Chem.* **1991**, *56*, 4815.
37. E. C. Constable, M. D. Ward, *J. Chem. Soc., Dalton Trans.* **1990**, 1405.
38. G. Lowe, T. Vilaivan, *J. Chem. Research (S)* **1996**, *8*, 386.
39. (a) SHELXL-93 Program for crystal structure determination, G. M. Sheldrick, University of Göttingen, Germany, **1993**; (b) G. M. Sheldrick, *Acta Crystallogr.* **1990**, *A46*, 467.
40. F. H. Allen, O. Kennard, D. G. Watson, L. Brammer, A. G. Orpen, R. Taylor, *J. Chem. Soc., Perkin Trans. 2* **1987**, S1.
41. R. K. Harris, A. C. Olivieri, *Prog. NMR Spectrosc.* **1992**, *24*, 435.
42. A. Mizuno, Y. Toda, M. Itoh, K. Kojima, Y. Kadoma, *J. Mol. Struct.* **1998**, *441*, 149.
43. G. A. Facey, T. J. Connolly, C. Bensimon, T. Durst, *Can. J. Chem.* **1996**, *74*, 1844.
44. F. Buyl, J. Smets, G. Maes, L. Adamowicz, *J. Phys. Chem.* **1995**, *99*, 14967.
45. Dipole moments were calculated to be 3.74 Debye and 7.82 Debye for the enol (**1a**) and keto (**1b**) tautomers respectively. Calculations were performed using the Gaussian-94 program at the Hartree-Fock (HF) level with the 6-311G basis set. M. J. Frisch, G. W. Trucks, H. B. Schlegel, P. M. W. Gill, B. G. Johnson, M. A. Robb, J. R. Cheeseman, T. Keith, G. A. Petersson, J. A. Montgomery, K. Raghavachari, M. A. Al-Laham, V. G. Zakrzewski, J. V. Ortiz, J. B. Foresman, J. Cioslowski, B. B. Stefanov, A. Nanayakkara, M. Challacombe, C. Y. Peng, P. Y. Ayala, W. Chen, M. W. Wong, J.

- L. Andres, E. S. Replogle, R. Gomperts, R. L. Martin, D. J. Fox, J. S. Binkley, D. J. Defrees, J. Baker, J. P. Stewart, M. Head-Gordon, C. Gonzalez, J. A. Pople, Gaussian, Inc., Pittsburgh PA, 1995.
46. Y. Akama, M. Shiro, T. Ueda, M. Kajitani, *Acta Crystallogr., Sect. B* 1995, 51, 1310.
47. S. O. Morgan, H.H. Lowry, *J. Phys. Chem.* 1930, 34, 2385.

Appendix II - X-Ray Crystallography

II.1 Bond Lengths for [7]-Helicene 18A and 18B

<i>(a) Molecule A</i>			<i>(b) Molecule B</i>		
Atom1	Atom2	Distance	Atom1	Atom2	Distance
Br	C12	1.913(9)	Br	C12	1.892(9)
O1	C4	1.379(10)	O1	C4	1.320(11)
O1	C30	1.439(8)	O1	C30	1.452(8)
O2	C21	1.363(9)	O2	C21	1.363(9)
O2	C40	1.452(10)	O2	C40	1.422(10)
N1	C4	1.287(11)	N1	C4	1.320(11)
N1	C5	1.379(11)	N1	C5	1.359(11)
N2	C20	1.387(10)	N2	C20	1.389(9)
N2	C21	1.287(11)	N2	C21	1.277(11)
C1	C2	1.395(12)	C1	C2	1.429(12)
C1	C5	1.409(11)	C1	C5	1.439(10)
C1	C28	1.464(12)	C1	C28	1.428(12)
C2	C3	1.357(12)	C2	C3	1.373(12)
C3	C4	1.419(10)	C3	C4	1.418(11)
C5	C6	1.405(12)	C5	C6	1.408(12)
C6	C7	1.361(12)	C6	C7	1.343(12)
C7	C8	1.408(10)	C7	C8	1.440(10)
C8	C9	1.408(12)	C8	C9	1.396(12)
C8	C28	1.399(12)	C8	C28	1.410(11)
C9	C10	1.360(10)	C9	C10	1.354(10)
C10	C11	1.396(11)	C10	C11	1.447(11)
C11	C12	1.455(11)	C11	C12	1.436(11)
C11	C27	1.435(12)	C11	C27	1.413(11)
C12	C13	1.346(12)	C12	C13	1.375(12)
C13	C14	1.414(12)	C13	C14	1.404(12)
C14	C15	1.417(12)	C14	C15	1.434(12)
C14	C26	1.392(11)	C14	C26	1.413(10)
C15	C16	1.358(12)	C15	C16	1.347(11)
C16	C17	1.442(12)	C16	C17	1.412(11)
C17	C18	1.422(12)	C17	C18	1.406(12)
C17	C25	1.406(12)	C17	C25	1.421(12)
C18	C19	1.359(11)	C18	C19	1.352(11)
C19	C20	1.452(13)	C19	C20	1.402(12)
C20	C24	1.399(12)	C20	C24	1.404(11)
C21	C22	1.405(12)	C21	C22	1.425(13)
C22	C23	1.367(10)	C22	C23	1.356(10)
C23	C24	1.407(13)	C23	C24	1.416(12)
C24	C25	1.455(10)	C24	C25	1.440(10)
C25	C26	1.451(12)	C25	C26	1.449(12)